

LOW LOSS SUBSTRATE INTEGRATED WAVEGUIDE N-WAY POWER DIVIDER

A THESIS SUBMITTED TO
THE GRADUATE SCHOOL OF NATURAL AND APPLIED SCIENCES
OF
MIDDLE EAST TECHNICAL UNIVERSITY

BY

PEJMAN MOHAMMADI

IN PARTIAL FULFILLMENT OF THE REQUIREMENTS
FOR
THE DEGREE OF DOCTOR OF PHILOSOPHY
IN
ELECTRICAL AND ELECTRONIC ENGINEERING

DECEMBER 2012

Approval of the thesis:

LOW LOSS SUBSTRATE INTEGRATED WAVEGUIDE N-WAY POWER DIVIDER

submitted by **PEJMAN MOHAMMADI** in partial fulfillment of the requirements for the degree of **Doctor of Philosophy in Electrical and Electronic Engineering Department, Middle East Technical University** by,

Prof. Dr. Canan Özgen
Dean, Graduate School of **Natural and Applied Sciences** _____

Prof. Dr. İsmet ERKMEN
Head of Department, **Electrical and Electronic Engineering** _____

Assoc. Prof. Dr. Şimşek Demir
Supervisor, **Electrical and Electronic Engineering Department, METU** _____

Examining Committee Members:

Prof. Dr. Canan Toker
Electrical and Electronic Engineering Dep., METU _____

Assoc. Prof. Dr. Şimşek Demir
Electrical and Electronic Engineering Dep., METU _____

Prof. Dr. Özlem Aydın Çivi
Electrical and Electronic Engineering Dep., METU _____

Prof. Dr. Gönül Turhan Sayan
Electrical and Electronic Engineering Dep., METU _____

Assoc. Prof. Dr. Ali Kara
Electrical and Electronic Engineering, Atılım University _____

Date: _____

I hereby declare that all information in this document has been obtained and presented in accordance with academic rules and ethical conduct. I also declare that, as required by these rules and conduct, I have fully cited and referenced all material and results that are not original to this work.

Name, Last Name: PEJMAN MOHAMMADI

Signature :

ABSTRACT

LOW LOSS SUBSTRATE INTEGRATED WAVEGUIDE N-WAY POWER DIVIDER

Mohammadi, Pejman

Ph.D., Department of Electrical and Electronic Engineering

Supervisor : Assoc. Prof. Dr. Şimşek Demir

December 2012, 97 pages

Substrate Integrated Waveguide (SIW) technology has been used in designing and fabricating SIW n-way power dividers. In this thesis employing this technology three-port and five-port SIW power dividers are designed and fabricated. These structures are compact in size and the design procedure can be expanded into n-port power dividers. These structures are used with microstrip transition parts however measurement of S-parameters of the main structure are required for comparison. This is carried out with a special algorithm based on TRL calibration method. This method is general for reconstructing the S-parameters of the n-port network. For the three-port SIW power divider the measured return loss is below 10 dB and transmission is measured between -3.5 dB and -4 dB over a frequency band from 9 GHz to 11 GHz. The measured amplitude balance is less than ± 0.5 dB from 9.5 GHz to 11 GHz and the measured phase difference between $\angle S_{21}$ and $\angle S_{31}$ is about 4° . There is a good agreement between simulation and measurement results over the frequency band from 9.5 GHz to 10.5 GHz for five-port SIW power divider. Based on the total loss mechanisms in SIW structure low loss SIW three-port and five-port power dividers have been designed. A three-port partially filled SIW power divider has been constructed. Its measurement results show that transmissions are between -3 dB and -3.5 dB from 8.75 GHz to 10 GHz and the return loss is less than 10 dB in the same frequency band. The measured amplitude balance is less than

± 0.2 dB over frequency band from 8.75 GHz to 10 GHz and the measured phase difference between $\angle S_{21}$ and $\angle S_{31}$ is about 4° .

Keywords: Substrate Integrated Waveguide, Power Divider, Low Loss, TRL Calibration

ÖZ

TABAN MALZEMESİNE TÜMLEŞİK DALGA KLAVUZU İLE DÜŞÜK KAYIPLI N-YOLLU GÜÇ BÖLÜCÜ

Mohammadi, Pejman

Doktora, Elektrik ve Elektronik Mühendisliği Bölümü

Tez Yöneticisi : Assoc. Prof. Dr. Şimşek Demir

Aralık 2012, 97 sayfa

Yüzey Tümlleşik Dalga Kılavuzu (YTDK) teknolojisi YTDK huzme oluřturma ađı tasarımı ve üretiminde kullanılmaktadır. Tez kapsamında, üç ve beř kapılı YTDK güç bölücü tasarlanmış ve üretilmiştir. Bu yapılar az yer kaplar ve tasarım adımları n-kapılı huzme oluřturma ađı oluřturmak için geliştirilebilir. Bu yapılar mikrořerit geçişlere gerek duyulmadan kullanıldığı için yapının ek geçişlerin etkisini içermeyen S-parametreleri ölçülmelidir. Bu ölçümler özel TRL kalibrasyon algoritması ile yapılmıştır. Bu metot n-kapılı ađın S-parametrelerini yeniden yapılandırmak için genelleştirilebilir.

Üç kapılı YTDK güç bölücü yapısında, -10 dB geriye dönüş kaybı ve 9 GHz - 11 GHz bant aralığında -3.5 dB ile -4 dB arasında geçiş değerleri ölçülmüştür. Ayrıca, ölçülen genlik dengesi 9 GHz - 11 GHz bant aralığında ± 0.5 dB'den azdır ve $\angle S_{21}$ ile $\angle S_{31}$ arasında ölçülen faz farkı yaklaşık ± 4 derece dir. Beř kapılı YTDK güç bölücünün ölçüm ve benzetim sonuçları 9 GHz - 11 GHz bant aralığında gayet uyumludur.

YTDK yapısındaki kayıp mekanizmaları incelenmiştir. Bu çalışmalara göre düşük kayıplı üç ve beř kapılı YTDK huzme oluřturma ađı tasarlanmıştır. Üç kapılı yarı doldurulmuş YTDK güç bölücü yapılmıştır. Bu yapının kalibrasyon ile yeniden yapılandırılmış S-parametreleri,

8.75 GHz -10 GHz bant aralığında -3 dB ile -3.5 dB arasında geçiş ve -10 dB'den az geriye dönüş kaybı göstermektedir. 8.75 GHz - 10 GHz bant aralığında ölçülen genlik dengesi ± 0.2 dB'den azdır ve $\angle S_{21}$ ile $\angle S_{31}$ arasında ölçülen faz farkı yaklaşık ± 4 derece dir.

Anahtar Kelimeler: Yüzey Tümlleşik Dalga Kılavuzu, Huzme Oluşturma Ağı, Düşük Kayıp, TRL Kalibrasyon

To my family

ACKNOWLEDGMENTS

It gives me a great pleasure in expressing my gratitude to all people who have supported me and had their contributions in making this thesis possible. First I must acknowledge to my supervisor Prof. Şimşek Demir for his supervision, valuable strategy and providing me this opportunity to study with him and get valuable experiences in working at the millimeter laboratory. I also would like to thank Prof. Özlem Aydın Çivi and Prof. Ali Kara for their contribution and innovative ideas to the research. I also would like to acknowledge Prof. Sencer Koç for his support at the millimeter wave laboratory and for sharing his great experience. I would to express my gratitude to Prof. Canan Toker and Prof. Gönül Turhan Sayan for their motivation and contribution in my thesis.

I would like to thank Amin Ronaghzadeh for his contribution in this thesis. He has always been a trust-able brother for me. Moreover I would like to thank the students in millimeter-wave laboratory namely Kağan Topallı, Mehmet Ünlü for their valuable experiences in METU , Omer Bayraktar Çağrı Çetintepe and İlker Comart for their motivation, and helping me during the research time. I would like to thank the millimeter wave staff Adam Ateş, Erdinc Yardakuc and Orhan Bardak for their support in fabrication process. I would like to thank my parents for their unconditional love and support. I also would like to express my deep appreciation toward my wife and kids, Sina and Sadra for their valuable encouragement and motivation during the study. The last but not the least, I would thank my dear brothers, Mehran and Ali for their supports.

TABLE OF CONTENTS

ABSTRACT	iv
ÖZ	vi
ACKNOWLEDGMENTS	ix
TABLE OF CONTENTS	x
LIST OF TABLES	xiii
LIST OF FIGURES	xiv
CHAPTERS	
1 INTRODUCTION	1
1.1 Overview	1
1.2 Thesis Motivation and Objectives	2
1.3 Thesis Contribution and Publication	4
1.4 Thesis Outline	4
2 SUBSTRATE INTEGRATED WAVEGUIDE	6
2.1 Introduction	6
2.2 Microstrip-to-Substrate Integrated Waveguide Transitions	6
2.3 CPW-to-Substrate Integrated Waveguide Transitions	8
2.4 Rectangular Waveguide Equivalent and Some Consideration on Design of Substrate Integrated Waveguide	10
2.5 Substrate Integrated Waveguide Based Components	12
3 SUBSTRATE INTEGRATED WAVEGUIDE POWER DIVIDER	18
3.1 Introduction	18
3.2 SIW Power Divider	20
3.3 E-Plane Power Divider	21

4	MEASUREMENT METHODS for SUBSTRATE INTEGRATED WAVEGUIDE POWER DIVIDER	27
4.1	Introduction	27
4.2	TRL Calibration Procedure	28
4.3	TRL Measurement of Three-Port device with Two-Port Network Analyzer	30
4.3.1	First Method:	31
4.3.2	Second Method:	33
4.4	Measurement of n-Port Scattering Matrix with Two-Port Network Analyzer	35
5	THREE-PORT AND FIVE-PORT SUBSTRATE INTEGRATED WAVEGUIDE POWER DIVIDER	39
5.1	Introduction	39
5.2	Three-Port Substrate Integrated Waveguide Power Divider Design, Simulation and Fabrication	40
5.2.1	SIW Design	42
5.2.2	Power Divider Design	42
5.2.3	TRL Calibration and Measurement Procedure	43
5.2.4	The Experimental Results of Three-Port SIW Power Divider	47
5.3	Five-Port Substrate Integrated Waveguide Power Divider Design, Simulation and Fabrication	50
5.3.1	Five-port SIW Power Divider Design Consideration	50
5.3.2	Experimental Results of Five-Port SIW Power Divider	51
6	LOW LOSS SUBSTRATE INTEGRATED WAVEGUIDE	57
6.1	Introduction	57
6.2	Wave Propagation Mechanisms in SIW	59
6.3	Dielectric Loss in SIW	60
6.4	Attenuation Constant Due to Dielectric Loss	63
6.5	Design of Partially Filled SIW Power Divider	67
6.5.1	SIW Design	67
6.5.2	Three-Port PSIW Power Divider Design	69
6.6	TRL Procedure	71
6.7	Experimental Results of Three-Port PSIW Power Divider	76

	76
6.8	Five-Port PSIW Power Divider Design	79
7	CONCLUSIONS	83
7.1	Thesis Summary and Conclusions	83
7.2	Suggestions for Future Studies	84
REFERENCES	88
VITA	97

LIST OF TABLES

TABLES

Table 3.1	Three-port SIW power divider dimensions(mm).	25
Table 5.1	Two-way SIW power divider dimensions (mm).	44
Table 5.2	Five-port SIW power divider dimension (mm).	52
Table 6.1	Dimensions of PSIW power divider (mm).	69
Table 6.2	Dimensions of five-ports PSIW power divider (mm).	80
Table 7.1	Dimensions of unequal SIW power divider (mm).	86

LIST OF FIGURES

FIGURES

Figure 1.1 Substrate Integrated Waveguide	1
Figure 2.1 Configuration of proposed transition of microstrip line to rectangular waveguide on the same substrate[3]	7
Figure 2.2 Electric field distributions (a) in rectangular waveguide (b) in microstrip line [3]	8
Figure 2.3 Equivalent topology for microstrip-to-SIW transition a) microstrip Line b) waveguide model of microstrip line c) top view of a microstrip taper d) microstrip-to-SIW step [10]	8
Figure 2.4 Schematic view of the proposed transition of coplanar waveguide and rectangular waveguide [14]	9
Figure 2.5 Configuration of the CPW-to-SIW transition [15]	9
Figure 2.6 Structure of the CPW-to-SIW transition (a) Top view (b) cross section showing the E-field gradation [15]	10
Figure 2.7 Schematic structure of a conventional rectangular waveguide [17]	10
Figure 2.8 Configuration of the substrate integrated waveguide synthesized using metallized via-hole arrays [20]	11
Figure 2.9 (a)Post in waveguide (b) Equivalent PI network [28]	13
Figure 2.10 (a)Photograph of the manufactured three-pole filter (b) Measured and simulated results for the three-pole Chebyshev filter [19]	13
Figure 2.11 (a) Photo of the assembled directional coupler and the two separate single layer PCB (b) Measured S-parameters of the directional coupler at the maximum coupling factor [37]	15

Figure 2.12 (a) HMSIW and SIW couplers (b) Measured and simulated S parameters of the proposed HMSIW 3-dB coupler. [40]	16
Figure 2.13 Photographs of the HMSIW-fed transverse resonant slot array antennas (a) X-band and (b) Ka-band [50]	17
Figure 2.14 Return loss of the HMSIW transverse slot array antenna over X-band.(a) X band (b)Ka-band [50]	17
Figure 2.15 Radiation patterns of the HMSIW transverse slot array antenna (a) 9.82GHz (b) 31.4GHz [50]	17
Figure 3.1 A lossless three port junction used as power divider	18
Figure 3.2 (a) The Wilkinson power divider (b) Simulation results	19
Figure 3.3 The main structure of multi-layer SIW (a) The first and the second layers with slots (b) The coupled E-fields	20
Figure 3.4 The E-plane waveguide or tee junction	21
Figure 3.5 (a,b)Two equivalent circuits for the E-plane tee (c) Side view	22
Figure 3.6 E-plane power divider	23
Figure 3.7 SIW power divider (a) top view (b) bottom view	23
Figure 3.8 SIW power divider equivalent circuit	24
Figure 3.9 Return Loss of SIW power divider with HFSS and ADS software	24
Figure 3.10 Picture of fabricated SIW power divider (a) Top view (b) Bottom view	25
Figure 3.11 Simulation and measurement of three-port SIW power divider	25
Figure 4.1 Block diagram of a network for TRL calibration	28
Figure 4.2 Signal flow graph of LINE	29
Figure 4.3 (a) TRL block diagram of SIW (b) Line (c) Short (d) Thru	30
Figure 4.4 A three-port device	31
Figure 4.5 An n-port network with three different loads connection	37
Figure 5.1 (a)Rectangular waveguide equivalent of three-port SIW power divider (b) Equivalent circuit of three-port SIW power divider	41

Figure 5.2 (a) Rectangular waveguide equivalent of three-port SIW power divider for TRL measurement (b) Equivalent circuit of three-port SIW power divider	41
Figure 5.3 Standards for SIW power divider (a) Thru (b) Line (c) Reflect	43
Figure 5.4 Three-port SIW power divider	44
Figure 5.5 (a) Measurement setup for three-port SIW power divider (b) Reflection measurement from Thru standard	45
Figure 5.6 Fabricated three-port SIW power divider (a) Bottomn view (b) Top view	47
Figure 5.7 Return loss of three-port SIW power divider from simulation and measurement	47
Figure 5.8 Transmission of three port SIW power divider from simulation and measurement	48
Figure 5.9 Isolation between output ports of the three port SIW power divider	48
Figure 5.10 Amplitude balance of three-port SIW power divider	49
Figure 5.11 Phase difference of three-port SIW power divider	49
Figure 5.12 Five-port SIW power divider	50
Figure 5.13 DUT of five-port SIW power divider	51
Figure 5.14 Picture of five-port SIW power divider	52
Figure 5.15 Transmission of five-port SIW power divider S_{21}	53
Figure 5.16 Transmission of five-port SIW power divider S_{31}	53
Figure 5.17 Transmission of five-port SIW power divider S_{41}	54
Figure 5.18 Transmission of five-port SIW power divider S_{51}	54
Figure 5.19 Isolation of five-port SIW power divider	55
Figure 5.20 Amplitude balance of five-port SIW power divider	55
Figure 5.21 Phase difference of five-port SIW power divider	56
Figure 6.1 Partially filled SIW	58
Figure 6.2 Surface current distribution of the rectangular waveguide	59
Figure 6.3 Top view of PSIW and its equivalent RW	61
Figure 6.4 DUT of proposed PSIW structure	64
Figure 6.5 Propagation constant in z direction of PSIW	65

Figure 6.6	Propagation constant in x direction of PSIW	65
Figure 6.7	Dielectric loss of PSIW	66
Figure 6.8	E-Field lines for PSIW top view	67
Figure 6.9	The current distribution on PSIW for TE_{10}	68
Figure 6.10	Proposed PSIW structure	68
Figure 6.11	(a) The proposed PSIW power divider (b) Configuration of PSIW with three different layers	70
Figure 6.12	TRL Standards (a) True (b) Line (c) Reflect	71
Figure 6.13	Signal flow graph for Line connection	72
Figure 6.14	(a) Three layers of fabricated PSIW (b) Top view (c) Bottom view	76
Figure 6.15	Simulation and measurement results of PSIW power divider (a-b) Trans- missions (c) Return Loss	77
Figure 6.16	(a) Amplitude balance (b) Phase balance of PSIW power divider	78
Figure 6.17	Five-port PSIW power divider	79
Figure 6.18	Configuration of five-port PSIW power divider	79
Figure 6.19	DUT of five-port PSIW power divider	80
Figure 6.20	Simulation results of five-port PSIW power divider, Return loss	81
Figure 6.21	Simulation results of five-port PSIW power divider, Transmissions	81
Figure 6.22	Simulation results of five-port PSIW power divider, Isolation	82
Figure 7.1	Unequal SIW power divider	86
Figure 7.2	Return Loss of Unequal SIW power divider	87
Figure 7.3	Transmissions of unequal SIW power divider	87

CHAPTER 1

INTRODUCTION

1.1 Overview

Low-cost, mass-producible, high-performance and high yield microwave and millimeter-wave technologies are critical for developing successful RF and microwave systems. At millimeter-wave frequencies, in particular, circuit-building blocks including antenna elements are closely related to each other via electromagnetic coupling and interconnect. In this case, circuit design should be made with a global consideration. Conventional waveguide technology is still the mainstream for designing high-performance millimeter-wave systems. However, this matured scheme is not suitable for low-cost mass-production. Tedious and expensive post fabrication tuning and assembling become a real problem for manufacturers. In addition, waveguide technique cannot be used to reduce the weight and volume. Substrate integrated waveguide (SIW) is a recent form of transmission line [1]. It is implemented by two periodic via-holes in grounded dielectric. A schematic view is shown in Figure 1-1.

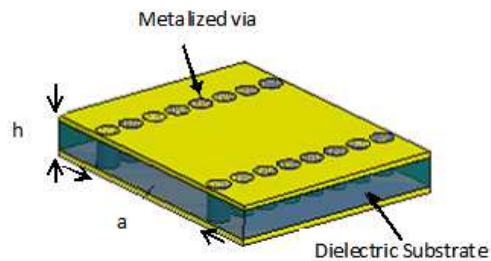


Figure 1.1: Substrate Integrated Waveguide

SIW structures similar to metallic rectangular waveguide are electromagnetic interference free. The side walls of the rectangular waveguide can be realized within the substrate by using a metallized post of vias and upper and lower walls are formed by two metals of printed circuit board (PCB). Some advantages like low cost, low loss and high density integration with microwave and millimeter wave components made it popularized in the past few years[2]-[4]. Moreover SIW technique permits to fabricate a complete circuit in planar form (including planar circuitry transitions, rectangular waveguide, and antenna), using a standard printed circuit board or other processing technique. In a SIW structure the electric field distribution fill the volume inside the waveguide and surface current propagate on a large total cross-sectional area of the waveguide walls, resulting in lower conductor loss [5]-[8]. As frequency of operation and circuit density continue to increase, closely spaced microstrip and strip line interconnects will no longer be viable options. Problems associated with signal integrity, cross coupling and radiation are becoming increasingly difficult to overcome.

The demand for wideband interconnects and compact electronic systems are continually increasing. These desires will employ the SIW technology in future ultra-high frequency and broadband applications and highly integrated systems. In order to improve dimensional design procedure significantly in term of accuracy, time and complexity, excessive use of global full-wave tuning and optimization should be avoided, especially in complicated structure where there are numerous dimensions and parameters to be tuned and optimized.

In a SIW component a global full-wave tuning is the most commonly used method, but this is typically very time consuming due to lots of metallized cylindrical via holes. So an accurate dimensional synthesis procedure has been developed for SIW design. For example some different strategies for microstrip-to-SIW transition with different geometries have been described [9]-[11]. In which the impedance variation follows different mathematical expressions, some of them extract from the classical theory.

1.2 Thesis Motivation and Objectives

In millimeter wave and microwave applications, SIW is an attractive guided-wave structure to realize components and subsystems. Hence one can find a number of the key elements devices implemented using SIW technology. Among these devices SIW power dividers serve the key elements for the realization of multiplexers, phase shifter and antenna beam forming

networks. There had been some efforts to design and produce the SIW-based power dividers. However, these SIW power dividers in the multi-way port environment have large size due to lateral port distribution. One goal of this thesis is to decrease the size of the structure and has a compact size power divider based on SIW technology. There are some papers about this problem earlier, but their structures have lateral form or they are designed for a specific number of ports. So by increasing the number of the ports the size of the structure become larger. In the proposed SIW power divider by stacking the PCB layers in proper position only the length of the SIW power divider will be increased and its width remain constant. Consequently the two-way SIW power divider could be considered as building block on n-way SIW power divider.

Another object of this thesis is to develop a method for measuring n-way scattering matrix with two-port voltage network analyzer (VNA). A modern VNA with True-Reflect-Line (TRL) calibration and appropriate standards can measure two-port non-coaxial (Device Under Test) DUT at desired reference planes. In contrast, due to lack of a multi-port counterpart of a full two-port TRL calibration, a multi-port VNA cannot measure a multi-port non-coaxial DUT up to the intrinsic ports as straightforwardly as measuring the coaxial one.

In the light of TRL calibration facility, removing of any transmission part effects will be achievable. There is a little systematic research in this area. Proposed method has some advantages in comparison with similar methods. By applying this method one can find the desired S-parameter individually. Its mathematical calculation is easy without any need for matrix inversion that must be done in similar algorithm [59-61].

One of the major issues for applicability of SIW to design of millimeter wave components is related to its losses. According to previous studies there are three sources of loss in SIW components. Ohmic loss, radiation loss and dielectric loss are investigated in a little paper[97]-[98]. It has been shown that the dielectric loss has more effect than two others in total loss of the structures. The third objective of this thesis is investigating the loss property of the SIW. A special method will be used for decreasing of the dielectric loss. This technique has been used to design and produce low loss power divider on SIW technology.

1.3 Thesis Contribution and Publication

This thesis presents a short review about the SIW technology, microwave and millimeter wave components which have been made based on SIW. Three SIW structure, i.e. filter, coupler and antenna have been reviewed, according to the subjects have been studied by the researcher until now. SIW power divider had a special interest in the thesis. Designing and manufacturing of some novel power dividers based on SIW will be carried out.

A new measuring method with TRL calibration for multi-port device will be established. The contributions of this thesis are summarized in the following three journal and conference papers:

1. P.Mohammadi, S.Demir, "Two layers substrate integrated waveguide power divider," General Assembly and Scientific Symposium, 2011 XXXth URSI, pp.1-4, 13-20 Aug. 2011.
2. P. Mohammadi and S. Demir, "Multi-layer substrate integrated waveguide e-plane power divider," Progress In Electromagnetics Research C, Vol. 30, 159-172, 2012.
3. P. Mohammadi and a. S. Demir, "Substrate Integrated Waveguide Unequal Power Divider with Adjustable Dividing Ratio," The first Iranian Conference on Electromagnetic Engineering (ICEME) Iran University Of Science And Technology in 26-27 Dec. 2012.

1.4 Thesis Outline

This thesis includes the results of the activities up to date in the framework of the mentioned objectives in 7 chapters. As mentioned above first chapter has an introduction about SIW technology. It has a clarification about the objective of the thesis in a short format.

Chapter 2 will start with a small introduction above the transition which must be used to connect the SIW to microstrip line or coplanar waveguide (CPW) line. It will be continued by reviewing the design equations for this transition parts. Different component based on SIW structure like filter, coupler, antennas, etc. will be provided which are found in literature. Finally general design rule, some consideration points for SIW design and rectangular waveguide equivalent formula are reviewed. This equation gives the length and width of transition parts which have been use to design the SIW power dividers and also SIW TRL standards in chapters 5 and 6.

Chapter 3 will be in progress with a beginning about power divider as a key element in de-

sign of the millimeter wave and microwave systems. This chapter includes E-plane power divider equivalent circuits. Resemblance between E-plane power divider and SIW power divider gives the design rules for SIW power divider design in chapter 5 and 6. Based on this theoretical background, a three-port SIW power divider designing and production with simulation and measurement results are also presented.

Chapter 4 presents the TRL calibration procedure for SIW-based component measurement. The difficulties due to n-port non coaxial device measurement with two-port VNA are reviewed. So a novel method for reconstruction the scattering parameters of an n-port device with non coaxial port in desired reference plane with two-port VNA will be implemented. This method will be used in chapter 5 and 6 to reconstruct the scattering parameters of three-port and five-port SIW power dividers.

Chapter 5 focuses on the three-port SIW power dividers and five-port SIW power dividers. Their design, simulation, production and measurement procedures will be investigated. In this chapter the two-way SIW power divider introduces as a building block of n-way SIW power divider. Their advantages especially compact size of the structures, in comparison with the comparable structures will be identified.

Chapter 6 will begin with the loss mechanisms study in SIW technology. It is carried on by introducing the method to decrease the loss in SIW. Then this method will apply to design the SIW low loss power divider. Measuring the fabricated case needs TRL calibration with two different error boxes. This low loss power divider measurement result will be compared with similar lossy one. Finally the expected scattering parameter will be exhibited.

The subjects of this thesis have been summarized in chapter 7. Future studies suggestions are provided for further improvement of the SIW power dividers and produce new type of an unequal SIW power divider.

CHAPTER 2

SUBSTRATE INTEGRATED WAVEGUIDE

2.1 Introduction

Although the hybrid and monolithic integrated circuits are used more and more in microwave and millimeter wave systems, metal waveguide still plays a major role in specific type of circuits like antenna, high-Q filters and high-Q oscillators. A critical point is to combine both systems via appropriate transitions. The excitation of waveguide with stripline and microstrip line has been reported in some papers [12]-[13]. The transition always consists of two or more separate pieces that require junction assembly, and a tuning mechanism is also generally essential. Furthermore the planar substrate has to be cut into a specific shape. However, they provide reasonably good results, but they typically are not very well suited for a simple and compact integration with the planar circuits.

Approximately ten years ago SIW was suggested. This waveguide is composed of two parallel row of metallic vias inserted in a dielectric substrate. It implements a waveguide on a piece of printed circuit board. However in order to connect active circuits to SIW or to measure S-parameters, mounting SMA connectors and microstrip-to-SIW transitions is required. At the following section a new integrated platform of microstrip line and rectangular waveguide is reviewed.

2.2 Microstrip-to-Substrate Integrated Waveguide Transitions

As the microstrip transmission line only has one ground conductor, the cross sectional electric field distribution propagates through both the substrate and the media above the substrate (usually air). Thus, the microstrip is said to propagate a quasi-TEM mode, in comparison to a

pure transverse electromagnetic (TEM) line, such as a stripline. In order to interconnect rectangular waveguides to planar transmission lines, an electromagnetic mode conversion must be accomplished to transmit signals between the planar TEM, or quasi-TEM, transmission line and the guided waveguide mode. The characteristic impedance of the planar transmission lines must be simultaneously matched to the frequency dependent wave impedance that relates the transverse electric and magnetic fields of the waveguide.

Transition from microstrip line to a substrate integrated waveguide with a tapered line has been proposed in [3]. Figure 2-1 shows this platform that completely integrated on the same substrate without any mechanical assembly or tuning. The 50Ω transmission line is connected to integrated waveguide by tapered section. Mode matching is done by tapered section. It transforms the quasi-TEM mode of the microstrip line into the TE_{10} mode in the waveguide. Design of this circuit is straightforward. By considering the dielectric properties 50Ω microstrip line is designed, then waveguide dimensions are determined by waveguide theory. Finally length "l" and width "d" of transition part should be determined.

Modelling and optimization in software over the desired frequency bandwidth is the most commonly used method, but this is typically very time consuming due to lots of metallized cylindrical via holes. Indeed, if analytical equation has been used, the design process would be speed up.

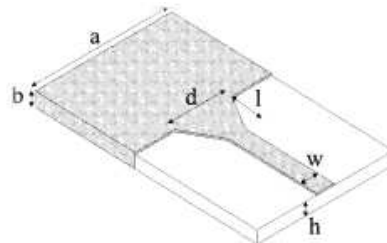


Figure 2.1: Configuration of proposed transition of microstrip line to rectangular waveguide on the same substrate[3]

Electric field distribution in microstrip line and rectangular waveguide is shown in Figure 2-2. The electric fields of two structures are approximately oriented in the same direction so the microstrip line is suitable to excite the integrated waveguide. The most important difference between RW and SIW is the dimension "b". The height or thickness "b" is reduced in SIW. But it does not influence the TE_{10} mode propagation because propagation constant of TE_{10} mode is only related to width "a". The design equation for microstrip-to-SIW transition has been

reported in [10]. According to Figure 2-3 the microstrip has been modeled by an equivalent TEM waveguide.

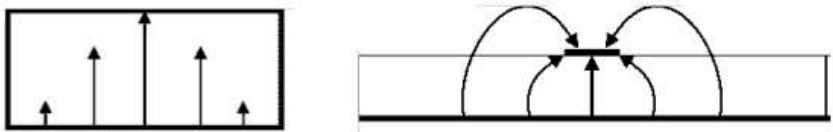


Figure 2.2: Electric field distributions (a) in rectangular waveguide (b) in microstrip line [3]

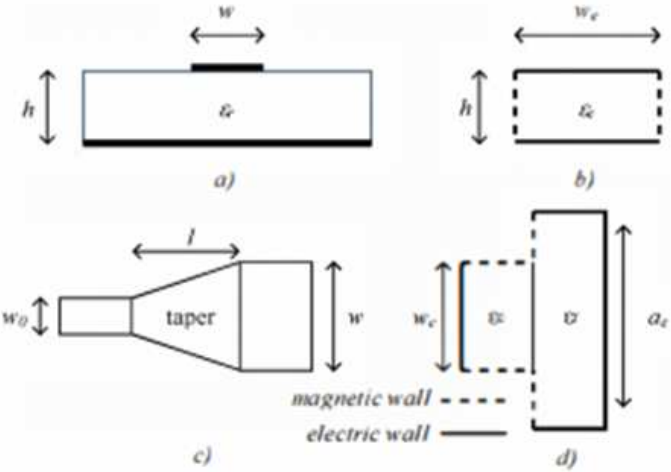


Figure 2.3: Equivalent topology for microstrip-to-SIW transition a) microstrip Line b) waveguide model of microstrip line c) top view of a microstrip taper d) microstrip-to-SIW step [10]

The width of the TEM waveguide, w_e is calculated to obtain the same impedance as in the microstrip line. The capacitance effects at the end of the SIW in the transition plane are not taken into account, because magnetic walls are used to close the SIW. Taper length must be chosen as a multiple of a quarter of a wavelength in order to minimize the return loss.

2.3 CPW-to-Substrate Integrated Waveguide Transitions

In the millimeter-wave frequency range the coplanar waveguide (CPW) is a very promising transmission line. In the platform shown in Fig.2-4 a coplanar waveguide (CPW) and a SIW

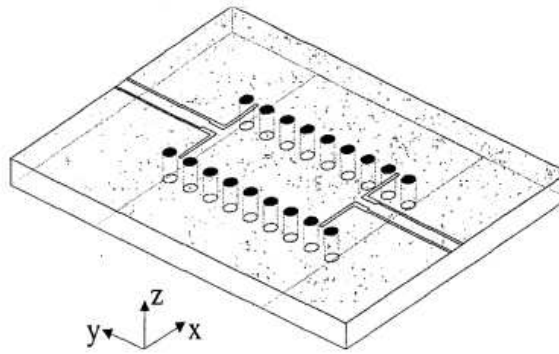


Figure 2.4: Schematic view of the proposed transition of coplanar waveguide and rectangular waveguide [14]

are fully integrated on the same substrate and they are interconnected via simple transition [14]-[16]. Increasing dielectric substrate height in order to decreasing the conductor loss, may not affect too much inherent CPW characteristics. So the substrate thickness can be increased to reduce conductor loss in the waveguide design without having adverse impact on planar components. Another proposed CPW-to-SIW transition which is using three metal layers is shown in Figure 2-5[15].

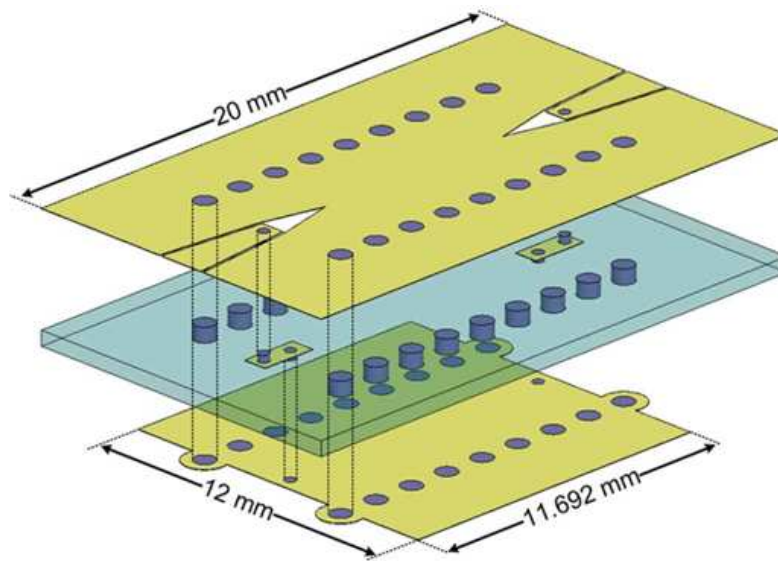


Figure 2.5: Configuration of the CPW-to-SIW transition [15]

An elevated-CPW (ECPW) intermediate section is inserted between a CPW and a SIW for gradual modification of the transmission mode as shown in Figure 2-6. The ECPW section

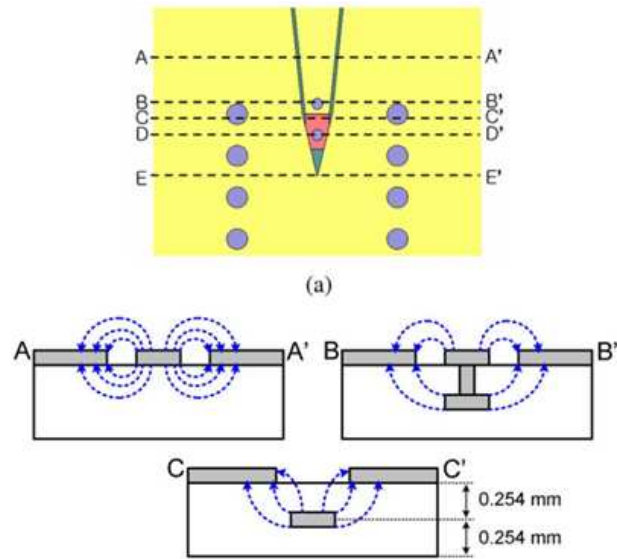


Figure 2.6: Structure of the CPW-to-SIW transition (a) Top view (b) cross section showing the E-field gradation [15]

(C-C') plays a role of the intermediary field matching between the horizontal CPW E-field (A-A') and the vertical SIW E-field (E-E') as a ridged waveguide.

2.4 Rectangular Waveguide Equivalent and Some Consideration on Design of Substrate Integrated Waveguide

The equivalence on propagation and cut-off frequency between SIW and RW has been investigated [17]. SIW can be modelled as a Rectangular waveguide (RW) as shown in Figure 2-7. Generally, a rectangular waveguide has horizontal length of “a” and vertical length of

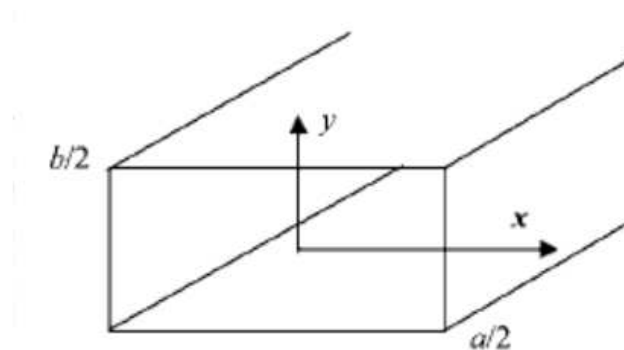


Figure 2.7: Schematic structure of a conventional rectangular waveguide [17]

“b” and its cut-off frequency is determined by t , a and b . Because length of vertical wall of SIW becomes height of substrate, “h” and horizontal length a is much longer than height of substrate ($a \gg b = h$) the cutoff frequency of the SIW is given by:

$$f_{cmn} = \frac{k_c}{2\pi} = \frac{1}{2\pi\sqrt{\mu\epsilon}} \sqrt{\left(\frac{m\pi}{a}\right)^2 + \left(\frac{n\pi}{b}\right)^2} \Rightarrow f_{10} = \frac{1}{2a\sqrt{\mu\epsilon}} \quad (2.1)$$

a' is the width of the SIW, W is the distance between two adjacent cylinders, R is the radius of the cylinder and a_e is the width of the equivalent RW. Rectangular waveguide width a can be written in term of a' [18]-[19]:

$$a' = \frac{2a}{\pi} \cot^{-1}\left(\frac{\pi W}{4a_e} \ln \frac{W}{4R}\right) \quad (2.2)$$

There is an empirical formula for equivalent width of SIW in [2].

$$W_{eff} = W - \frac{D^2}{0.95b} \quad (2.3)$$

where W_{eff} is equivalent width, W is the SIW width and D is via diameter and b is distance between adjacent vias. A schematic view of the SIW is shown in Figure 2-8 [20].

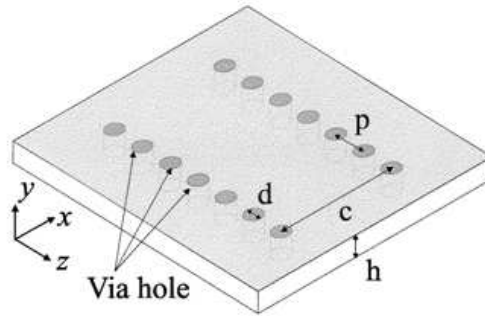


Figure 2.8: Configuration of the substrate integrated waveguide synthesized using metallized via-hole arrays [20]

The distance between two arrays (c) determines the propagation constant of the fundamental mode, and the via holes parameters (d and p) are set to minimize the radiation loss as well as the return loss. In order to insure that the synthesized waveguide section become radiation less or free of leakage loss, parametric effect of p and d have been studied [20]. These studies show that the pitch must be kept small to reduce the loss between adjacent points. The loss tends to decrease as the post gets smaller for a constant ratio d/p , which is conditioned by fabrication process. To obtain good results the ration $\frac{d}{p} \geq 0.5$ and $\frac{d}{c} < 0.4$ must be chosen.

2.5 Substrate Integrated Waveguide Based Components

Design and production costs of millimeter-wave systems are probably the most critical issue in the assessment of their commercial vitality. The potentials of the SIW for production of low cost, low loss and mass production passive component have been developed. With the emerging development of the SIW-based component and circuits, the design of an entire communication system based on these new interconnect system is possible. At the following a few critical components such as SIW-based filter coupler and antennas will be studied.

Rapid development of communication systems in the microwave and millimeter wave band need filters with low insertion loss, compact size, good selectivity, high quality and easy fabrication process for mass production. Available filters at microwave and millimeter wave bands [21]-[27] have a large size and are very hard to integrate with planar structure. SIW filters [28]-[34] can be easily integrated with planar structures and are very good candidate for mass production. The design and performance of millimeter wave Butterworth and Chebyshev filter with SIW has been reported [28]. First of all the filter specification are established, f_1 and f_2 defining the bandwidth. This filter is centered at f_0 with the frequency fractional bandwidth equal to:

$$\omega = \frac{f_2 - f_1}{f_0} \quad (2.4)$$

The guide wavelength is then computed for the center and band edge frequencies ($\lambda_{g0}; \lambda_{g1}; \lambda_{g2}$). The guide wavelength fractional bandwidth is defined as:

$$\omega_\lambda = \frac{\lambda_{g1} - \lambda_{g2}}{\lambda_{g0}} \quad (2.5)$$

and normalized prototype frequency at f_a is computed with:

$$\frac{\omega'}{\omega_1} = \frac{2}{\omega_\lambda} \left(\frac{\lambda_{g0} - \lambda_{ga}}{\lambda_{g0}} \right) \quad (2.6)$$

The specification for the out of band rejection at f_a gives the minimum order need for the filter. Inductive post equivalent circuit which is used to SIW fabrication is shown in Figure 2-9.

Using the moment method S-matrix of the structure can be calculated. From the S-parameters the equivalent circuit can be computed. Then impedance invertors have been computed from the circuit element. An iterative method is implemented to find the required post diameter knowing the desired invertors. In this way the design procedure of SIW filter has been completed. The manufacture filter with its simulation and measurement results are shown in

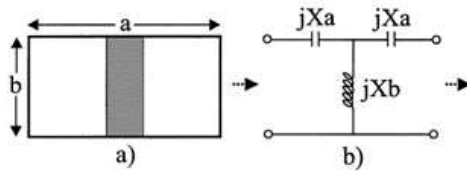


Figure 2.9: (a)Post in waveguide (b) Equivalent PI network [28]

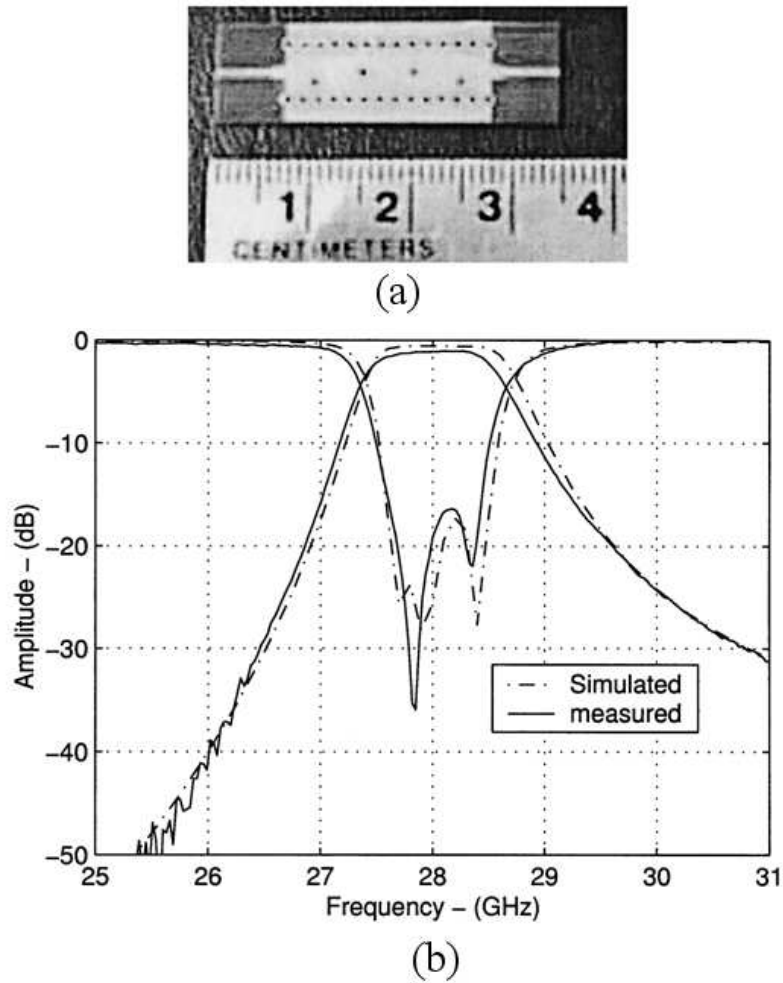


Figure 2.10: (a)Photograph of the manufactured three-pole filter (b) Measured and simulated results for the three-pole Chebyshev filter [19]

Figure 2-10[19]. Simulation and measurement results show the response of the Chebyshev filter at 28GHz. 1 GHz bandwidth has been achieved. This filter has been designed and fabricated without need for tuning.

Dual mode filter are widely used to improve the out of band rejection. However in typical design tuning screw or small metallic piece have been used for the mode conversion in the

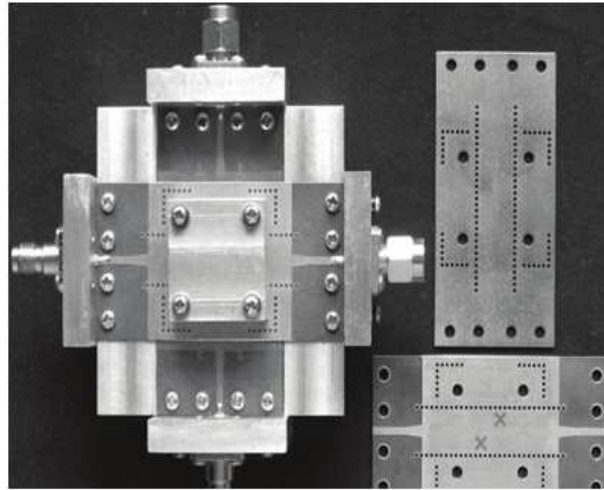
cavity. This method is not suitable for SIW. So by using the method in [33] the SIW dual mode filter has been realized [28].

A directional network is a four-port network in which portion of the forward and reverse traveling wave on a line are separately coupled to two of the ports. As a result, it finds extensive use in system that requires the measurement of amplitude and phase for travelling wave. In its most common form the directional coupler consist of two transmission lines and a mechanism for coupling signals between them. Many type of directional coupler have been developed over the years and have been classified as either discrete-type or distribute-type couplers [35]-[36]. Several SIW couplers have successfully been designed and have been demonstrated theoretically and experimentally [37]-[43].

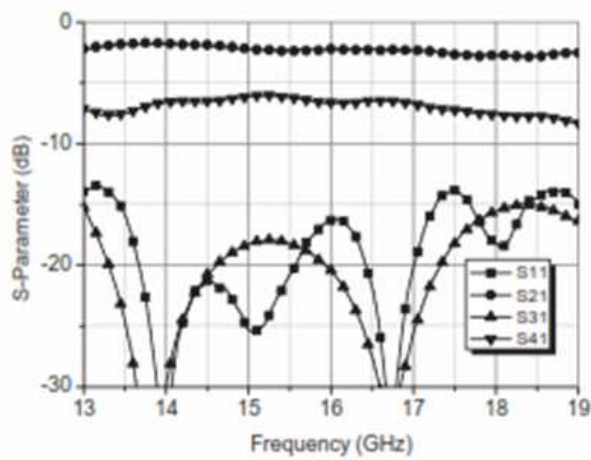
A double layer wide band compact size directional coupler with two SIWs crossed over each other has been shown in Figure 2-11[37]. The coupling is realized by the cross slots between upper layer SIW and lower layer SIW.

According to measured data in Figure 2-11(b) large range of coupling coefficient and wide band characteristic has been achieved. A half mode SIW (HFSIW) 3dB coupler has been reported in [40] as shown in Figure 2-12(a). It keeps the good performance of SIW coupler with nearly a half reduction in size. Simulation and measurement results are in a good agreement which is shown in Figure 2-12(b). The E-field is of the maximum value at the vertical center plane along the propagation direction in SIW when it works only in the dominate mode. So the center plane can be considered as an equivalent magnetic wall. Based on this idea the SIW can be bisect with the fictitious magnetic wall and each half of the SIW becomes a HMSIW structure and the new structure can almost keep the original field distribution in its own part because of its large width-to-height ratio and be considered to support the guided wave modes in the half open structure.

Slot array antennas with different feed network have been studied and developed. Rectangular waveguide feeding network for slot array antenna is a most common one. A design procedure that accounts for external coupling between slots in the array fed by dielectric filled waveguide was reported by Elliot [44]. The conventional rectangular waveguide-fed slot array antennas present the advantages of low loss and high power handling capacity. Nevertheless, their incompatibility with integrated planar components creates a hurdle for their external application in microwave and millimeter wave integrated circuits. To overcome this drawback SIW based antennas with integration capacity has been investigated [45]-[55]. The half mode SIW transverse slot array antennas have been reported [50]. It not only maintains the advantages



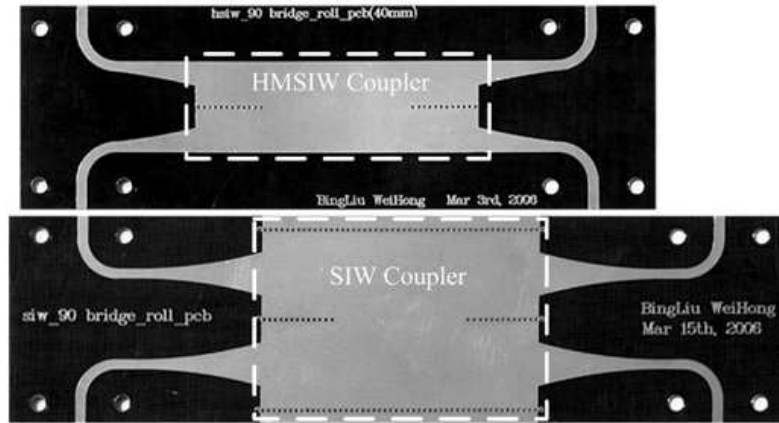
(a)



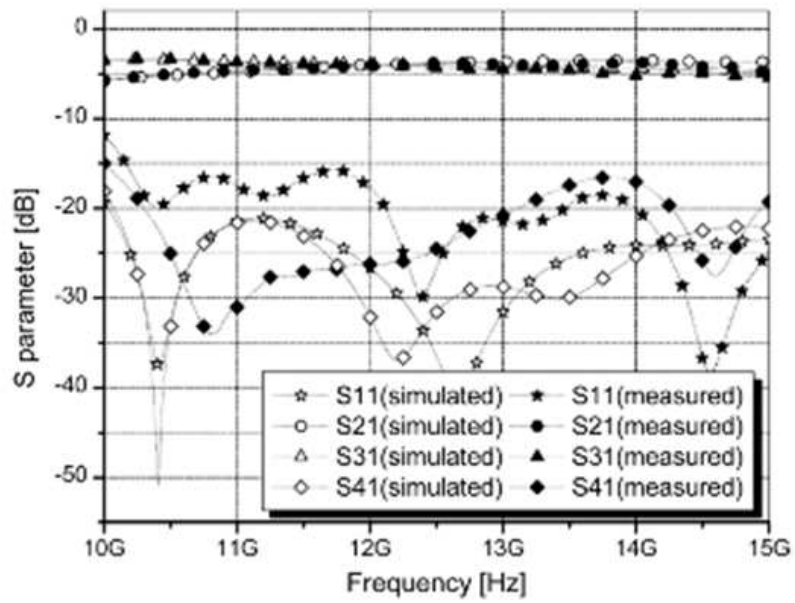
(b)

Figure 2.11: (a) Photo of the assembled directional coupler and the two separate single layer PCB (b) Measured S-parameters of the directional coupler at the maximum coupling factor [37]

characteristics of slot array antenna fed by the SIW, but also it is more compact, as its size is reduced by nearly half. A sketch of an HMSIW-fed transverse slot array antenna is shown in Figure 2-13 and its properties are shown in Figures 2-14 and 2-15 respectively.

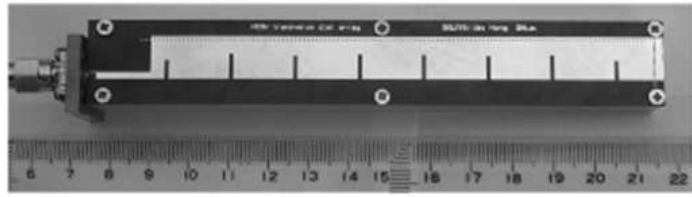


(a)

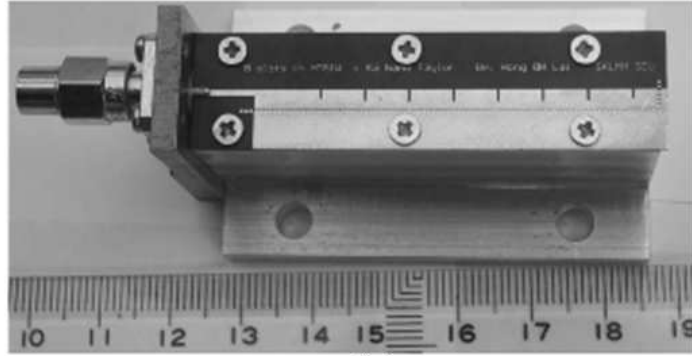


(b)

Figure 2.12: (a) HMSIW and SIW couplers (b) Measured and simulated S parameters of the proposed HMSIW 3-dB coupler. [40]



(a)



(b)

Figure 2.13: Photographs of the HMSIW-fed transverse resonant slot array antennas (a) X-band and (b) Ka-band [50]

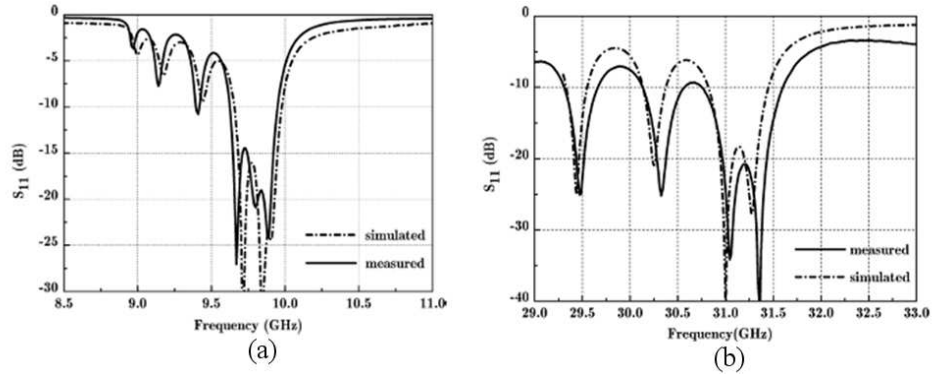


Figure 2.14: Return loss of the HMSIW transverse slot array antenna over X-band.(a) X band (b)Ka-band [50]

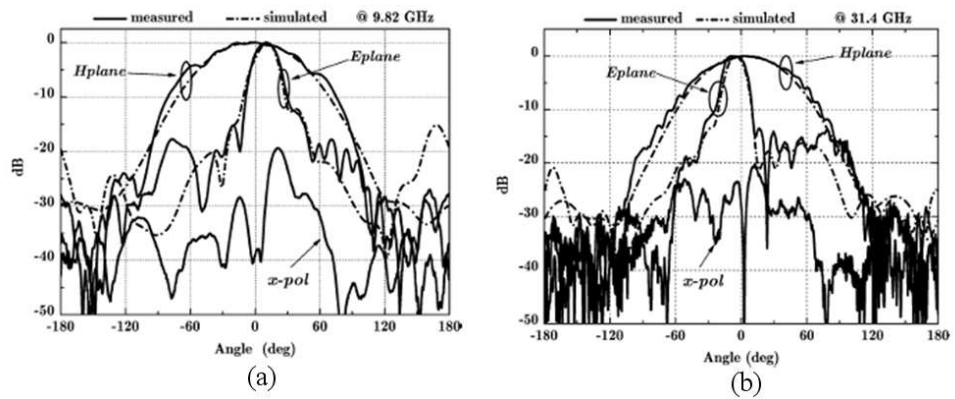


Figure 2.15: Radiation patterns of the HMSIW transverse slot array antenna (a) 9.82GHz (b) 31.4GHz [50]

CHAPTER 3

SUBSTRATE INTEGRATED WAVEGUIDE POWER DIVIDER

3.1 Introduction

Power dividers are used to divide the input power into a number of smaller amounts of power for exciting the radiating elements in an array antenna. They are also used in balanced amplifiers both as power divider and power combiner [35]. A fundamental property of a lossless reciprocal three-port junction is that not all three ports can be simultaneously matched. If we assume that all three ports can be matched, then $S_{11} = S_{22} = S_{33} = 0$ and the scattering matrix has the form:

$$[S] = \begin{pmatrix} 0 & S_{12} & S_{13} \\ S_{21} & 0 & S_{23} \\ S_{13} & S_{23} & 0 \end{pmatrix} \quad (3.1)$$

If we want to use a lossless three-port junction to split or divide input power P_1 into fraction $\alpha P_1 = P_2$ and $(1 - \alpha)P_1 = P_3$ at port 2 and port 3 this is readily accomplished [35]. For a three-port junction shown in Figure 3.1, Z_2 and Z_3 can be chosen so that the input port 1 is matched and the desired power split is obtained.

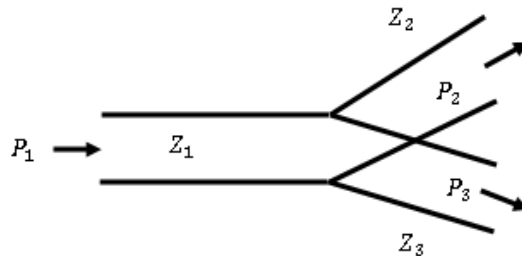


Figure 3.1: A lossless three port junction used as power divider

If the input is matched, then the input power is $P_1 = \frac{1}{2}Y_1|V_1^+|^2$. Since $V_2^- = V_3^- = V_1^+$ because of the parallel connection of all three lines, the power relation can be written as:

$$P_1 = \frac{1}{2}Y_1|V_1^+|^2 + \frac{1}{2}Y_3|V_1^+|^2 \quad (3.2)$$

For an impedance match it requires $Y_1 = Y_2 + Y_3$ and in order to obtain the desired power division, it requires that:

$$\frac{Y_2}{Y_3} = \frac{\alpha}{1 - \alpha}$$

This type of lossless power divider will not have matched output ports and since S_{23} will not be zero it also does not have isolation between the output ports. If there is a shunt susceptance at the junction, such as would occur from excitation of evanescent mode in a waveguide T or Y junction, the input port can still be matched by placing a suitable shunt-compensating susceptance at the appropriate position in the input line. Wilkinson power divider is illustrated in Figure 3-2. It consists of two quarter wave sections with characteristic impedance Z_2 and Z_3 connected in parallel with the input line, which has the characteristic impedance Z_c .

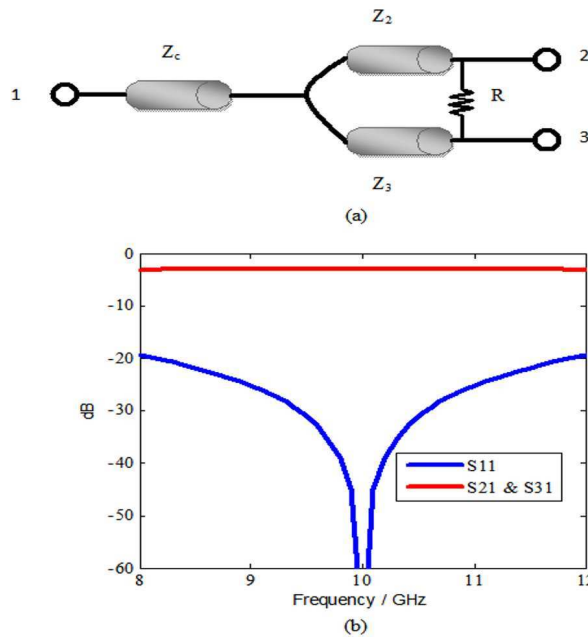


Figure 3.2: (a) The Wilkinson power divider (b) Simulation results

A resistor R is connected between port 2 and port 3. Wilkinson developed an N -way power divider that would split the input power into output power at N ports and that would also provide the isolation between the output ports. A unique feature of the Wilkinson power

divider is the use of resistor connected between the various output ports. When the output ports are terminated in the correct load impedance, there is no current in the resistor; so they do not absorb any power. If one port is matched, then the reflected power from that port is partly absorbed by the resistor network and partly returned to the input, but no power is coupled into the other ports as long as they remain properly terminated. The above theory about power divider has been developed by using the advantages of the SIW technology. At the following section power division will be carried out by using two SIW parts which are attached together. The electromagnetic wave has been propagated from lower layer to upper layer via an aperture.

3.2 SIW Power Divider

Power dividers are widely used in microwave and millimeter wave circuits. Array antenna feeding network is an example which need desired power division ratio at a specified bandwidth. SIW is a dielectric filled waveguide structure that has the similar propagation modes as rectangular waveguide, but manufacturing of such a waveguide structure requires only a normal Print Circuit Board (PCB) process and results in the merit of low cost and mass production ability. The main structure of proposed SIW power divider is shown in Figure 3-3. It includes two PCB layers with the same electrical properties. The electromagnetic wave is coupling from bottom layer to upper through a slot.

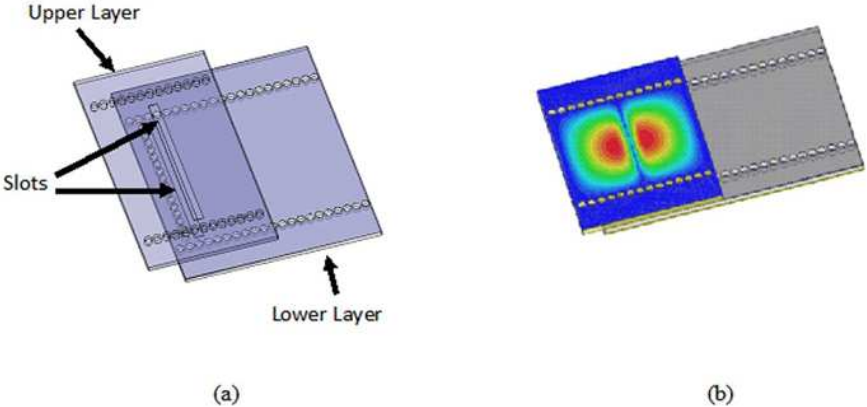


Figure 3.3: The main structure of multi-layer SIW (a) The first and the second layers with slots (b) The coupled E-fields

The above proposed structure need to transition parts to connect to microstrip lines. RO4003

with dielectric constant $\epsilon_r = 3.38$, $\tan(\delta) = 0.0027$ and $h=0.51$ mm has been used to design of the SIW power divider. The distance between vias, and via diameters are $p=0.8$ mm, $d=1$ mm respectively.

3.3 E-Plane Power Divider

The three-port waveguide configuration in Figure 3-4 is known as E-plane or series tee[56]. Port 1 is usually designated as E-arm and port 2 and port 3 as coupler arms. The width of the all three guide is the same, which is the most common arrangement. Associated with the propagating waves are conduction currents in the inner walls of the waveguides. The longitudinal or power currents that follow along the broad walls are also indicated. Since the common current flows in the three guides, the E-plane tee may be represented by three series connection of transmission lines.

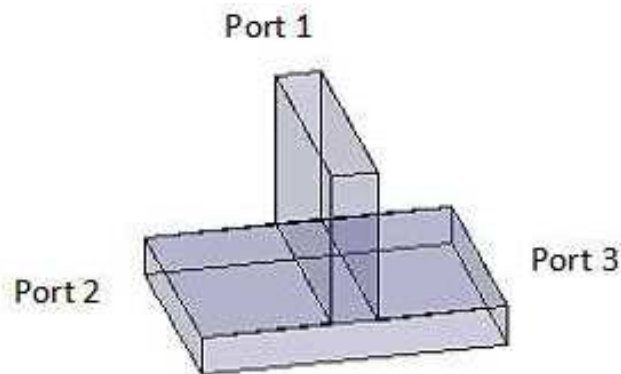


Figure 3.4: The E-plane waveguide or tee junction

The equivalent circuit for E-plane waveguide is shown in Figure 3-5 *a, b, c*. The reactive effects associated with the localized higher-order mode may be accounted for by either of equivalent circuits in Figure 3-5. Susceptance values as well as values for n, d and d' are given in [56]. The circuit in part b of Figure 3-6 is particularly useful to determine the effect of mismatched terminations on the power divisions. The data in [56] indicates that for $b' \leq b$, X is quite small and may be neglected. Because of the impedance transforming properties of transmission lines, it is important that the terminal planes for the equivalent circuits be specified. The lines lengths in Figure 3-5 are necessary to make the terminal planes in both circuits the same. The planes are defined in Figure 3-5 c. The turn ratio n of the transformer

is frequency sensitive, it has been decreased when the frequency is increased.

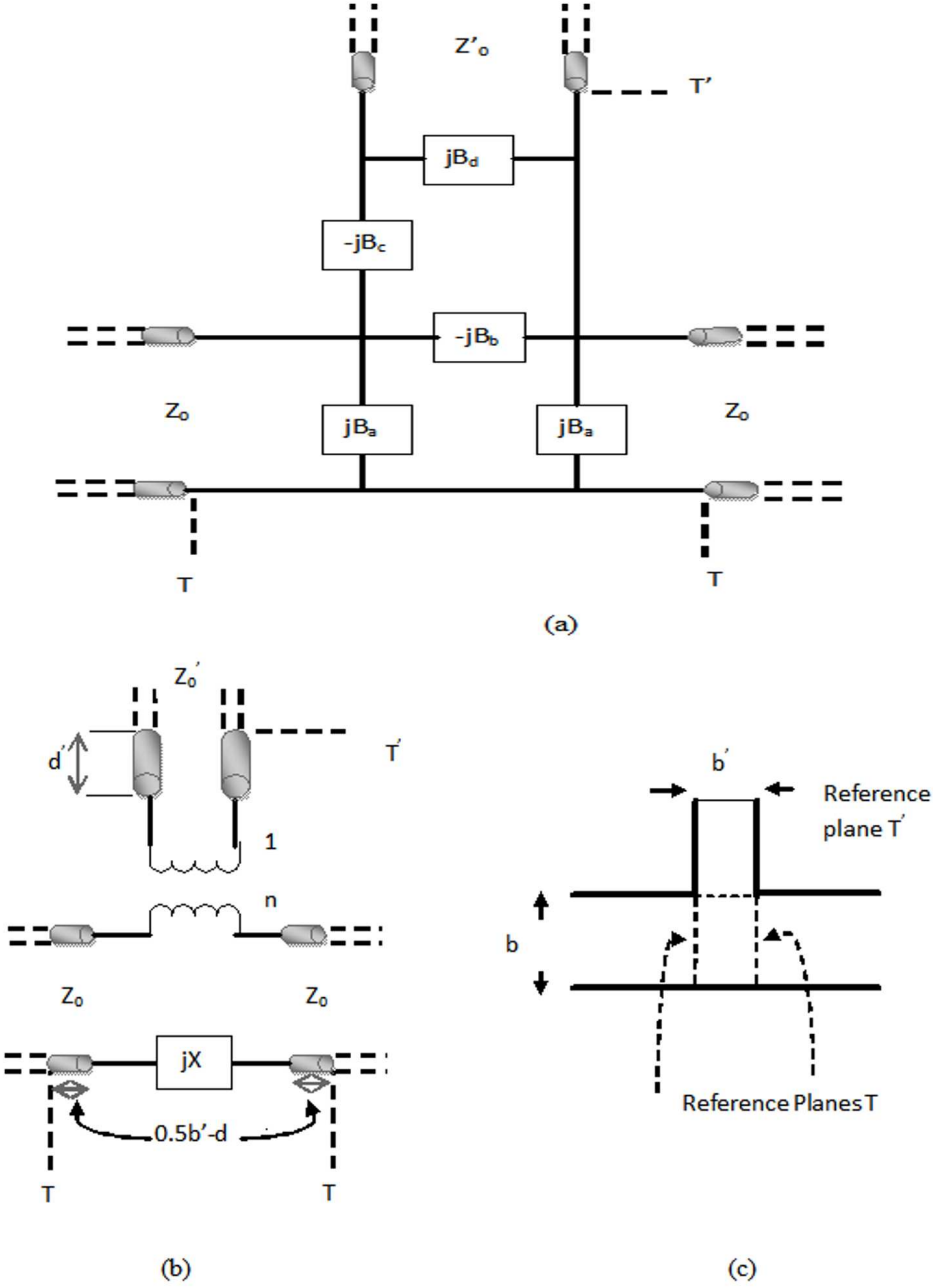


Figure 3.5: (a,b)Two equivalent circuits for the E-plane tee (c) Side view

Due to similarity of SIW power divider with E-plane power divider it is suitable to use E-Plane power divider design procedure for designing SIW power divider. For our case RO4003 substrate with $b = b' = 0.51mm$, as shown in Figure 3-6 has been used. By using the cut-off frequency formula and also operation frequency equal to 10 GHz, $a=11$ mm in Figure 3-6 is

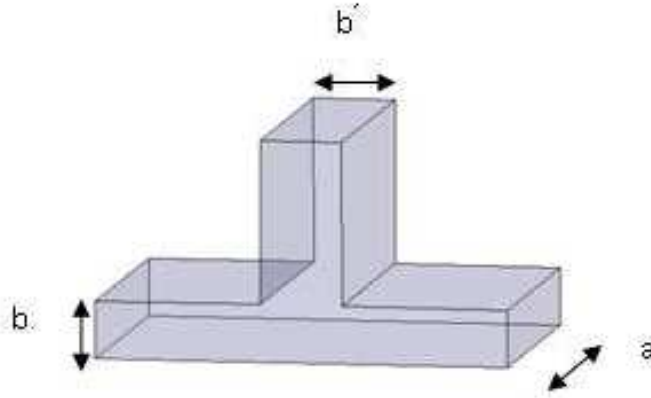


Figure 3.6: E-plane power divider

achieved. Other parameters (d, d' and n) can be calculated from plotted data in [56]. Characteristic impedance of waveguide is also considered from $Z_o = \frac{b}{a} \sqrt{\frac{\mu_r \lambda_g}{\epsilon_r \lambda}}$ [36]. However $a=11$ mm, $b = b' = 0.51$ mm, $Z_o = Z' = 17.46\Omega$, $n=0.98$, $d=0.035$ mm, $d' = 0.06$ mm are the parameters of SIW power divider. This procedure is easy to simulation in comparison with EM simulation. So it can be used for finding the initial value of the device parameters then it can be optimized by using EM simulator. By applying the procedure for design of E-Plane junction the SIW parameters in Figure 3-3 has been found. Transition parts length and widths have been calculated by using the method which has been explained in part 2-4. The complete SIW power divider with using HFSS software is shown in Figure 3-7. The equivalent circuit

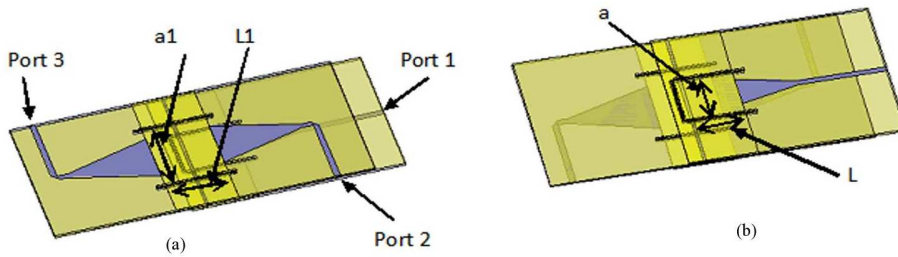


Figure 3.7: SIW power divider (a) top view (b) bottom view

for this structure in ADS software with mention of Figure 3-5b has been illustrated in Figure 3-8. Simulation results from these two SIW power divider is shown in Figure 3-9. This SIW power divider has been fabricated as shown in Figure 3-10. RO4003 with dielectric constant $\epsilon_r = 3.38$, $\tan(\delta) = 0.0027$ and $h = 0.51$ mm has been used for fabrication of the structure. Dimensions of this three-port SIW power divider are exhibited in Table I. Simulation

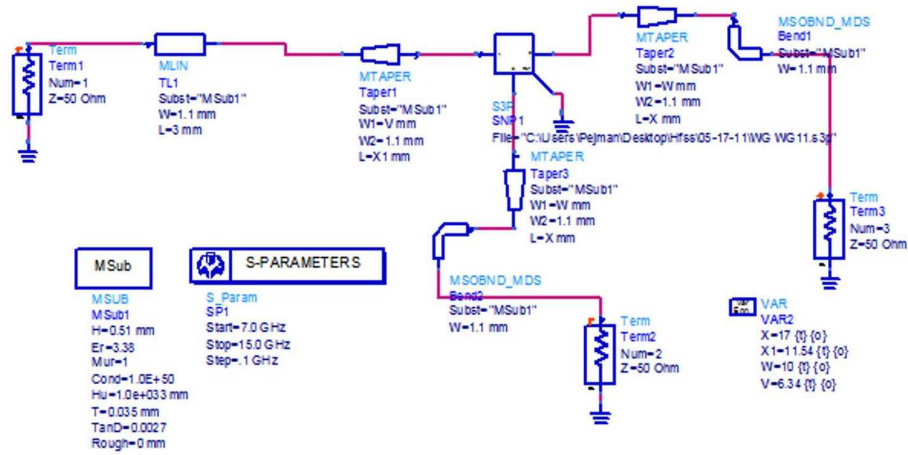


Figure 3.8: SIW power divider equivalent circuit

from HFSS and measurement results also is shown in Figure 3-11. There is good agreement between simulation and measurement results.

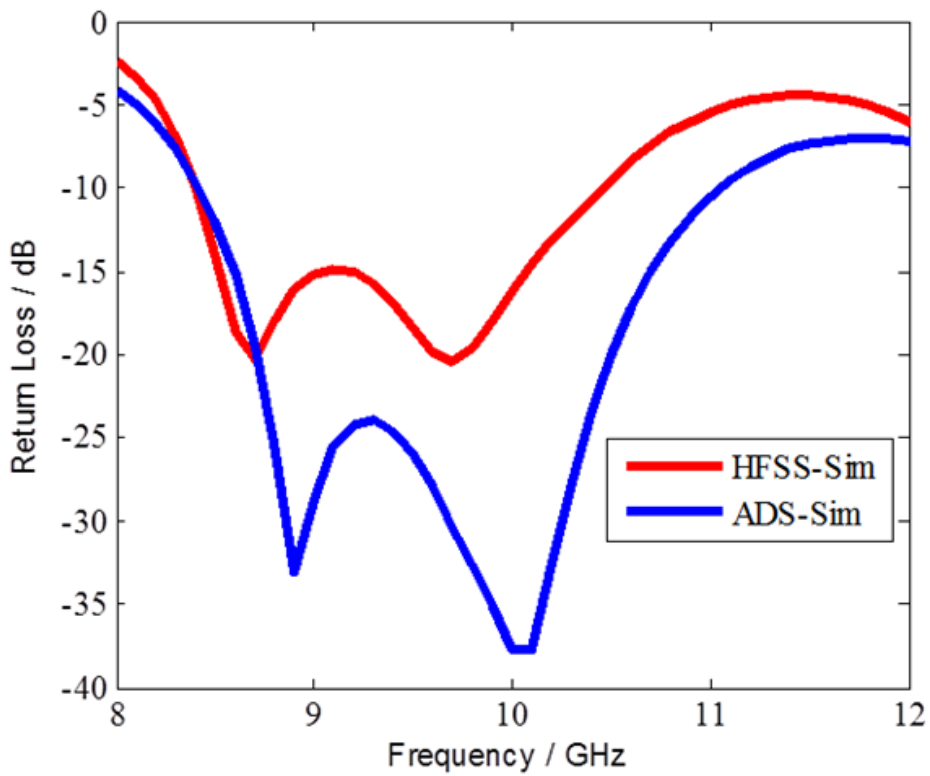


Figure 3.9: Return Loss of SIW power divider with HFSS and ADS software

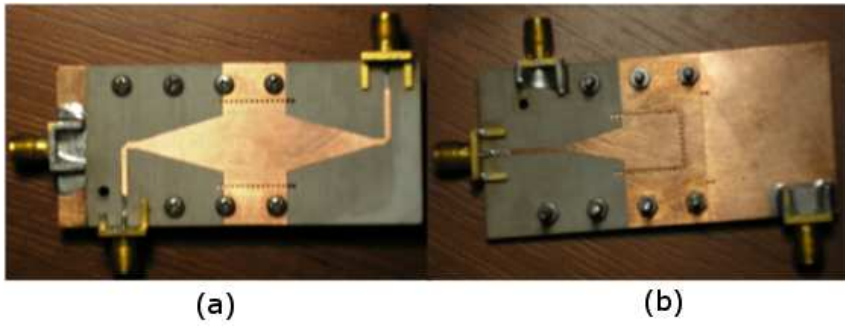


Figure 3.10: Picture of fabricated SIW power divider (a) Top view (b) Bottom view

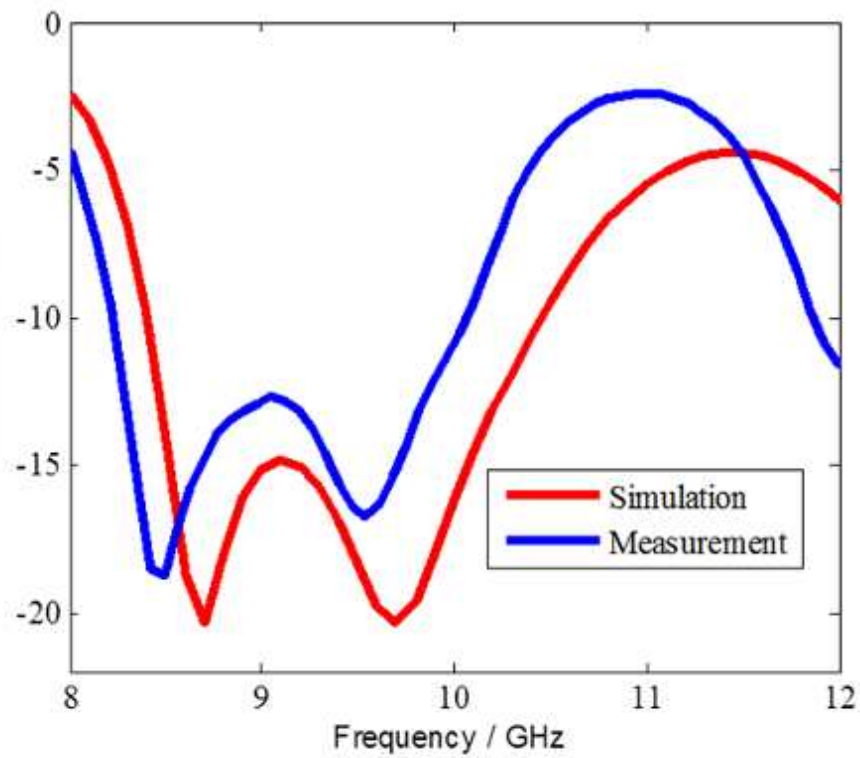


Figure 3.11: Simulation and measurement of three-port SIW power divider

Table 3.1: Three-port SIW power divider dimensions(mm).

	Length	Width
First Layer (L)	10	10.4
Second Layer (L1)	12.5	16
Slot	10.4	0.5
Transition Part on First Layer	11.84	6.3
Transition Part on Second Layer	17.7	11

The EM simulation result with HFSS software is more similar to measurement result. The EM simulation needs more time and memory, in comparison with ADS simulation. The suitable approach is that the structure firstly has been simulated with ADS software then by considering the results, EM simulation has been accomplished for optimization of the response. For SIW structure by increasing the dimension of the structure simulation time and required memory will be increased, specially it depends on the number of vias. The width and length of the transition parts are usually must be optimized. The via diameter and distance between them are conditioned by fabrication instrument. The metallization process must be done carefully. The amplitude of the current in metallization instrument and time schedule for each part must be selected properly according the metallization area. Any mistake changes the thickness of the PCB copper due to metallization and measurement then results will be changed.

CHAPTER 4

MEASUREMENT METHODS for SUBSTRATE INTEGRATED WAVEGUIDE POWER DIVIDER

4.1 Introduction

A network analyzer measures the S-parameters as ratio of complex voltage amplitudes. The primary reference plane for such a measurement is generally at some point within the analyzer itself. It is desired to measure the S-parameters in intended reference plane. Removing the loss effect and phase delay of connectors, cables and transition parts is also preferred. So we need the standards which must be characterized at the same media type as the device under test (DUT). During measurement calibration, a series of known devices (standards) are connected. The systematic effects are determined as the difference between the measured and known responses of the standards. Once characterized, these errors can be mathematically related by solving a signal flow graph. The process of mathematically removing these systematic effects is called "error-correction".

The Thru-Reflect-Line (TRL) is an approach to two-Port calibration that relies on transmission lines rather than a set of discrete impedance standards. There are some consideration points about the TRL standards. Thru must have the properties as follows:

- It can be either a zero length or non zero length, zero length is achievable by directly connecting the error box together and it is preferred.
- It cannot be at the same electrical length as the line.
- Characteristic impedance of thru and line standards define the reference impedance of the calibration.

Line must have the properties as follows:

- Its characteristic impedance and propagation constant must be as the true standards.
- If its electrical length is specified within $\frac{1}{4}$ wavelength, more accurate results will be achieved.
- It cannot be the same as true standards.
- The phase difference between thru and line must be greater than 20 degree and less than 160 degree. This means in practice that a single LINE standard is only usable over an 8:1 frequency range (Frequency Span / Start Frequency). Therefore, for broad frequency coverage, multiple lines are required.

Reflect must have the properties as follows:

- It can be anything with a high reflection.
- The short circuit is preferred to open circuit, for avoiding any radiation loss.

At the following section the block diagram of the TRL calibration in general form will be exhibited, and also suitable TRL standards for SIW structure will be shown.

4.2 TRL Calibration Procedure

TRL block diagram is shown in Figure 4.1. It includes two error boxes and DUT [57]. By using the TRL

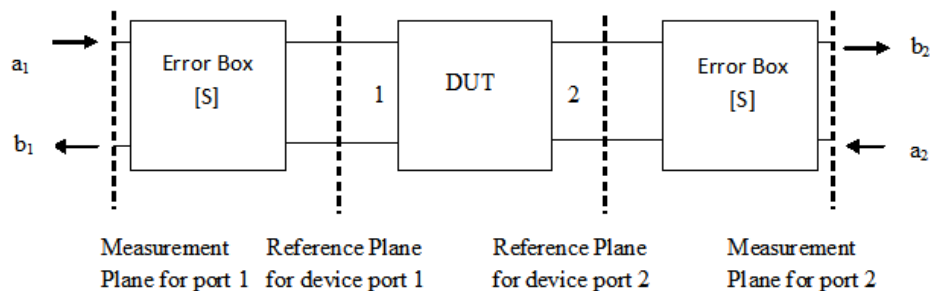


Figure 4.1: Block diagram of a network for TRL calibration

calibration procedure, firstly the error box has been characterized, and then the error corrected

S-parameters of the DUT can be calculated from measured data. To avoid confusion in notation the measured S-parameters for the Thru, Reflect, and Line connection, will denote as the [T], [R], and [L] matrices, respectively.

$$T = \begin{pmatrix} T_{11} & T_{12} \\ T_{21} & T_{22} \end{pmatrix} \quad R = \begin{pmatrix} R_{11} & R_{12} \\ R_{21} & R_{22} \end{pmatrix} \quad L = \begin{pmatrix} L_{11} & L_{12} \\ L_{21} & L_{22} \end{pmatrix}$$

Signal flow graph of the LINE is shown in Figure 4-2. Similar flow graphs has been used to True and Reflect. By considering Figure 4-1 and using the signal flow graph, S parameters for the three TRL components can be write as follows: [57]

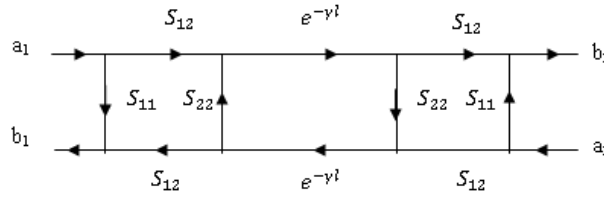


Figure 4.2: Signal flow graph of LINE

$$R_{11} = S_{11} + \frac{S_{12}^2 \Gamma_L}{1 - S_{22} \Gamma_L} \quad (4.1)$$

$$T_{11} = S_{11} + \frac{S_{22} S_{12}^2 e^{-2\gamma l}}{1 - S_{22}^2 e^{-2\gamma l}} \quad (4.2)$$

$$T_{12} = \frac{S_{12}^2 e^{-\gamma l}}{1 - S_{22}^2 e^{-2\gamma l}} \quad (4.3)$$

$$L_{11} = \frac{b_1}{a_1} = S_{11} + \frac{S_{22} S_{12}^2 e^{-2\gamma l}}{1 - S_{22}^2 e^{-2\gamma l}} \quad (4.4)$$

$$L_{12} = \frac{S_{12}^2 e^{-\gamma l}}{1 - S_{22}^2 e^{-2\gamma l}} \quad (4.5)$$

γ is the propagation constant and l and $l1$ is length of the Line and Thru respectively. There are five equations and five unknowns ($S_{11}, S_{12}, S_{22}, e^{(-\gamma l1)}, e^{(-\gamma l)}$).

$e^{(-\gamma l1)}$ can be eliminated from (4-2) and (4-3) and also $e^{(-\gamma l)}$ can be eliminated from (4-4) and (4-5). So there are two new equations with three unknowns (S_{11}, S_{12}, S_{22}). These two new equations with (4-1) could be used to find the S-parameters. The solution is straightforward but lengthy.

So $S = \begin{pmatrix} S_{11} & S_{12} \\ S_{21} & S_{22} \end{pmatrix}$ matrices are completely defined.

The TRL algorithm which is described above can be used to measure the SIW structure. For measuring S-parameters of main SIW structure the effects of transition part must be removed. So the appropriate TRL standards have been defined as shown in Figure 4-3. Coaxial connectors or probe pads and transition parts have been used to adopt the SIW structures to VNA for measuring. The side effect, like attenuation, phase delay and discontinuity not only change the measurement results, but also causes that the results become unsuitable to predicting how the design behaves when integrated with other components in final applications.

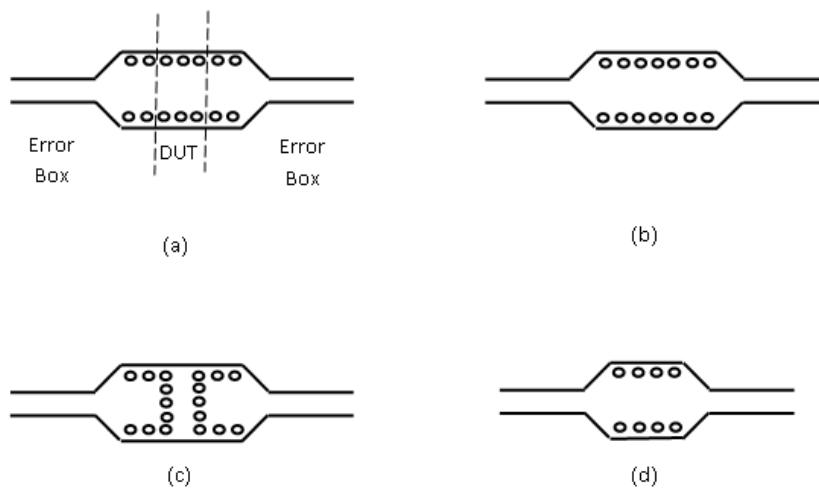


Figure 4.3: (a) TRL block diagram of SIW (b) Line (c) Short (d) Thru

The TRL standards have been used to calibration of vector network (VNA). Then the S-parameters of the main SIW can be reconstructed. But if the number of ports is more than 2, the effect of other ports must be considered. However the algorithm for reconstruction the S-parameter of n-port device from measured data with two-port VNA must be established. Firstly for the three-port device some algorithm will be introduced then a novel algorithm for n-port will be developed.

4.3 TRL Measurement of Three-Port device with Two-Port Network Analyzer

Measuring the S-parameters of a DUT with respect to 50Ω requires, by definition, that all ports of the DUT are terminated with a 50Ω load. With a two-port VNA only two ports of

a DUT can be terminated with the internal 50Ω loads of the VNA. This means that if the DUT has more than two-ports, all remaining ports must be terminated with an external 50Ω load. Depending on the type of the port of the DUT, different load must be used. This remark makes the procedure for reconstruction the S-parameters of DUT from measured data. For example experimental characterization of three-port devices, such as coupler, power divider, T-junction and etc. require de-embedding of the actual device from the transition used to connectorize it. This is the case that device ports cannot be directly accessed or connected to network analyzer [58].

4.3.1 First Method:

A three-port device is shown in Figure 4-4. TRL measurement has been done by connecting port 2 and port 3 to VNA. The error boxes effect has been removed from these ports, but from port 1 reflection coefficient Γ has been seen. So we need a method to construct the S-parameters of DUT. In this method the S-parameters of three-port device has been converted to two-port device. It is done as following.

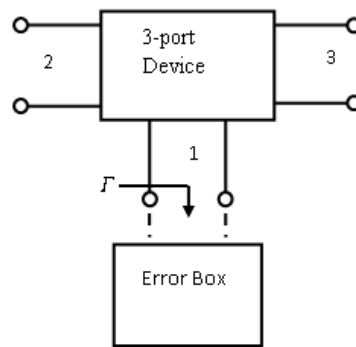


Figure 4.4: A three-port device

For the structure in Figure 4-4 S-parameters of DUT is defined as:

$$\bar{S} = \begin{pmatrix} S_{11} & S_{12} & S_{13} \\ S_{21} & S_{22} & S_{23} \\ S_{31} & S_{32} & S_{33} \end{pmatrix}$$

$$\bar{S}^m = \bar{S}_{ee} + \bar{S}_{ei}(\bar{C} - \bar{S}_{ii}) \quad (4.6)$$

\bar{S}^m : Measured S-parameters

\bar{S}_{ee} : S-parameters of external ports

\bar{S}_{ii} : S-parameters of internal ports

\bar{S}_{ei} : S-parameters of internal and external ports

\bar{C} : Connectivity matrix

The (4.6) can be applied for a three-port device by considering the port 2 and 3 as external port and port 1 as internal port.

a) Measurement from port 2 and 3:

$$\begin{pmatrix} S^{m23} & S^{m23} \\ S^{m23} & S^{m23} \end{pmatrix} = \begin{pmatrix} S_{22} & S_{23} \\ S_{32} & S_{33} \end{pmatrix} + \begin{pmatrix} S_{21} & 0 \\ S_{31} & 0 \end{pmatrix} \left(\begin{pmatrix} 0 & 1 \\ 0 & 1 \end{pmatrix} - \begin{pmatrix} S_{11} & 0 \\ 0 & \Gamma \end{pmatrix} \right)^{-1} \begin{pmatrix} S_{12} & S_{13} \\ 0 & 0 \end{pmatrix}$$

b) Measurement from port 1 and 2 :

$$\begin{pmatrix} S^{m12} & S^{m12} \\ S^{m12} & S^{m12} \end{pmatrix} = \begin{pmatrix} S_{11} & S_{12} \\ S_{21} & S_{22} \end{pmatrix} + \begin{pmatrix} S_{13} & 0 \\ S_{23} & 0 \end{pmatrix} \left(\begin{pmatrix} 0 & 1 \\ 0 & 1 \end{pmatrix} - \begin{pmatrix} S_{33} & 0 \\ 0 & \Gamma \end{pmatrix} \right)^{-1} \begin{pmatrix} S_{31} & S_{32} \\ 0 & 0 \end{pmatrix}$$

In the above matrix Γ is the reflection coefficient and S^{mij} is the measured S-parameter from port i and j.

The Symmetry conditions are given below:

$$S_{22} = S_{33} \quad S_{23} = S_{32} \quad S_{21} = S_{12} = S_{13} = S_{31} \quad (4.7)$$

From the measured data in matrix a and b unknown S-parameters after some algebra can be found as follows:

$$S_{22} = \frac{\Gamma(S_{23}^{m23} - S_{22}^{m23})^2 - S_{22}^{m12}}{\Gamma(S_{22}^{m12} + 2S_{22}^{m23} - 2S_{23}^{m12} - 1)} \quad (4.8)$$

$$S_{23} = S_{22} - S_{22}^{m23} + S_{23}^{m23} \quad (4.9)$$

$$S_{21} = \frac{S_{12}^{m23}(1 - \Gamma S_{22})}{1 + \Gamma(S_{23} - S_{22})} \quad (4.10)$$

$$S_{11} = S_{11}^{m23} - \frac{\Gamma S_{21}^2}{1 - \Gamma S_{22}} \quad (4.11)$$

$$S_{33} = S_{33}^{m23} - \frac{\Gamma S_{21}^2}{1 - \Gamma S_{11}} \quad (4.12)$$

So the unknown S-parameters of DUT are found. This method is simple and straightforward.

4.3.2 Second Method:

The goal of this method is obtain S-parameters S_N with respect to 50Ω of an N-port device [59]. This technique is fully general and can be applied for arbitrary terminations. Assume the port i and j of structure connected to VNA, and all other ports are connected with a load with known reflection coefficient Γ_k ($k = 1, 2, \dots, N, k \neq i, j$; Γ_i and Γ_j) are the reflection coefficients of the load that will be used to terminate ports i and j if they are not connected with the VNA. The S-matrix of the N-port DUT according the definition in [23] can be writing as:

$$\begin{pmatrix} b_I \\ b_J \end{pmatrix} = \begin{pmatrix} S_{II} & S_{IJ} \\ S_{JI} & S_{JJ} \end{pmatrix} \begin{pmatrix} a_I \\ a_J \end{pmatrix} \quad (4.13)$$

With:

$$X_I = (X_j \ X_i)^T \quad X_I = (X_1 \dots \ X_{i-1} \ X_{i+1} \ \dots \ X_{j-1} \ X_{j+1} \ \dots \ X_N)^T \quad (4.14)$$

The relationship between the measured S-parameters and S-parameters of DUT can be derived as follows:

$$S^{m(i,j)} = S_{II} + S_{IJ} \cdot (\Gamma_{JJ}^{-1} - S_{JJ})^{-1} \cdot S_{JI} \quad (4.15)$$

The measure S-parameters are the complex non linear function of the S-parameter of the N-port DUT. By definition of Σ_{II} as:

$$\Sigma_{II} = (\Gamma_{II}^{-1} - S^{m(i,j)})^{-1} \quad (4.16)$$

it can be prove that:

$$\Sigma_{II} = ((\Gamma^{-1} - S^N)^{-1})_{II} \quad (4.17)$$

With the knowledge of the measured S-parameters $S^{m(i,j)}$ and the reflection coefficient Γ_i and Γ_j the II block matrix of the Σ matrix has been found.

$$\Sigma = (\sigma_{i,j}) = (\Gamma^{-1} - S^N)^{-1} \quad (4.18)$$

In other words, the elements $\sigma_{ii}, \sigma_{ij}, \sigma_{ji}, \sigma_{jj}$ have been found. By repeating the S-parameter measurement for all possible 2-port combination $(i, j)(i = 2, \dots, N; j = 1, \dots, i)$ the complete Σ matrix will be found. Once The S-matrix is completely determined (2-18) can be used to determine S^N .

$$S_N = \Gamma^{-1} - \Sigma^{-1} \quad (4.19)$$

This method has been applied for three-port DUT at the subsequent. Again by considering the Figure 4-4 three different measurement set i.e. measurement from port (1, 2), (1, 3) and (2, 3) have been applied. The result at the matrix form can be written as follows:

$$S_N = \Gamma^{-1} - \Sigma^{-1} =$$

$$\begin{pmatrix} \Gamma^{-1} & 0 & 0 \\ 0 & \Gamma^{-1} & 0 \\ 0 & \Gamma^{-1} & 0 \end{pmatrix} - \begin{pmatrix} \sigma_{11} & \sigma_{12} & \sigma_{13} \\ \sigma_{21} & \sigma_{22} & \sigma_{23} \\ \sigma_{31} & \sigma_{32} & \sigma_{33} \end{pmatrix}^{-1} \quad (4.20)$$

$$\Sigma_{12} = \left(\begin{pmatrix} \Gamma^{-1} & 0 \\ 0 & \Gamma^{-1} \end{pmatrix} - \begin{pmatrix} S_{11}^{m12} & S_{12}^{m12} \\ S_{21}^{m12} & S_{22}^{m12} \end{pmatrix} \right)^{-1} \begin{pmatrix} \sigma_{11} & \sigma_{12} \\ \sigma_{21} & \sigma_{22} \end{pmatrix} = \left(\begin{pmatrix} \Gamma^{-1} - S_{11}^{m12} & -S_{12}^{m12} \\ -S_{21}^{m12} & \Gamma^{-1} - S_{22}^{m12} \end{pmatrix} \right)^{-1}$$

$$\Sigma_{13} = \left(\begin{pmatrix} \Gamma^{-1} & 0 \\ 0 & \Gamma^{-1} \end{pmatrix} - \begin{pmatrix} S_{11}^{m13} & S_{12}^{m13} \\ S_{21}^{m13} & S_{22}^{m13} \end{pmatrix} \right)^{-1} \begin{pmatrix} \sigma_{11} & \sigma_{13} \\ \sigma_{31} & \sigma_{33} \end{pmatrix} = \left(\begin{pmatrix} \Gamma^{-1} - S_{11}^{m13} & -S_{12}^{m13} \\ -S_{21}^{m13} & \Gamma^{-1} - S_{22}^{m13} \end{pmatrix} \right)^{-1}$$

$$\Sigma_{23} = \left(\begin{pmatrix} \Gamma^{-1} & 0 \\ 0 & \Gamma^{-1} \end{pmatrix} - \begin{pmatrix} S_{22}^{m23} & S_{23}^{m23} \\ S_{32}^{m23} & S_{33}^{m23} \end{pmatrix} \right)^{-1} \begin{pmatrix} \sigma_{22} & \sigma_{23} \\ \sigma_{32} & \sigma_{33} \end{pmatrix} = \left(\begin{pmatrix} \Gamma^{-1} - S_{22}^{m23} & -S_{23}^{m23} \\ -S_{32}^{m23} & \Gamma^{-1} - S_{33}^{m23} \end{pmatrix} \right)^{-1}$$

Data from measurement of port 1 and 2:

$$\Delta_{12} = (\Gamma^{-1} - S_{11}^{m12})(\Gamma^{-1} - S_{22}^{m12}) - S_{12}^{m12} S_{21}^{m12}$$

$$\sigma_{11} = \frac{\Gamma^{-1} - S_{22}^{m12}}{\Delta_{12}} \quad \sigma_{12} = \frac{S_{12}^{m12}}{\Delta_{12}} \quad (4.21)$$

$$\sigma_{21} = \frac{S_{21}^{m12}}{\Delta_{12}} \quad \sigma_{22} = \frac{\Gamma^{-1} - S_{11}^{m12}}{\Delta_{12}}$$

Data from measurement of port 1 and 3:

$$\begin{aligned}
\Delta_{13} &= (\Gamma^{-1} - S_{11}^{m13})(\Gamma^{-1} - S_{33}^{m13}) - S_{13}^{m13} S_{31}^{m13} \\
\sigma_{11} &= \frac{\Gamma^{-1} - S_{33}^{m13}}{\Delta_{13}} & \sigma_{13} &= \frac{S_{13}^{m13}}{\Delta_{13}} \\
\sigma_{31} &= \frac{S_{31}^{m13}}{\Delta_{13}} & \sigma_{33} &= \frac{\Gamma^{-1} - S_{11}^{m13}}{\Delta_{13}}
\end{aligned} \tag{4.22}$$

Data from measurement of port 2 and 3:

$$\begin{aligned}
\Delta_{23} &= (\Gamma^{-1} - S_{22}^{m23})(\Gamma^{-1} - S_{33}^{m23}) - S_{23}^{m23} S_{32}^{m23} \\
\sigma_{22} &= \frac{\Gamma^{-1} - S_{33}^{m23}}{\Delta_{23}} & \sigma_{23} &= \frac{S_{23}^{m23}}{\Delta_{23}} \\
\sigma_{32} &= \frac{S_{32}^{m23}}{\Delta_{23}} & \sigma_{33} &= \frac{\Gamma^{-1} - S_{22}^{m23}}{\Delta_{23}}
\end{aligned} \tag{4.23}$$

And finally (4-20) give all unknown parameters of DUT. This method can characterize an N-port DUT using a two-port VNA and N termination with a known reflection coefficient. The method is exact and does not use any assumption.

4.4 Measurement of n-Port Scattering Matrix with Two-Port Network Analyzer

In order to measure the multi-port scattering matrix of an n-port network, a special multi-port VNA need to design [60]. The multi-port VNA requires specific calibration methods[60]-[63]. Another approach is using a two-port VNA with all other (n-2) ports of the test network connected with perfect terminators based on the definition of the scattering matrix. In practice, the imperfect terminators must be taken into consideration where using a two-port VNA to measure an n-port network accurately. The rigorous method for solving the scattering matrix of a multiport network using a two-port VNA with known terminator was described [64]-[66]. In [67] n-port scattering matrix is calculated directly from C_2^n sets of two-port scattering matrices. In [68] an approach from the port reduction point-of-view has been proposed. As a terminator is connected to an n-port network the order of measured ports is reduced by one. With their method, the n-port scattering matrix can be reconstructed from (n-1) ports scattering matrix by connecting n known terminator to each port one at a time. This port reduction

process can be continued to reduce the port order, and the resulting minimal reduced port order is three.

In [59] C_2^n combinations of two-port measurement have been performed, with other n-2 unused ports have been terminated in perfectly matched load. A match loads not always accessible to application such as millimeter wave or broadband. It has been explained how an imperfect match load degraded the accuracy of the measured S-parameters. Then the concept of virtual auxiliary termination has been introduced [69]. This concept is applied in the multi-port S-matrix measurement with the use of two-port VNA and leaving the rest of the ports of the DUT unconnected. This method is so long and need too remedy. Since there is some matrix inversion, it could be numerically difficult under certain circumstance and sometimes matrix with a large condition number is known as ill condition has been appeared.

A modern VNA with TRL calibration and appropriate standards can measure two-port non-coaxial DUT at desired reference planes. In contrast, due to lack of a multi-port counterpart of a full two-port TRL calibration, a multi-port VNA cannot measure a multi-port non-coaxial DUT up to the intrinsic ports as straightforwardly as measuring the coaxial one [69]- [76]. At the following a new method will be introduced which has less mathematical calculation and each scattering matrix will be calculated individually.

In this method three different load i.e. short circuit (S.C), open circuit (O.C) and 50Ω has been used as auxiliary termination. An n-port network with a termination (by reflection coefficient Γ_k) that is connected at the k^{th} port is shown in Figure 4-5. All other ports are connected to 50Ω . The relationship between S_{ij}^k (measurement scattering matrix) of this reduced (n-1)-port network and S_{ij} (true scattering matrix) of this n-port network is given as [69]:

$$S_{ij}^{(k)} = S_{ij} + \frac{S_{ik}S_{kj}\Gamma_k}{1 - S_{kk}\Gamma_k} \quad i, j, k = 1, \dots, n, j \neq k \quad (4.24)$$

This formula can be applied for the three different loads, the results are given below:

a) 50Ω termination

$$S_{ij\alpha}^{(k)} = S_{ij} + \frac{S_{ik}S_{kj}\Gamma_\alpha}{1 - S_{kk}\Gamma_\alpha} \quad k \neq i, j \quad (4.25)$$

b) Short circuit (S.C.) termination

$$S_{ij\beta}^{(k)} = S_{ij} + \frac{S_{ik}S_{kj}\Gamma_\beta}{1 - S_{kk}\Gamma_\beta} \quad k \neq i, j \quad (4.26)$$

c) Open circuit (O. C.) termination

$$S_{ij\theta}^{(k)} = S_{ij} + \frac{S_{ik}S_{kj}\Gamma_\theta}{1 - S_{kk}\Gamma_\theta} \quad k \neq i, j \quad (4.27)$$

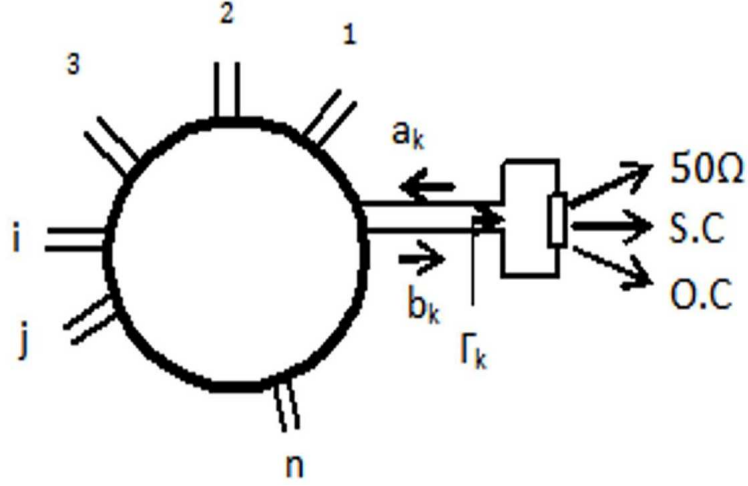


Figure 4.5: An n-port network with three different loads connection

From (2-25)-(2-26)-(2-27) the two unknown, S_{ij} and S_{kk} , can be derived as follows.

$$S_{kk} = \frac{A(\Gamma_\alpha - \Gamma_\theta) - (\Gamma_\alpha - \Gamma_\beta)}{A\Gamma_\beta(\Gamma_\alpha - \Gamma_\theta) - \Gamma_\theta(\Gamma_\alpha - \Gamma_\beta)} \quad (4.28)$$

$$A = \frac{S_{ij\alpha}^{(k)} - S_{ij\beta}^{(k)}}{S_{ij\alpha}^{(k)} - S_{ij\theta}^{(k)}} \quad k \neq i, j$$

$$S_{ik}S_{kj} = \frac{(S_{ij\alpha}^{(k)} - S_{ij\beta}^{(k)})(1 - S_{kk}\Gamma_\alpha)(1 - S_{kk}\Gamma_\beta)}{\Gamma_\alpha - \Gamma_\beta} \quad (4.29)$$

$$S_{ij} = S_{ij\alpha}^{(k)} - \frac{S_{ik}S_{kj}\Gamma_\alpha}{1 - S_{kk}\Gamma_\alpha} \quad k \neq i, j \quad (4.30)$$

$\Gamma_\alpha, \Gamma_\beta$ and Γ_θ are reflection coefficients of port k when it is connected to 50Ω, S.C and O.C loads, respectively.

Thus, in order to measure return loss from port k, it is sufficient to connect 3 different loads to this port, then the S-parameter from two other ports must be measured. Therefore in this

method one can compute the desired S-parameter individually, but in other method all parameters will be found simultaneously.

CHAPTER 5

THREE-PORT AND FIVE-PORT SUBSTRATE INTEGRATED WAVEGUIDE POWER DIVIDER

5.1 Introduction

Power dividers are building blocks of many microwave and millimeter wave integrated circuits and systems. Antenna feed networks are one of the power divider applications. In general, SIW has a relatively large footprint compared to conventional printed circuit counterparts. Some advantages such as being low cost, low loss and suitable for high density integration with microwave and millimeter wave components have popularized SIW in the past few years. Conventional technologies for designing high quality power dividers, including a metal rectangular waveguide or microstrip line are either bulky or unable to provide low insertion loss.

An acceptable performance with considerably decreased size can be offered by SIW technology as a potential solution to the compact communication application. Moreover a multilayer SIW keeps all the advantages of a conventional multilayer PCB structure and will further resolve the problem of radiation from the microstrip feed lines due to its closed structure. Several power dividers based on SIW have been reported [77]-[97]. SIW power divider has the advantages of planar structure and conventional rectangular waveguide power divider, so it is a promising device for planar microwave circuits. Compact size SIW power dividers [77]-[79] and multilayer SIW power dividers [80]-[81] have been reported by researcher. In some SIW power dividers chip resistors have been used to realizing wideband device [82]-[84].

In some applications of SIW power dividers like beam forming network, the main part of SIW must be connected to a beam forming network directly . therefore TRL calibration procedure

can be performed for measuring the desired S-parameters. With the use of TRL calibration function and appropriate TRL standards, a modern VNA can measure a two-port DUT in a desired reference plan. Due to the lack of an established multi-port counterpart of the two-port TRL, a method for measuring the multi-port non-coaxial DUT up to the intrinsic ports has been developed in section 4.4. This method will be applied for three-port and five-port SIW power dividers.

At the following section a novel SIW power divider and its design procedure will be introduced. The design procedure will start by using the waveguide equivalent of SIW and by taking into account the similarity of the SIW with E-plane power divider. Firstly a three-port and then a five-port SIW power dividers will be designed and simulated. Then S-parameters will be reconstructed from measurement data. Finally the measurement results will be compared with simulation results.

5.2 Three-Port Substrate Integrated Waveguide Power Divider Design, Simulation and Fabrication

In this subsection a novel three-port SIW power divider will be introduced. This SIW power divider and its equivalent circuit are shown in Figure 5-1. The above structure will be designed by considering the size reduction, which is a key criterion for microwave and millimeter wave systems. Main part of SIW power divide consists of two layers which are attached together. Electromagnetic waves are propagated from lower layer to upper layer via slots. The width of the first layer is different from the second layer in order to match the input port. Width of the first layer is determined by considering the cut-off frequency and then width of the second layer is computed for matching the input port.

This structure will be completed for measuring by connecting the transitions and microstrip parts. Measuring the main structure without any transitions or microstrip parts is intended. Therefore TRL calibration technique will be applied to remove the effects of transition and microstrip parts. By considering some difficulties in measurement, the same error box in two output ports is preferred in TRL procedure. So it is preferred to have the same output width at three ports as shown in Figure 5-2. The equivalent circuit of this structure is also shown in Figure 5-2. In order to measure the SIW with VNA, above structure must be connected to 50Ω microstrip line. So the transition part between SIW and microstrip line is necessary. The

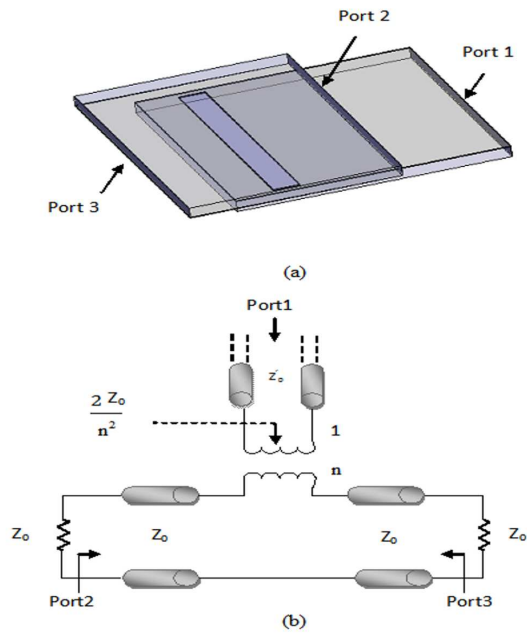


Figure 5.1: (a) Rectangular waveguide equivalent of three-port SIW power divider (b) Equivalent circuit of three-port SIW power divider

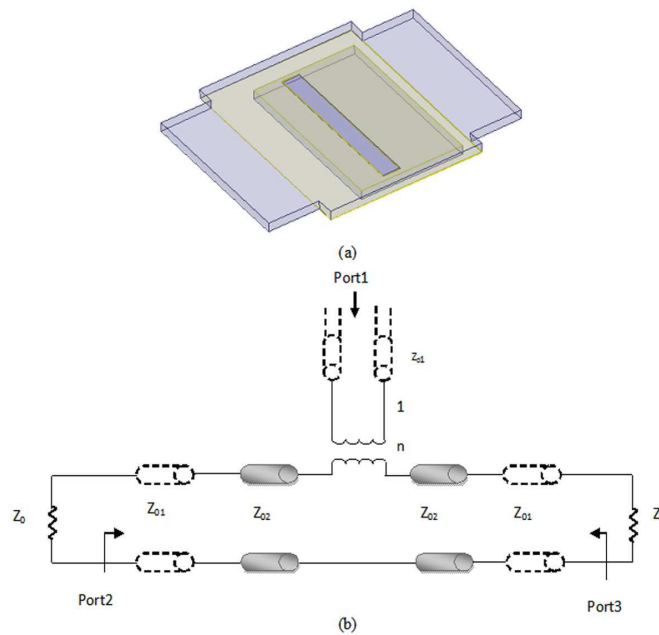


Figure 5.2: (a) Rectangular waveguide equivalent of three-port SIW power divider for TRL measurement (b) Equivalent circuit of three-port SIW power divider

most common transition part has a tapered form. It not only matches the two lines with different characteristic impedance but also transforms the quasi-TEM mode of the microstrip

line into the TE_{10} mode in the waveguide as it has been explained in section 2.4.

5.2.1 SIW Design

SIW is a quasi-rectangular waveguide formed by periodic via-hole connection between two metal layers and TE_{10} is the dominant mode. With the knowledge of pitch between consecutive vias and via diameters, SIW can be replaced by an equivalent dielectric filled rectangular waveguide. The equivalent width (a_e) is computed using the (2-2) or (2-3). The cut-off frequency for rectangular waveguide is given as follows:

$$f_{cmn} = \frac{k_c}{2\pi\sqrt{\mu\epsilon}} = \frac{1}{2\pi\sqrt{\mu\epsilon}} \sqrt{\left(\frac{m\pi}{a_e}\right)^2 + \left(\frac{n\pi}{b}\right)^2} \quad (5.1)$$

$$f_{c10} = \frac{1}{2a_e\sqrt{\mu\epsilon}} \quad (5.2)$$

Where $b = 0.51\text{mm}$ is the substrate thickness, a_e is the equivalent width of SIW, ϵ and μ are the permittivity and permeability of the substrate, respectively.

5.2.2 Power Divider Design

The similarity of SIW power divider with E-plane power divider encourages the researcher to use the E-plane power divider design procedure for designing SIW counterpart. Equivalent circuits of E-plane power divider which have been used in this design shown in Figure 5-1(b) and 5-2(b). The reactive effect associated with the localized higher-mode can be accounted in equivalent circuit. According to the data in [56] X is quite small and negligible. For SIW structure b' is the substrate thickness, and $b = b'$.

$$Z_0 = \frac{b}{a} \frac{\sqrt{\mu_r} \lambda_g}{\sqrt{\epsilon_r} \lambda} \quad (5.3)$$

Z_0 is the characteristic impedance of the rectangular waveguide and $n=0.98$. For SIW power divider in Figure 5-1 Z'_0 is the characteristic impedance of the input line (the first layer in SIW power divider) and Z_0 is the characteristic impedance of the two output lines (the second layer in SIW power divider). As mentioned above for the SIW equivalent circuit $b = b'$ is known parameter, so the width of the SIW "a" is the only variable to achieve the desired response. The design steps for SIW power divider are as follows:

1- The first layer width is determined by cut-off frequency in (5-2) and the characteristic

impedance of the first layer Z'_0 is calculated from(5-3).

2- The characteristic impedance of the second layer Z_0 is calculated from equivalent circuit for matching the input ports.

3- Width of the second layer is calculated from(5-3)

The above three steps can be developed to design an n-way SIW power divider. However, the dimensions of different layers must be optimized due to effect of slot in different layers.

5.2.3 TRL Calibration and Measurement Procedure

The S-parameters of SIW power divider without the microstrip transition parts are achievable in the light of TRL calibration technique. The three TRL standards for SIW structure are shown in Figure 5-3. All of them have the same error box in two ports. For avoiding any radiation effects the reflect standard is a short circuit. The thru standard is made by connecting two error boxes directly together. The design steps for SIW power divider is continued as follows:

4- TRL standards are designed.

5- Transition part is calculated from [10] by considering the width of the input port.

SIW power divider design procedure has been completed with the above 5 steps. The full

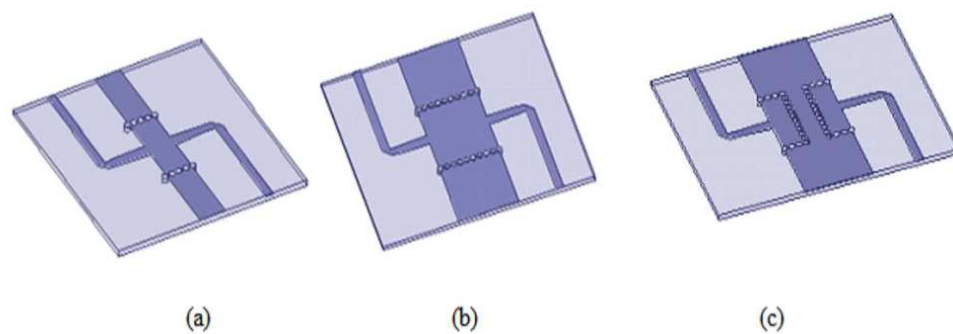


Figure 5.3: Standards for SIW power divider (a) Thru (b) Line (c) Reflect

structure has been shown in Fig.5-4. According to the Fig.5.2 (a) its output has the same width, and it is suitable for TRL calibration technique measurement with the standards shown in Fig. 5-3. So by using the above TRL standards the effect of microstrip line, tapered transition and error box have been removed. The DUT which is measured is exactly the same as shown in Figure 5-1(a). The three-port SIW power divider dimensions are shown in

Table.1. Superior simulation results will be accomplished with small width-slot, but due to fabrication restriction 1 mm width for slot has been chosen.

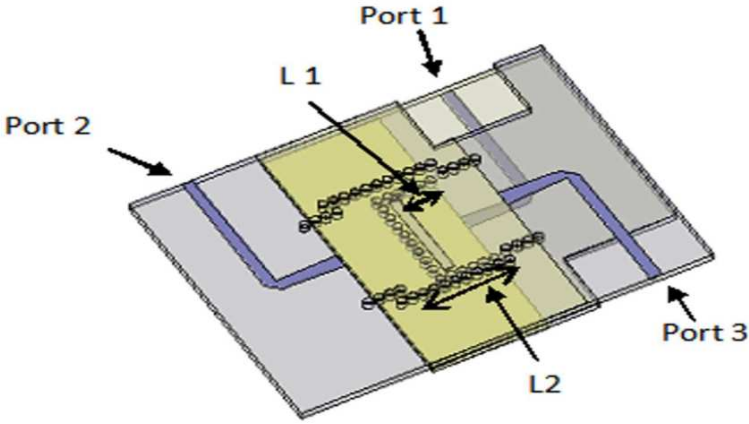


Figure 5.4: Three-port SIW power divider

Table 5.1: Two-way SIW power divider dimensions (mm).

	Length	Width
First Layer (L1)	4	9.1
Second Layer (L2)	9	11.5
Slot	8	1
Transition Part	4.6	1.5

The measuring method in section 4.4 has been used for three-port SIW power divider measurement. In this method the measurement setup will be need as shown in Figure 5-5(a). In this setup port one has been connected to three different loads, O.C, S.C and 50Ω. Three reflection coefficients $\Gamma_\alpha, \Gamma_\beta$ and Γ_θ are related to port k when it is connected to 50Ω, S.C and O.C loads respectively. These reflection coefficients have been measured by using the thru standards as shown in Fig. 5-5(b). In designing the TRL standards thru has zero length and it is made by directly connecting the two error boxes. The equations (4-28)-(4-30) with $k=1, i=2$ and $j=3$ can be written as:

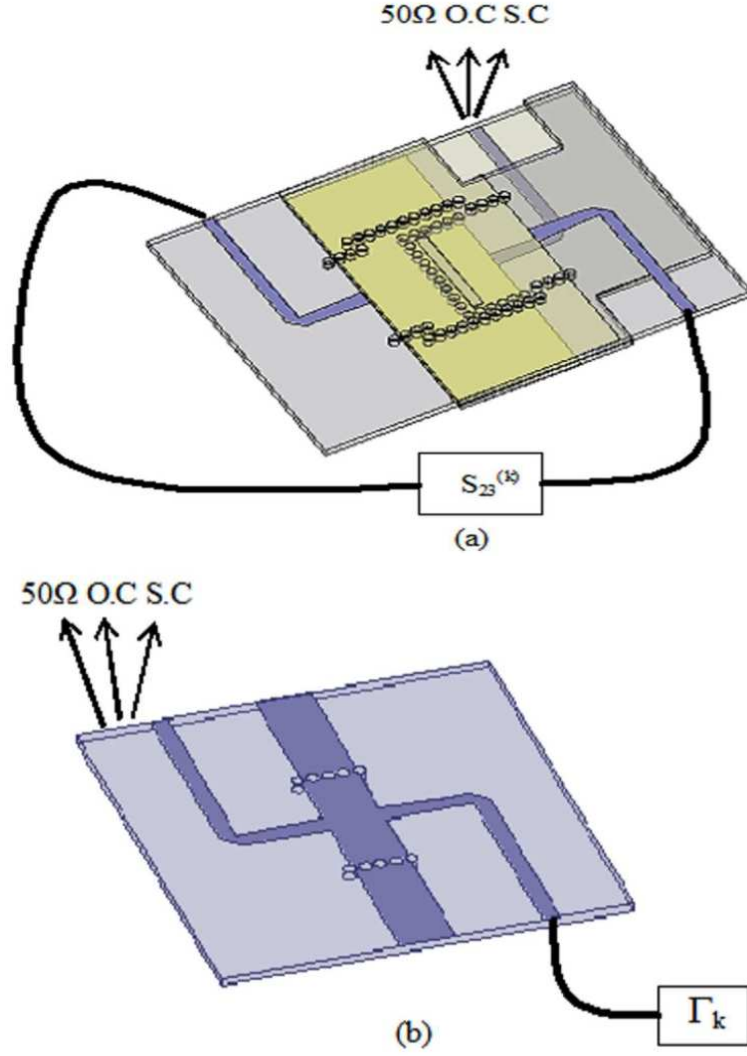


Figure 5.5: (a) Measurement setup for three-port SIW power divider (b) Reflection measurement from Thru standard

$$S_{11} = \frac{A(\Gamma_\alpha - \Gamma_\theta) - (\Gamma_\alpha - \Gamma_\beta)}{A\Gamma_\beta(\Gamma_\alpha - \Gamma_\theta) - \Gamma_\theta(\Gamma_\alpha - \Gamma_\beta)} \quad (5.4)$$

$$A = \frac{S_{23\alpha}^{(1)} - S_{23\beta}^{(1)}}{S_{23\alpha}^{(1)} - S_{23\theta}^{(1)}}$$

$$S_{21}S_{13} = \frac{(S_{23\alpha}^{(1)} - S_{23\beta}^{(1)})(1 - S_{11}\Gamma_\alpha)(1 - S_{11}\Gamma_\beta)}{\Gamma_\alpha - \Gamma_\beta} \quad (5.5)$$

$$S_{23} = S_{23\alpha}^{(1)} - \frac{S_{21}S_{13}\Gamma_\alpha}{1 - S_{11}\Gamma_\alpha} \quad (5.6)$$

In the above equations $S_{23\alpha}^{(1)}$, $S_{23\beta}^{(1)}$ and $S_{23\theta}^{(1)}$ are the S-parameters measured from port 2 and 3 when port 1 is connected to 50Ω , S.C and O.C loads respectively. The measurement setup for reconstruction of the transmission of three-port SIW power divider is similar to Figure 5-5(a) but the measurement port must be changed. The equations (4-28)-(4-30) with $k=2, i=1$ and $j=3$ can be written as:

$$S_{11} = \frac{A(\Gamma_\alpha - \Gamma_\theta) - (\Gamma_\alpha - \Gamma_\beta)}{A\Gamma_\beta(\Gamma_\alpha - \Gamma_\theta) - \Gamma_\theta(\Gamma_\alpha - \Gamma_\beta)} \quad (5.7)$$

$$A = \frac{S_{13\alpha}^{(2)} - S_{13\beta}^{(2)}}{S_{13\alpha}^{(2)} - S_{13\theta}^{(2)}}$$

$$S_{12}S_{23} = \frac{(S_{13\alpha}^{(1)} - S_{13\beta}^{(1)})(1 - S_{22}\Gamma_\alpha)(1 - S_{22}\Gamma_\beta)}{\Gamma_\alpha - \Gamma_\beta} \quad (5.8)$$

$$S_{13} = S_{13\alpha}^{(1)} - \frac{S_{21}S_{13}\Gamma_\alpha}{1 - S_{11}\Gamma_\alpha} \quad (5.9)$$

In the above equations $S_{13\alpha}^{(2)}$, $S_{13\beta}^{(2)}$ and $S_{13\theta}^{(2)}$ are the S-parameters measured from port 1 and 3 when port 2 is connected to 50Ω , S.C and O.C loads respectively. The reconstruction procedure for S_{12} is similar to S_{13} and it is written from equations (4-28)-(4-30) with $k=3, i=1$ and $j=2$ as follows:

$$S_{33} = \frac{A(\Gamma_\alpha - \Gamma_\theta) - (\Gamma_\alpha - \Gamma_\beta)}{A\Gamma_\beta(\Gamma_\alpha - \Gamma_\theta) - \Gamma_\theta(\Gamma_\alpha - \Gamma_\beta)} \quad (5.10)$$

$$A = \frac{S_{12\alpha}^{(3)} - S_{12\beta}^{(3)}}{S_{12\alpha}^{(3)} - S_{12\theta}^{(3)}}$$

$$S_{13}S_{32} = \frac{(S_{12\alpha}^{(3)} - S_{12\beta}^{(3)})(1 - S_{33}\Gamma_\alpha)(1 - S_{33}\Gamma_\beta)}{\Gamma_\alpha - \Gamma_\beta} \quad (5.11)$$

$$S_{12} = S_{12\alpha}^{(3)} - \frac{S_{21}S_{13}\Gamma_\alpha}{1 - S_{11}\Gamma_\alpha} \quad (5.12)$$

At the next section above mentioned formula will be used to reconstruct the measurement results of three-port SIW power divider.

5.2.4 The Experimental Results of Three-Port SIW Power Divider

The fabricated three-port SIW power divider is shown in Figure 5-6. It is made of RO4003 with thickness $h=0.51$ mm. The simulation results of DUT in Figure 5-4 and measurement results which have been constructed from fabricated case are compared at the following Figures. According to Figure 5-7 there is a good agreement between simulation and measurement results from 9 GHz to 11 GHz. The return loss below 10 dB has been achieved at the same frequency band. Transmissions in Figure 5-8 are between -3.5 dB to -4 dB at the same

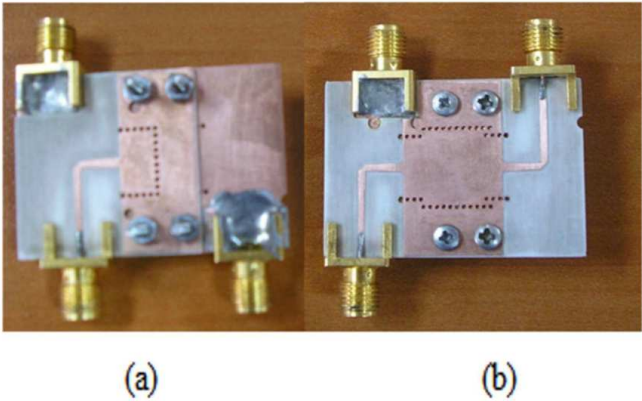


Figure 5.6: Fabricated three-port SIW power divider (a) Bottomn view (b) Top view

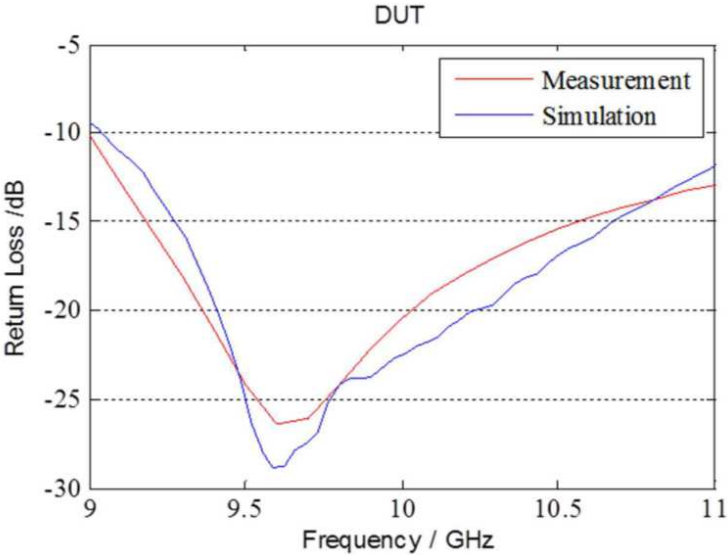


Figure 5.7: Return loss of three-port SIW power divider from simulation and measurement

frequency band. Figure 5.9 shows a poor isolation between port 2 and port 3 as expected, because there is not any resistance between output ports. Amplitude balance in Figure 5-10

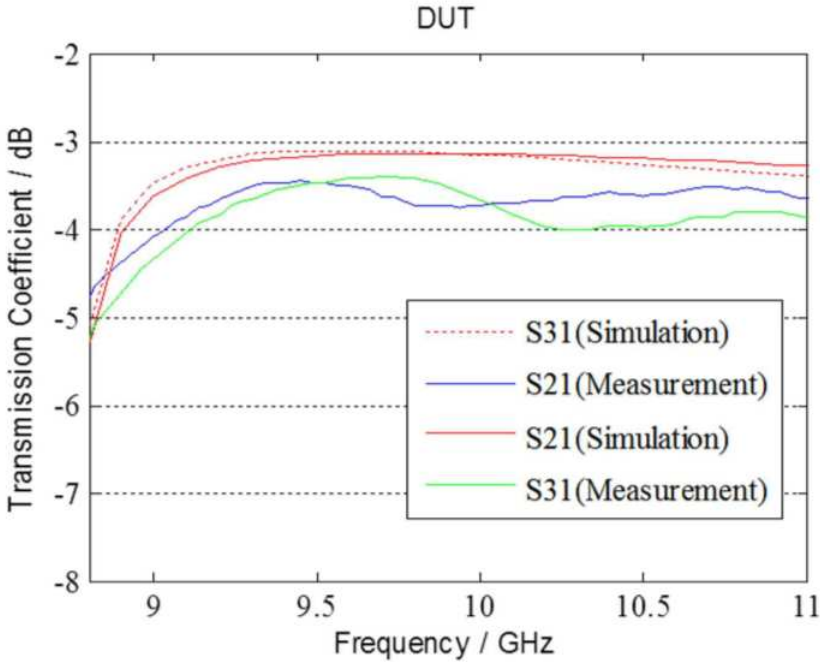


Figure 5.8: Transmission of three port SIW power divider from simulation and measurement

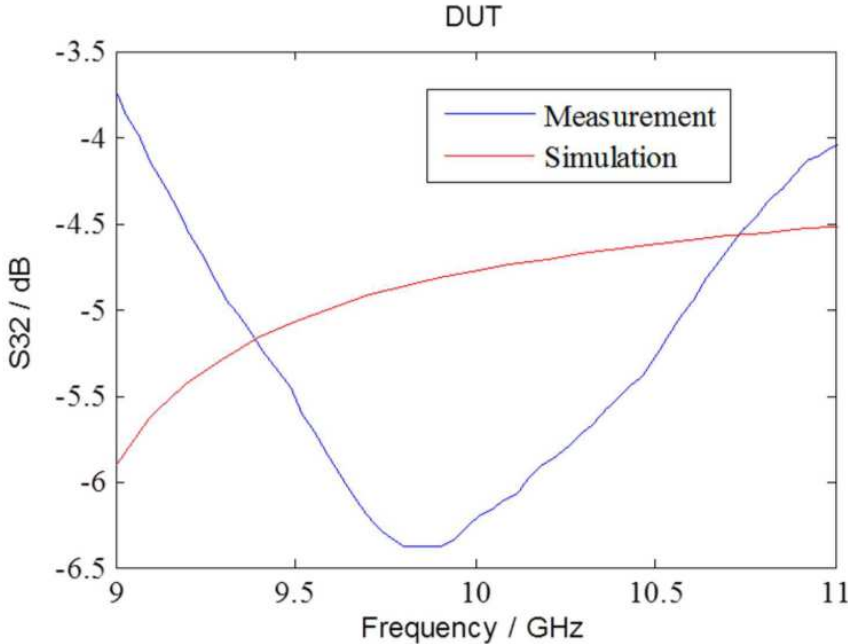


Figure 5.9: Isolation between output ports of the three port SIW power divider

is less than $\pm 0.5dB$ from 9.5 GHz to 11 GHz. Phase difference in Figure 5-11 between $\angle S_{21}$

and $\angle S_{31}$ is about $\pm 4^\circ$. The amplitude balance and phase balance is not too sensitive to frequency of operation in design frequency band.

Therefore this SIW power divider is suitable for some applications like amplifier, because the non sensitivity to operation frequency is an important factor for these applications. In the all above mentioned cases simulation and measurement results are in a good agreement with each other.

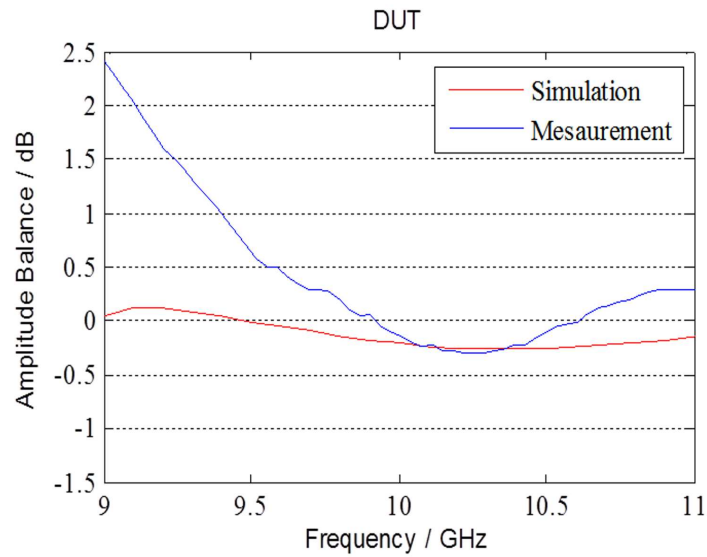


Figure 5.10: Amplitude balance of three-port SIW power divider

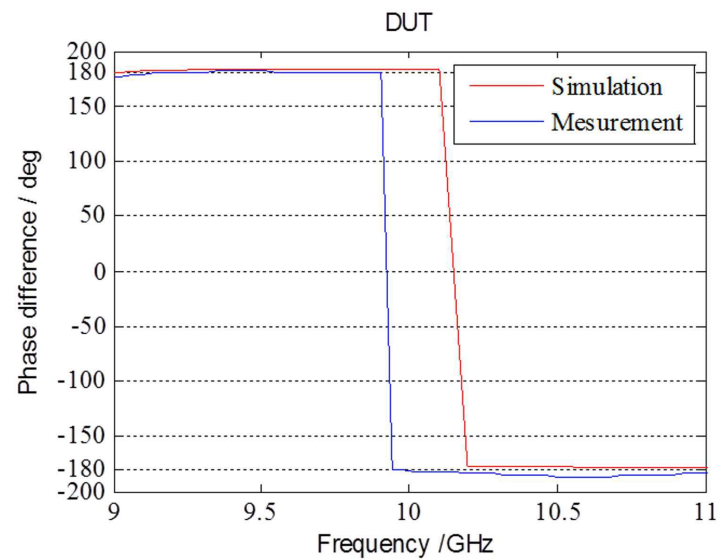


Figure 5.11: Phase difference of three-port SIW power divider

5.3 Five-Port Substrate Integrated Waveguide Power Divider Design, Simulation and Fabrication

5.3.1 Five-port SIW Power Divider Design Consideration

In this subsection a five-port SIW power divider power divider design is presented. The steps in designing a five-port SIW power are similar to that of a three-port SIW power divider. The firstly by considering the operation frequency and cut-off frequency the width of the first layer has been determined then width of the second layer and width of the third layer have been determined by considering the equivalent circuit and matching the input port.

This SIW power divider is shown in Figure 5-12. It consists of three PCB layers. There is one slot in the first layer and two slots in the second layer. The electromagnetic wave has been propagated from these slots. The TRL standards are the same as three-port SIW power dividers, so the widths of the output port are the same. The measurement set up in part 4-4 has been used for reconstruction of the S-parameters of the DUT. DUT of a five-port SIW

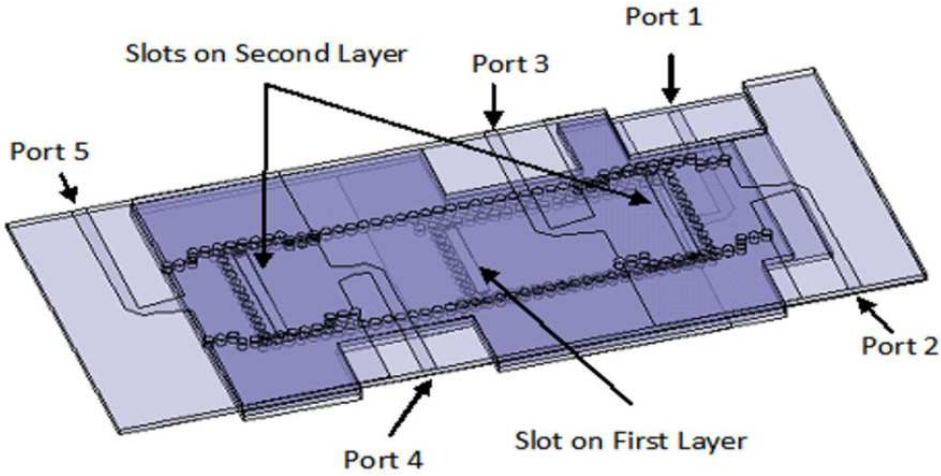


Figure 5.12: Five-port SIW power divider

power divider is shown in Figure 5-13. Three layers are presented separately. There are two slots in the second layer for propagating the electromagnetic waves from the first layer to the third layer. The widths of the slots are the same in all layers and it is 1 mm. The slots of the first and the second layer are surrounded by vias in order to avoid any radiation from the end of the structure. The slot-position is symmetric with respect to upper layer. The slot-position

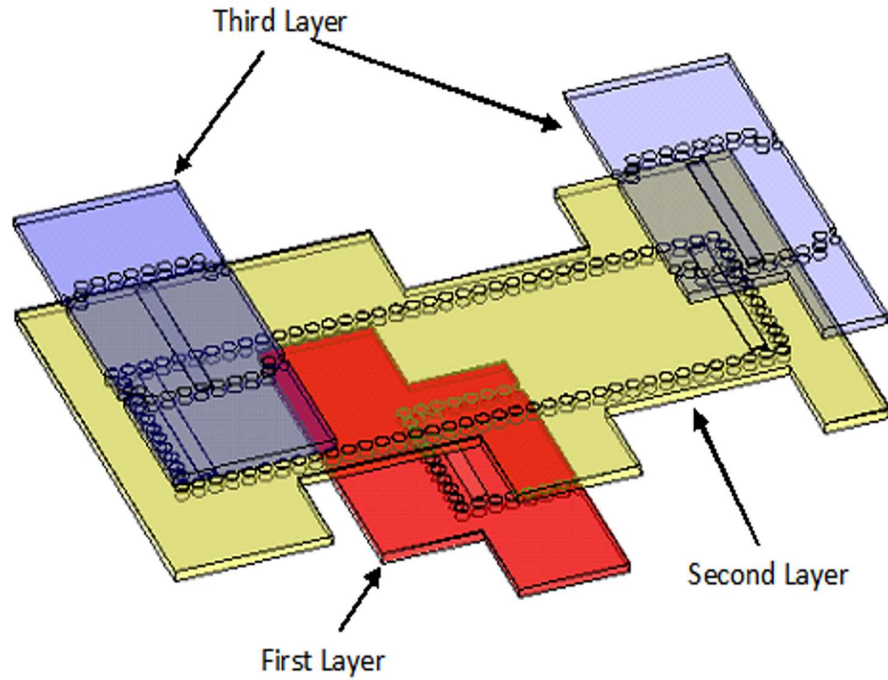


Figure 5.13: DUT of five-port SIW power divider

affects the input return loss and the amount of power which has been transferred to each port. By using the set up mentioned actually the S-parameters of the Figure 5.13 has been measured. Output of this structure can be connected directly to microstrip array antenna as a feed network, therefore its electrical performance must be known. This is an equal power divider, but by changing the width of the output ports the amount of power which is transferred to each port can be change. So the unequal power divider can be accomplished.

5.3.2 Experimental Results of Five-Port SIW Power Divider

The fabricated five-port SIW power divider is shown in Figure 5-14. It is made of RO4003 with thickness $h=0.51$ mm. Its dimension is given in Table 5.2. This is fabricated and measured in microwave laboratory of METU University. Three layers have been attached together with screw.

The simulation and measurement results are shown in Figures 5-15, 5-16, 5-17, and Figure 5-18. A good agreement is seen between simulation and measurement results of DUT over the frequency band from 9.5 GHz to 10.5 GHz. The measured data have been obtained based

on TRL calibration and reconstruction method. The isolation between port 4 and port 5 is shown in Figure 5-19. The isolation between the other ports is the same as S_{45} . There is not a good isolation as expected because there is not any resistance between output ports.

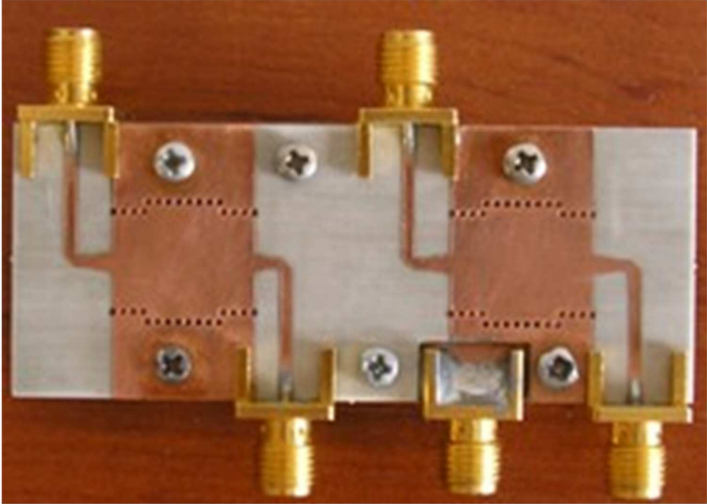


Figure 5.14: Picture of five-port SIW power divider

Table 5.2: Five-port SIW power divider dimension (mm).

	Length	Width
First Layer	8.2	9
Second Layer	32	11
Third Layer	7	11
Transition Part	2.6	2

The measured amplitude difference and phase difference between S_{21} and S_{31} of five-port SIW power divider are shown in Figure 5-20 and Figure 5-21 respectively. Amplitude balance is less than ± 0.5 dB from 9.5 GHz to 10.8 GHz, and phase balance is approximately $\pm 0.5^\circ$.

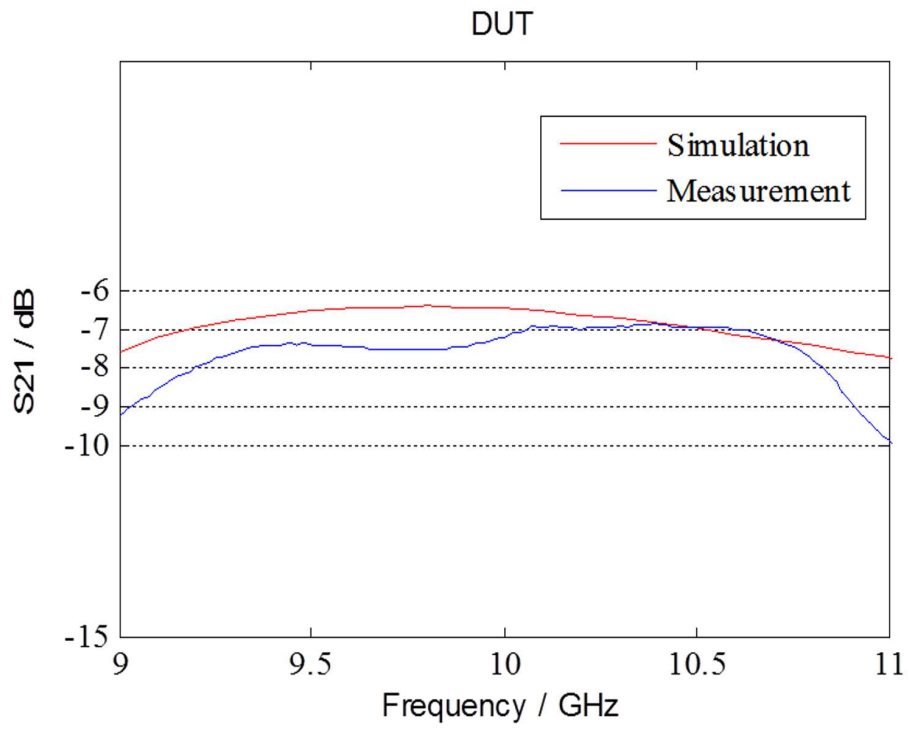


Figure 5.15: Transmission of five-port SIW power divider S_{21}

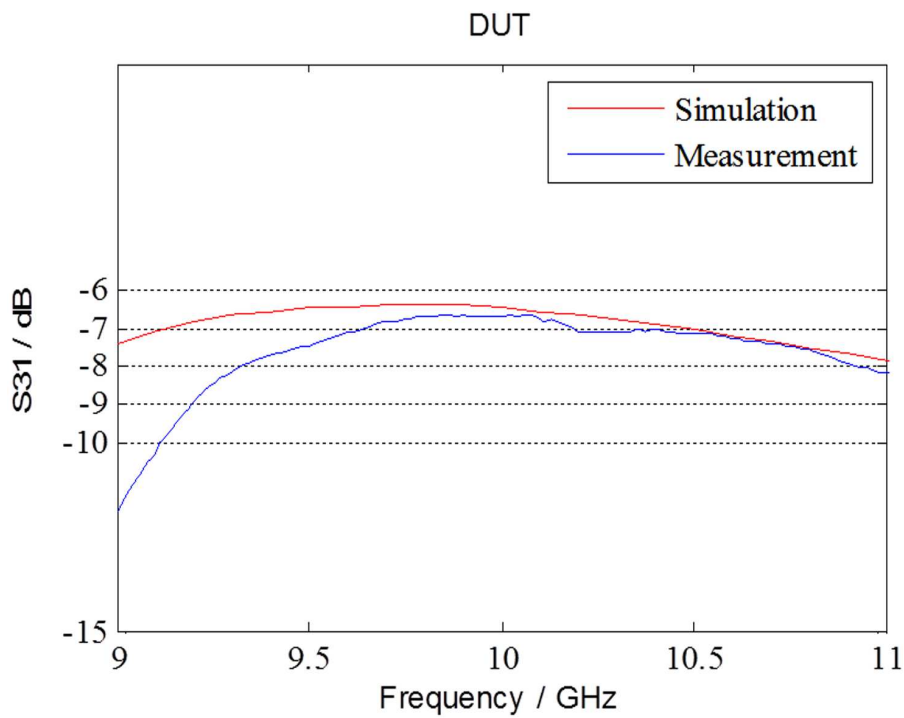


Figure 5.16: Transmission of five-port SIW power divider S_{31}

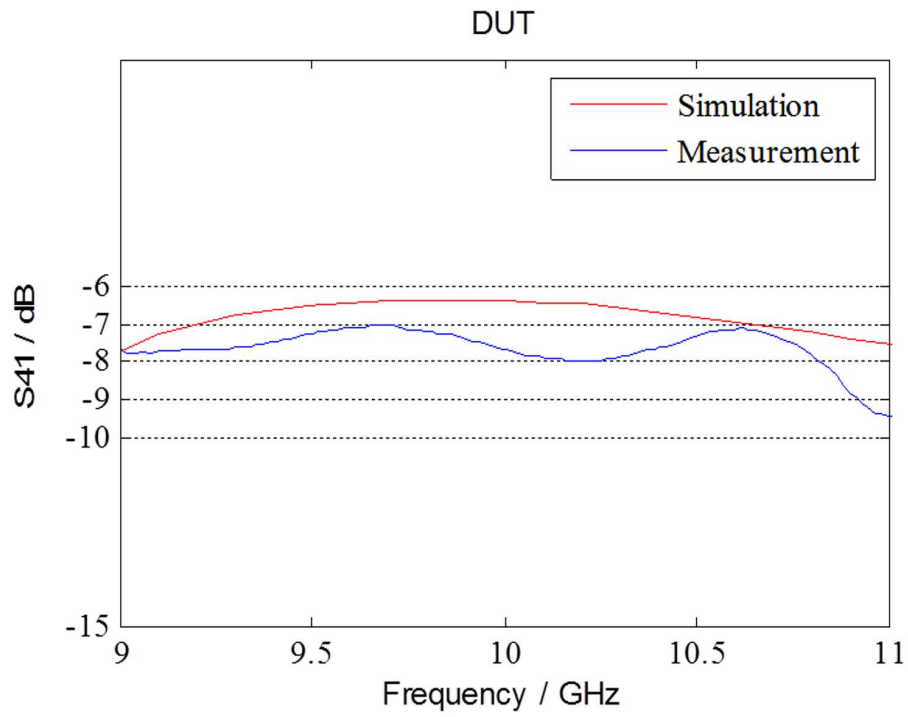


Figure 5.17: Transmission of five-port SIW power divider S_{41}

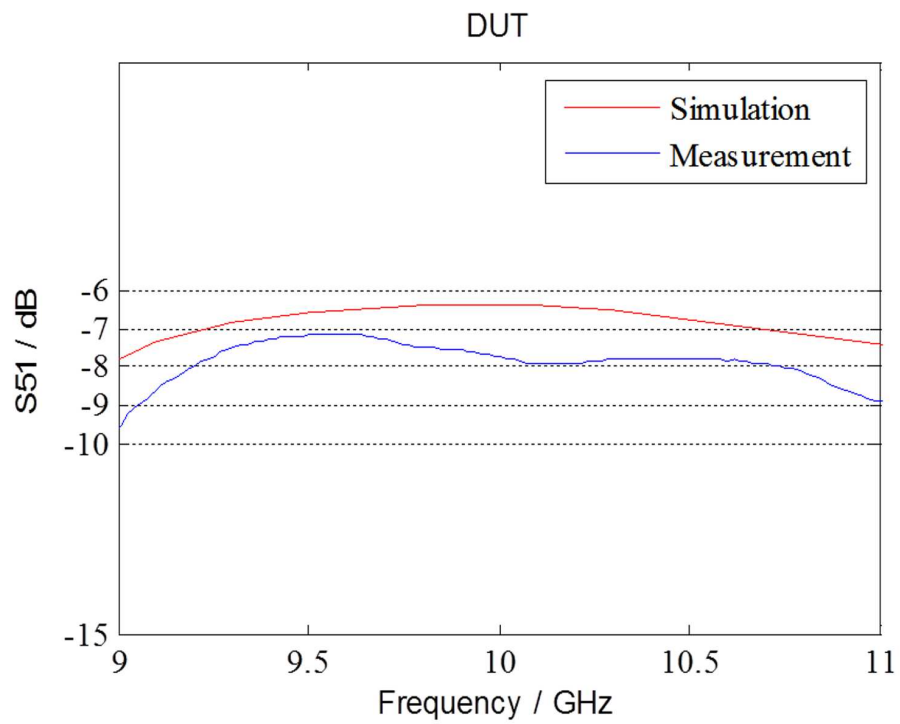


Figure 5.18: Transmission of five-port SIW power divider S_{51}

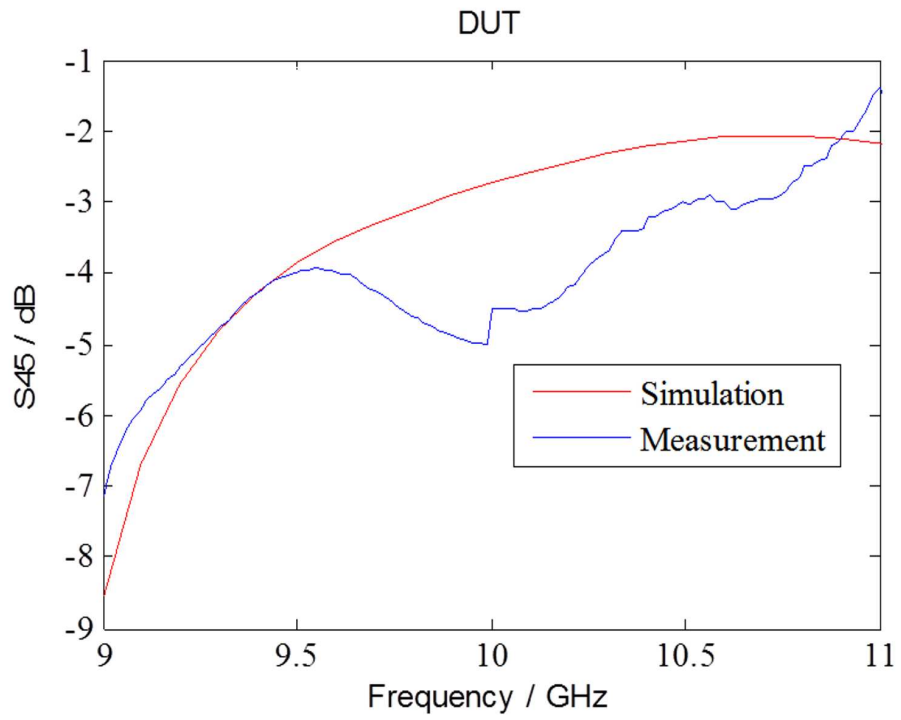


Figure 5.19: Isolation of five-port SIW power divider

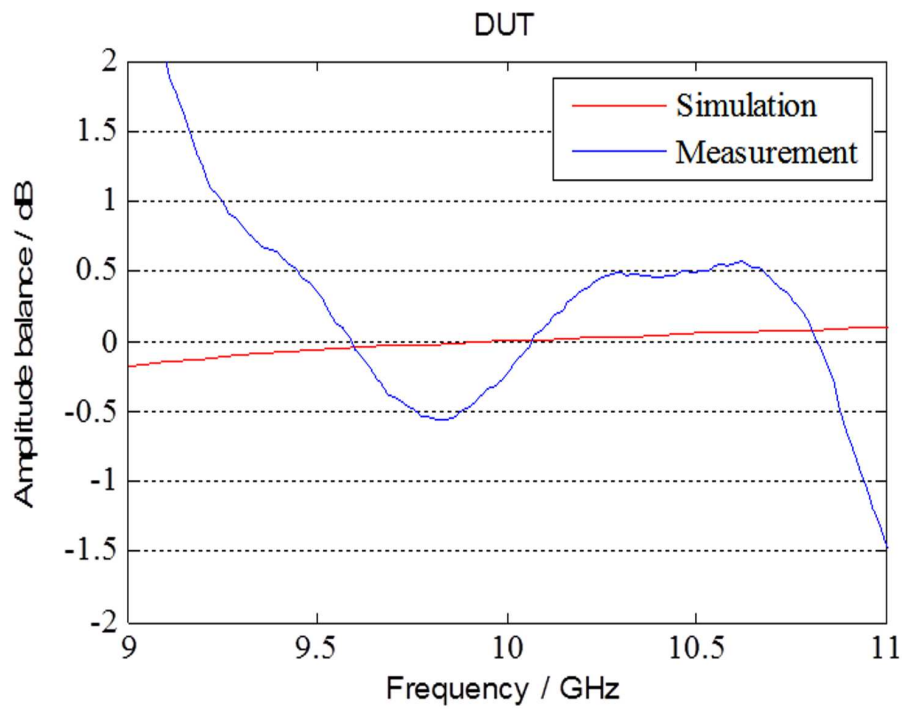


Figure 5.20: Amplitude balance of five-port SIW power divider

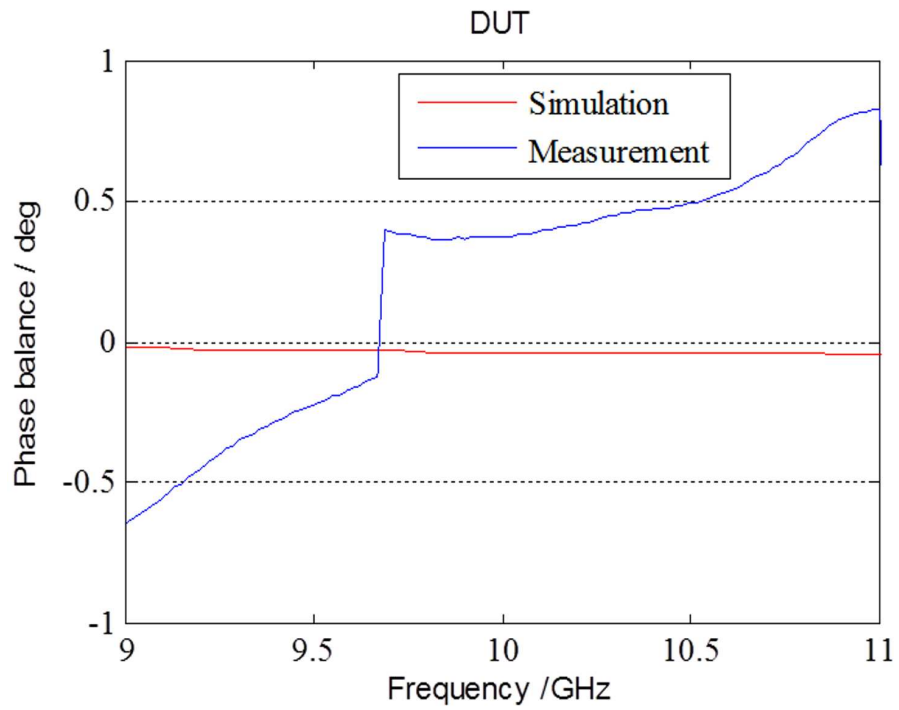


Figure 5.21: Phase difference of five-port SIW power divider

The phase balance and amplitude balance are not too sensitive to operation frequency in desired band. There are similar results between other output ports.

CHAPTER 6

LOW LOSS SUBSTRATE INTEGRATED WAVEGUIDE

6.1 Introduction

Compact and low loss integrated components are the key element in designing telecommunication systems which are operating in the microwave and millimeter-wave frequency range. Metallic waveguides have also been widely adopted, but sometimes their use is unpractical because of weight and size and integration problems with planar structure. Substrate integrated waveguide (SIW) is an interesting alternative that solves these problems. Like metallic rectangular waveguide (RW), substrate integrated waveguide is an electromagnetic-interference-free-component. Compared with rectangular waveguide, SIW has well known advantages like low loss, low cost and high density integration with microwave and millimeter wave components. Integrated rectangular waveguide concepts have been studied in previous chapters. One of the major issues for the applicability of SIW in millimeter-wave components design is related to its losses.

Loss mechanisms in SIW have been discussed in some papers [97]-[98]. Wave mechanism and leakage characteristic of SIW have been reported in [99]-[103]. SIW structures suffer from ohmic loss, radiation loss and dielectric loss. Since the SIW is not completely shielded due to gap between slots, there is a radiation loss from the possibility of the leakage wave through these gaps. Ohmic loss is related to finite conductivity of metal walls and finally dielectric loss is due to the loss tangent of dielectric material. It is shown that all these losses can be minimized if the vias have large diameters and closely spaced.

Dielectric loss is the major source of loss in SIW and it is significantly larger than two other losses. So decreasing the dielectric loss would have significant role in decreasing the total dissipated power in SIW. The main idea in order to get low dielectric loss is using air instead

of dielectric in SIW as a transmission medium. Removing the dielectric substrate from the middle part of the SIW as illustrated in Figure 6-1 is a desired method to decrease the dielectric loss.

Partially filled SIW (PSIW) in Figure 6-1 has been covered with two metal covers like up

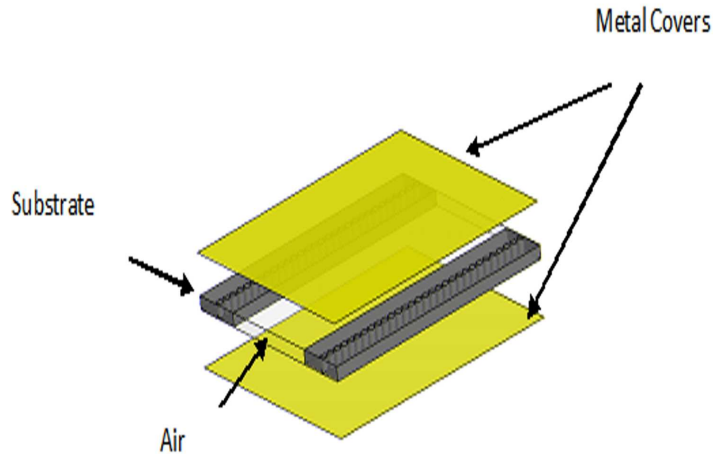


Figure 6.1: Partially filled SIW

and down wall of waveguide. The low loss SIW with this technique has been designed and fabricated. Then a low loss power divider has been produced based on this technology. Power dividers are the key element in microwave and millimeter wave systems. However, available SIW power dividers in the multi-way port environment have large size due to lateral port distribution and the loss problems. In the available SIW power dividers the size problem has been improved by stacking the layers, but the loss problem still exists.

In our proposed PSIW power divider both problems have been investigated and improved. Firstly the size reduction has been achieved by stacking the layers. Then by increasing the number of ports only the length of the structure is increased and its width remains unchanged. Secondly by removing the dielectric the loss can be decreased. The comparison of S-parameters of this power divider with similar power dividers [103] shows that total loss has been decreased due to decrease in dielectric loss. The low profile property of SIW can be developed and utilized in multilayer structures [78], somewhat similar to the presented configuration in the current study. However, this study is much more convenient for applications like antenna array feed network designs.

In order to measure the SIW structure, tapered transition parts have been used. These parts can change the loss property of the structures. Hence the S-parameters of the main structure is a matter of concern and not a transitions parts. This leads to use thru-reflect-line (TRL) calibration technique. In the light of appropriate PSIW TRL standards the unwanted effects of transition parts will be removed. This procedure has been explained at the following sub-sections.

6.2 Wave Propagation Mechanisms in SIW

In order to investigate the loss mechanism in SIW, firstly the wave propagation mechanism in SIW and its similarity and dissimilarity with rectangular waveguide will be discussed. The effect of vias in SIW will be similar to the effect of slots on the narrow wall of RW. Radiation loss will be appears due to leakage wave in SIW. The propagation characteristic of SIW is similar to classical rectangular waveguide, with a few basic differences.

The mode of an SIW practically coincides with a subset of the mode of RW. Due to the gaps between metal vias, only TE_{m0} ($m = 1, 2, \dots$) modes can exist in SIW [101]. In particular, the fundamental mode is similar to the TE_{10} mode of a RW, with vertical electrical current density on the side walls. Surface current distribution of the RW at TE_{10} mode is shown in Figure 6-2. It can be seen that the surface currents on narrow walls are parallel to SIW vias. The SIW structure can be regarded as a special RW with a series of slots on the bilateral

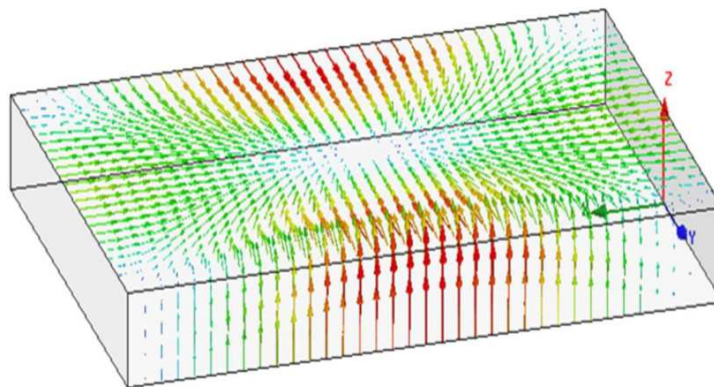


Figure 6.2: Surface current distribution of the rectangular waveguide

narrow walls. If the slots cut the currents, a large amount of radiation may appear. This is

a well established design principal of waveguide slot antenna. However, if the slots are cut along the directional of current flowing, there is only very little radiation. The vias at the SIW structure do not cut the surface current, on the narrow walls, so the mode can be presented in the structure. The other TE_{m0} modes have similar surface currents on the narrow walls. This is why TE_{m0} mode can exist in the SIW structures.

If the TM modes propagate in a RW with slot in the narrow walls, transverse magnetic fields will produce a longitudinal surface current. The transverse slots cutting these currents will bring about a large amount of radiation. By the same reason, those slots will also yield a large amount of radiation if $TE_{mn}(n \neq 0)$ mode travel in the RW with slots on the narrow walls. Therefore slots radiation suggests that only TE_{10} mode would be allowed in the structure.

6.3 Dielectric Loss in SIW

As mentioned in introduction, there are three sources for losses in SIW, and dielectric loss is larger than two other losses. In order to calculate the dielectric loss constant, PSIW must be analytically analyzed. For modeling and analysis of SIW structure some techniques have been reported [104]-[106]. These analyses may briefly be classified into the following groups:

- 1) Analysis based on full wave technique.
- 2) Analysis based on the method of moment (MOM).
- 3) Analysis based on surface impedance.

The advantages and disadvantages of these methods have been discussed in relevant papers. PSIW will be analyzed based on the surface impedance concept at the subsequent procedure. Firstly the partially filled rectangular equivalent waveguide of PSIW will be established. Then by using the well known formula for electric field and magnetic field in partially filled rectangular waveguide, surface impedance of the structure will be calculated. Finally dielectric loss constant based on known field distribution in partially filled waveguide will be worked out. Top view of PSIW in Figure 6-1 and proposed equivalent RW is shown in Figure 6-3. Both structures include two dielectric parts in corners with an air part in middle of the structures. At PSIW "d" is the width of air part and "a'" is width of total structure. In equivalent RW also "d" is air part width and "a" is width of RW. As shown in Figure 6-3 the metallized via

are replaced by RW walls in equivalent RW. The distance between adjacent vias is "w".

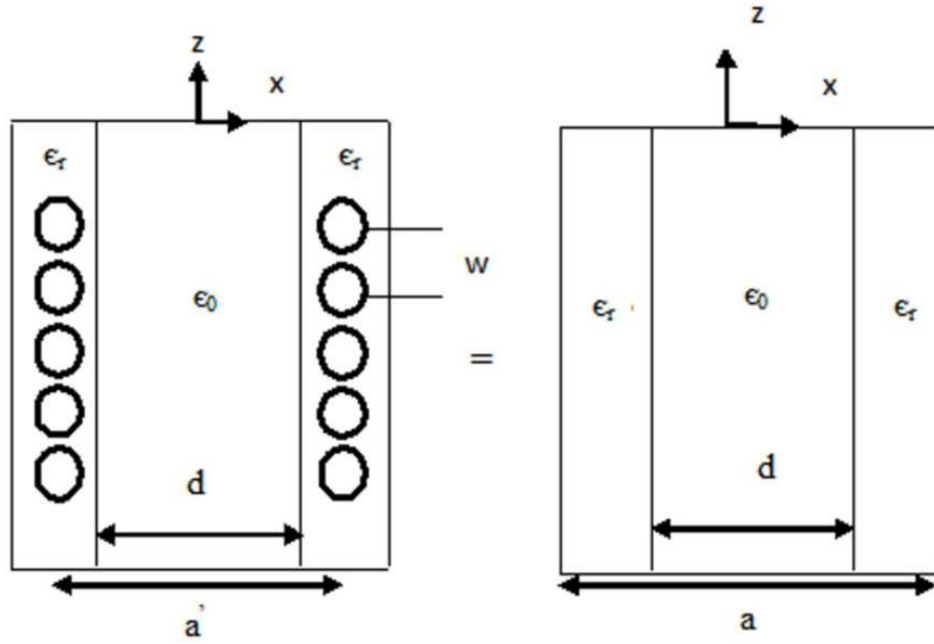


Figure 6.3: Top view of PSIW and its equivalent RW

For TE_{10} mode propagation in a rectangular waveguide functions are: [107]

$$\begin{aligned}
 E_x &= 0 & H_x &= \frac{1}{\hat{z}} \left(\frac{\partial^2}{\partial x^2} + k^2 \right) \Psi \\
 E_y &= -\frac{\partial \Psi}{\partial z} & H_y &= \frac{1}{\hat{z}} \frac{\partial^2 \Psi}{\partial x \partial y} \\
 E_z &= \frac{\partial \Psi}{\partial y} & H_z &= \frac{1}{\hat{z}} \frac{\partial^2 \Psi}{\partial x \partial z} \\
 \hat{z} &= j\omega\mu
 \end{aligned} \tag{6.1}$$

$$\Psi = \begin{cases} A \sin k_{x1} \left(\frac{a}{2} + x \right) \cos(k_{y1} y) & \text{if } -\frac{a}{2} \leq x \leq \frac{d}{2} \\ B \cos(k_{x0} x) \cos(k_{y0} y) & \text{if } -\frac{d}{2} \leq x \leq \frac{d}{2} \\ A \sin k_{x1} \left(\frac{a}{2} - x \right) \cos(k_{y1} y) & \text{if } \frac{d}{2} \leq x \leq a. \end{cases} \tag{6.2}$$

In the above formulas k_{x1} and k_{y1} are the propagation constant of dielectric part in x and y direction respectively. k_{x0} and k_{y0} are related to air part of PSIW. The surface impedance of the structures is given as follows [104]:

$$\eta_{s0} = \frac{j\omega\mu W}{4} \ln \frac{W}{4R} \quad (6.3)$$

R is the radius of cylinder and W is space between two cylinders and $\omega = 2\pi f$. The surface impedance for RW is :

$$\eta_s = \frac{E_y}{H_z} \quad \text{at} \quad x = \frac{a'}{2} \quad (6.4)$$

$$\begin{aligned} E_y &= -\frac{\partial \Psi}{\partial z} = jk_z \Psi \\ H_y &= -\frac{1}{z} \frac{\partial^2 \Psi}{\partial x \partial y} \end{aligned} \quad (6.5)$$

Then, η_s due to RW can be calculated by using (6-4) and (6-5). The equality $\eta_{s0} = \eta_s$ gives:

$$\begin{aligned} \frac{W}{4} \ln \frac{W}{4R} &= \frac{1}{\sqrt{(\omega^2 \mu \epsilon - k_z^2)}} \tan\left(\frac{(a - a')}{2} \sqrt{(\omega^2 \mu \epsilon - k_z^2)}\right) \\ \frac{W}{4} \ln \frac{W}{4R} &= C \end{aligned} \quad (6.6)$$

C is a constant value because after designing the SIW, the value of R and W are constant. Boundary condition will be applied as follows:

$$E_z(y = 0, b) = 0 \quad \Rightarrow \quad k_{y1} = k_{y0} = \frac{n\pi}{b} \quad n = 0, 1, 2, \dots \quad (6.7)$$

b is the height of PSIW Continuity of fields at $x = \frac{d}{2}$:

$$E_y\left(x = \frac{d}{2}\right) \quad \Rightarrow \quad A \sin\left(k_{x1} \frac{(a - d)}{2}\right) = B \cos\left(k_{x0} \frac{d}{2}\right) \quad (6.8)$$

$$H_y\left(x = \frac{d}{2}\right) \quad \Rightarrow \quad k_{x1} \cos\left(k_{x1} \frac{(-d + a)}{2}\right) = B k_{x0} \sin\left(k_{x0} \frac{d}{2}\right) \quad (6.9)$$

from (6-8)and (7-8)⇒

$$k_{x1} \cotan\left(k_{x1} \frac{(a - d)}{2}\right) = k_{x0} \tan\left(k_{x0} \frac{d}{2}\right) \quad (6.10)$$

it is known that:

$$k_{x1}^2 = \omega^2 \mu \epsilon = k_z^2 + k_{y1}^2 + k_{x1}^2 \quad (6.11)$$

$$k_{x0}^2 = \omega^2 \mu_0 \epsilon_0 = k_z^2 + k_{y1}^2 + k_{x1}^2 \quad (6.12)$$

k_{x1} and k_{x0} are the wave numbers in dielectric substrate and free space respectively. For TE_{10} mode ($n=0$) $k_{y1} = k_{y0}$ so by using (6-10),(6-11) and (6-12) one can write:

$$\sqrt{\omega^2 \mu \epsilon - k_z^2} \cotan\left(\sqrt{\omega^2 \mu \epsilon - k_z^2} \left(\frac{a-d}{2}\right)\right) = \sqrt{\omega^2 \mu_0 \epsilon_0 - k_z^2} \tan\left(\sqrt{\omega^2 \mu_0 \epsilon_0 - k_z^2} \left(\frac{d}{2}\right)\right) \quad (6.13)$$

from (6-6) it can be found that:

$$a = a' + \frac{2}{\sqrt{\omega^2 \mu \epsilon - k_z^2}} \tan^{-1} C \sqrt{\omega^2 \mu \epsilon - k_z^2} \quad (6.14)$$

then a can be substituted by a' in (7-14) and it becomes:

$$\begin{aligned} \sqrt{\omega^2 \mu \epsilon - k_z^2} \cotan\left(\sqrt{\omega^2 \mu \epsilon - k_z^2} \left(\frac{a'}{2} + \frac{2}{\sqrt{\omega^2 \mu \epsilon - k_z^2}} \tan^{-1} C \sqrt{\omega^2 \mu \epsilon - k_z^2}\right)\right) - \\ \sqrt{\omega^2 \mu_0 \epsilon_0 - k_z^2} \tan\left(\sqrt{\omega^2 \mu_0 \epsilon_0 - k_z^2} \left(\frac{d}{2}\right)\right) = 0 \end{aligned} \quad (6.15)$$

In equation (6-15) the only unknown is k_z and it can be found by a proper MATLAB program. This is done for our design. Then the equivalent RW length can be found from (6-14).

6.4 Attenuation Constant Due to Dielectric Loss

Attenuation constant due to dielectric loss can be found by using the well known formula.

$$\alpha_d = \frac{P_d}{2P} \quad (6.16)$$

$$P_d = \frac{1}{2} \omega \epsilon'' \int |E|^2 dv$$

$$P = \frac{1}{2} \text{Re} \int [E \times H^*] ds$$

$\alpha_d \Rightarrow$ Attenuation constant due to dielectric loss

$P_d \Rightarrow$ Power loss due to dielectric

$P \Rightarrow$ Power through the waveguide

$$P_d = \frac{\omega \epsilon'' lb A^2 k_z^2}{2} \left(\frac{a-d}{2} - \frac{\sin(k_{x1}(a-d))}{2k_{x1}} \right) \quad (6.17)$$

$$P = \frac{B^2 k_z b}{2\omega\mu} (k^2 - k_{x0}^2) \left(\frac{d}{2} + \frac{\sin(k_{x0}d)}{2k_{x0}} \right) + \frac{k_z A^2 b}{2\omega\mu} (k^2 - k_{x1}^2) \left(\frac{a-d}{2} - \frac{\sin k_{x1}(a-d)}{2k_{x1}} \right) \quad (6.18)$$

In order to examine the analytical results, you can consider the following example. A PSIW has been simulated with Ansoft HFSS software, and the simulation results have been compared with analytical results. PSIW is shown in Figure 6-4.

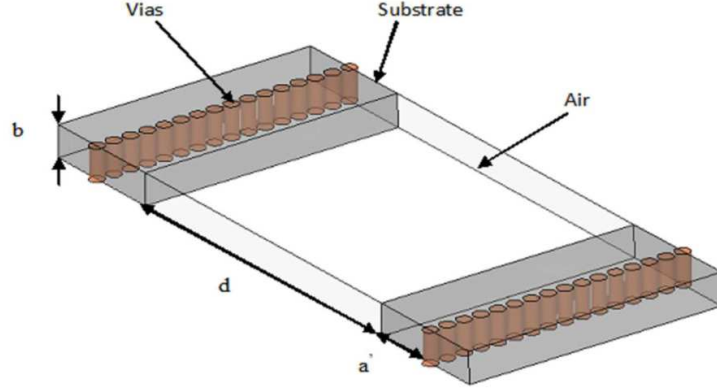


Figure 6.4: DUT of proposed PSIW structure

For this structure $d = 19$ mm, $a' = 3$ mm and substrate is RO4003 with $b = 0.51$ mm. Propagation constant in z direction due to PSIW which has been found from simulation and analytical solution is shown in Figure 6-5. According to this Figure, the cut-off frequency is about 6 GHz. There is a good agreement between them.

K_{x0} and K_{x1} are the propagation constant in x direction due to air part and dielectric part of PSIW respectively. Both are shown in Figure 6-6.

Dielectric losses in Figure 6-7 are in a good agreement with each other. The analytical dielectric loss was computed from (6.16), (6.17) and (6.18) for the above PSIW structure. The high degree of similarity between the two results in Figure 6-6 shows that the proposed equivalent circuit and analytical method are valid.

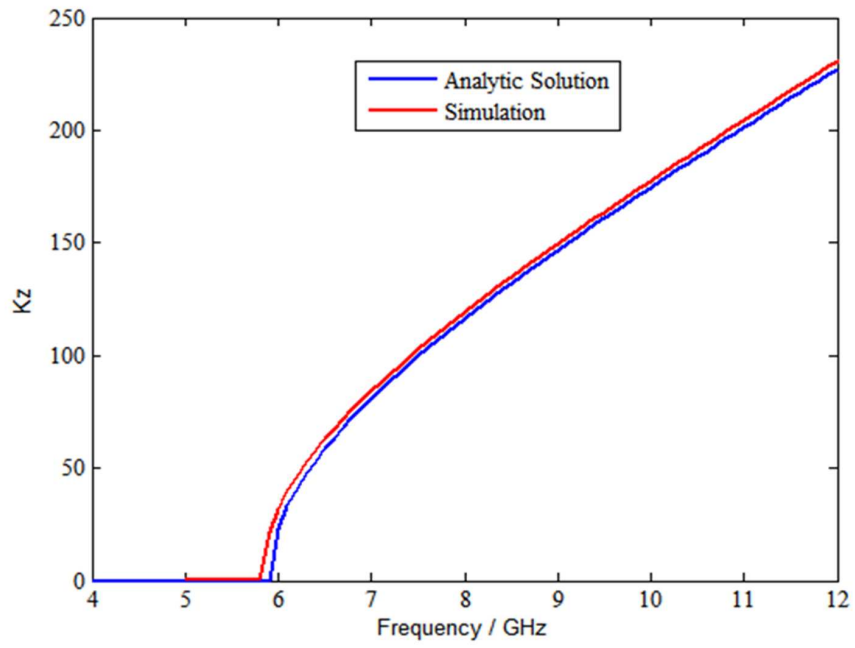


Figure 6.5: Propagation constant in z direction of PSIW

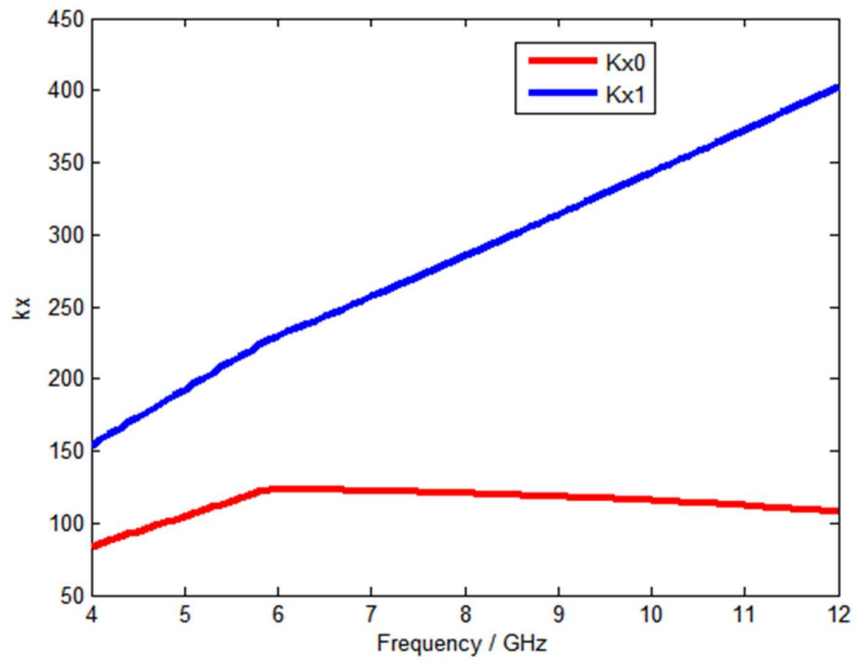


Figure 6.6: Propagation constant in x direction of PSIW

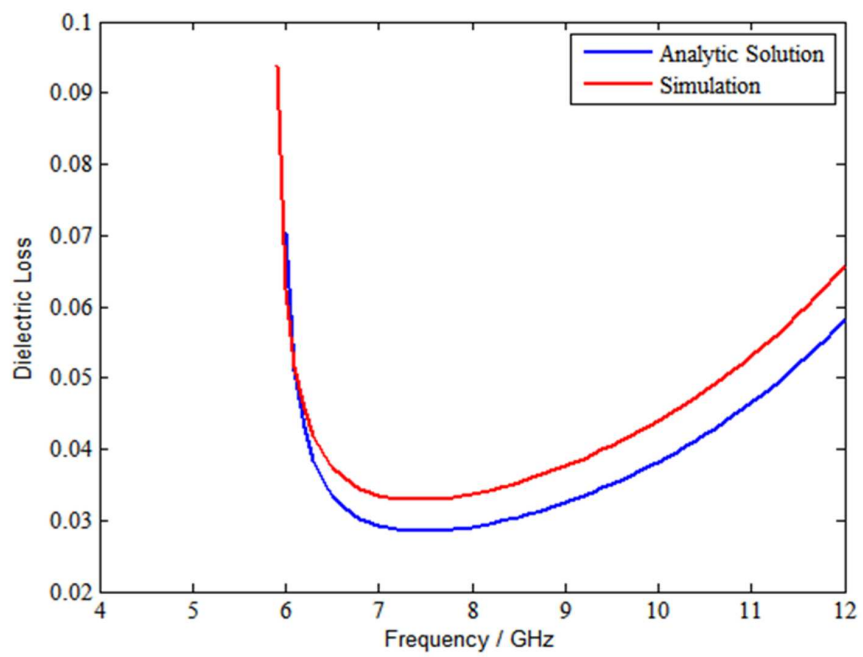


Figure 6.7: Dielectric loss of PSIW

6.5 Design of Partially Filled SIW Power Divider

6.5.1 SIW Design

PSIW is a synthetic rectangular waveguide formed by top and bottom metal covers and two sidewalls of metallic via-holes. PSIW operates in TE_{mo} modes. With the knowledge of pitch between consecutive vias and via diameters, it can be replaced by an equivalent rectangular waveguide as mentioned in subsection 6-3. The equivalent width (a_e) is computed using the method presented in [3]. The cut-off frequency for dominant mode of rectangular waveguide is given as follows:

$$f_{cmm} = \frac{k_c}{2\pi} = \frac{1}{2\pi\sqrt{\mu_0\epsilon_0}} \sqrt{\left(\frac{m\pi}{a_e}\right)^2 + \left(\frac{n\pi}{b}\right)^2} \quad (6.19)$$

$$f_{10} = \frac{1}{2a_e\sqrt{\mu_0\epsilon_0}} \quad (6.20)$$

where b is the substrate thickness, a_e is the equivalent width of SIW, μ_0 and ϵ_0 are the permittivity and permeability of the free space, respectively. By using the above formula width of the first layer will be calculated based on the cut-off frequency. The electrical field lines of a PSIW at TE_{10} mode are shown in Figure 6-8. This is similar to rectangular waveguide field lines. The discussion about SIW wave propagation mechanism in subsection 6.2 can be

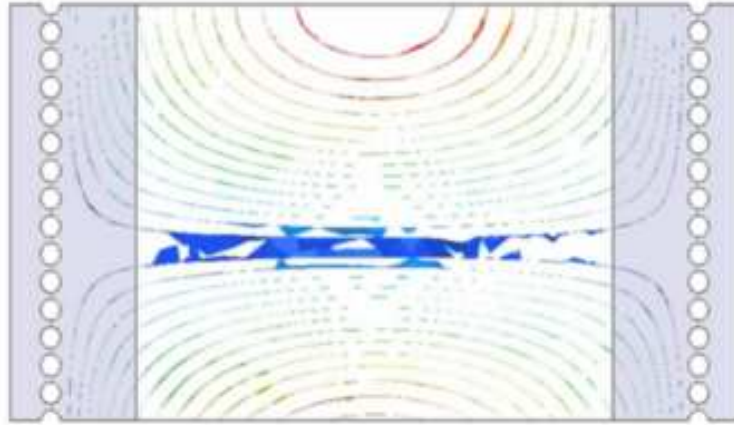


Figure 6.8: E-Field lines for PSIW top view

developed to PSIW structure. The main part of the transmission media in PSIW is filled with air and a small part at the corner are dielectric substrate. So cut-off frequency which can be found from (6-18) may be a little different from the one that is achieved through simulation.

Current distribution for TE_{10} is shown in Figure 6-9. The vias of PSIW are parallel to current

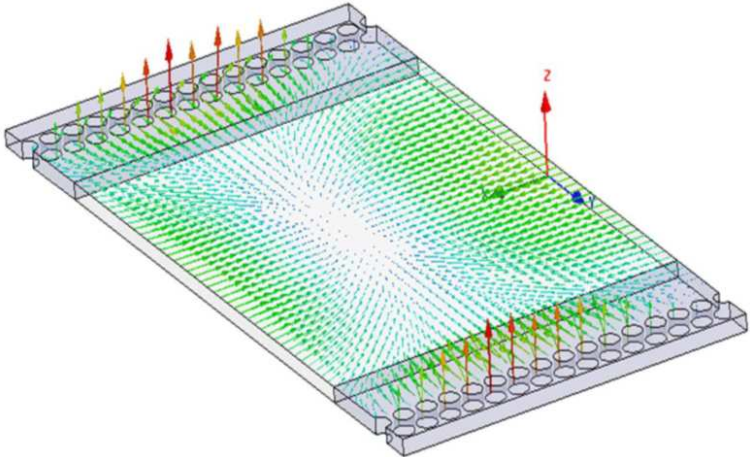


Figure 6.9: The current distribution on PSIW for TE_{10}

distribution, so there is a little amount of radiation. Generally, low radiation loss of the SIW structure can be obtained with large and closely spaced vias.

The proposed PSIW in Figure 6-4 must be adopted so that it can be measured with vector network analyzer (VNA). The adopted PSIW is shown in Figure 6-10. Two tapered parts

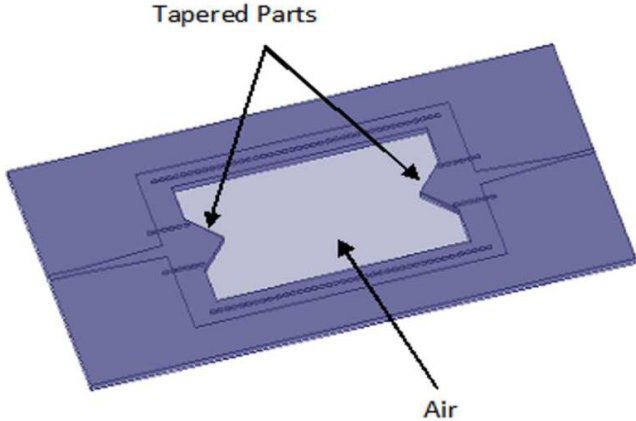


Figure 6.10: Proposed PSIW structure

for reducing the unwanted effect of changing in the transmission media from air to dielectric have been made. The electromagnetic wave is propagating from dielectric to air in input side of the PSIW line and from the air to dielectric at output side of the PSIW line by using the tapered sections. There are two covering parts in top and bottom of the PSIW line. These

covering parts are easily attached to the tapered parts without having any effect on electrical performance of the component. There are two other tapered parts in connection points between SIW and microstrip line. Their task is mode matching of the SIW to microstrip line.

6.5.2 Three-Port PSIW Power Divider Design

The similarity of PSIW power divider with E-plane power divider encourages the researcher to use E-plane power divider design procedure for designing PSIW counterpart. E-plane SIW power divider design procedure and its equivalent circuits are given in [56] and [103]. Our proposed PSIW power divider is illustrated in Figure 6-11. It consists of three layers. The first and the second layers are made from RO4003 with $\epsilon_r=3.55$ and $\tan\delta=0.0027$ which is cut in middle part. The second layer is cooper with 0.3 mm thickness. The thickness of copper layer affects the S-parameters of the structure. Experimental experience indicates that thin copper layer is suitable for covering the structure. But if a very thin layer is selected, the copper easily bends, making the height of the structure changed and this will produce a bad effect on the results. Thus the optimum thickness of the copper layer between the available copper in laboratory is 0.3 mm thickness. There is a slot in the second layer for propagating the electromagnetic wave from layer 1 to layer 3. The minimum width of the slots produce good results but it is possible to have 1 mm slot width with available instruments. This technology of manufacturing E-plane PSIW power dividers is very simple and efficient. By increasing the number of ports only the length of the structure is increased and its width remains unchanged. Therefore this method could be developed to design an n-way PSIW power divider. The dimension of PSIW power divider without transition parts is shown in Table 6-1.

Table 6.1: Dimensions of PSIW power divider (mm).

	Length	Width
First Layer	4	16
Slot	16.6	1
Third Layer	8	20.6
Transition Part	4.6	1.5

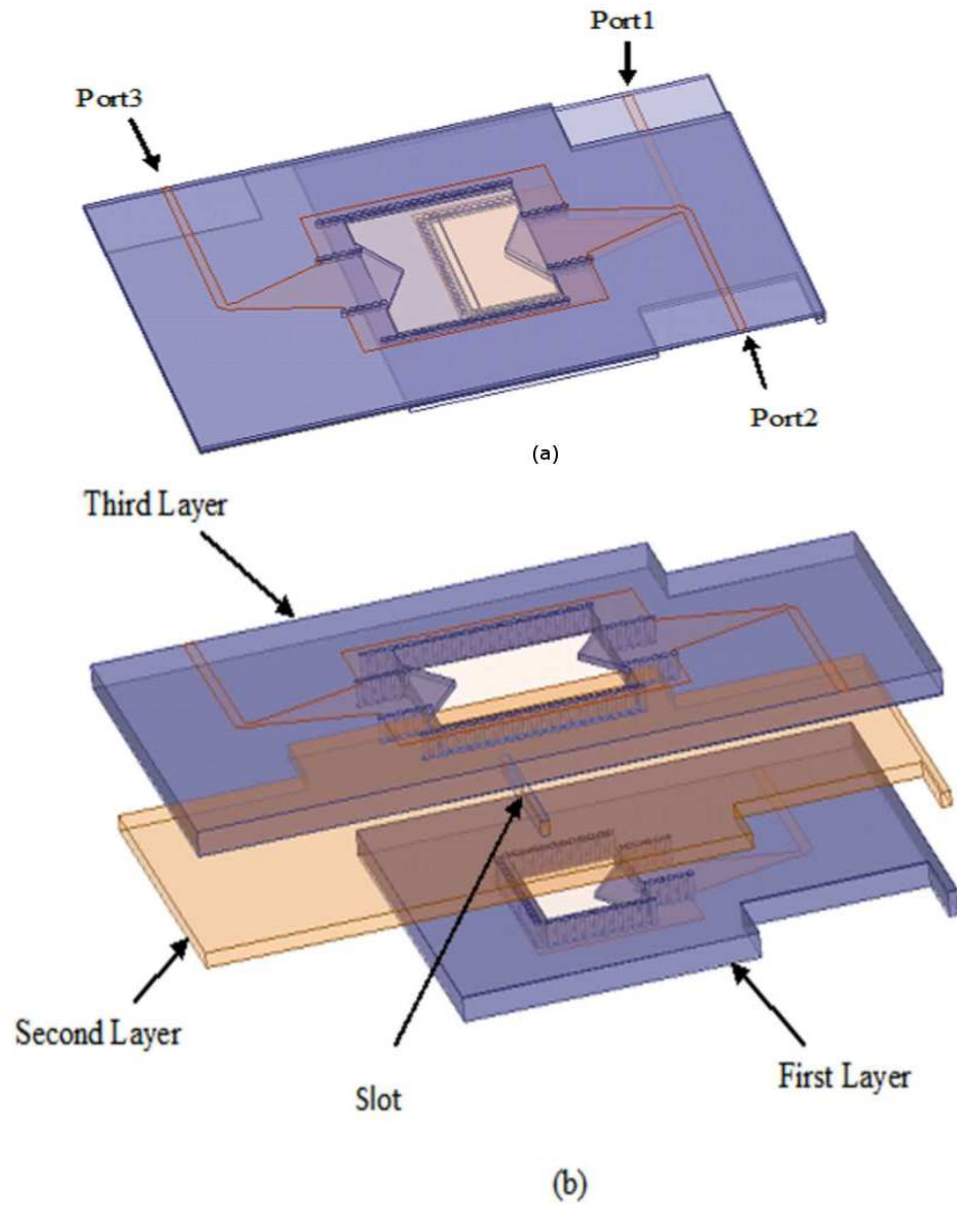


Figure 6.11: (a) The proposed PSIW power divider (b) Configuration of PSIW with three different layers

6.6 TRL Procedure

In order to measure the SIW structures, they must be connected to microstrip line with transition parts. These tapered parts and microstrip line affect the loss of SIW structure. So their contributions must be removed. This is achievable in the light of TRL calibration. Three TRL calibration standards which have been used for PSIW power divider measurement are shown in Figure 6-12.

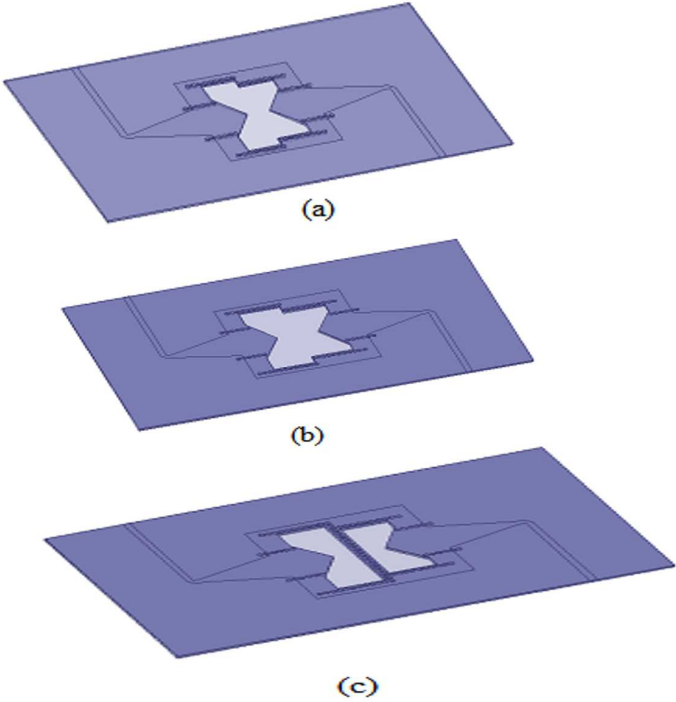


Figure 6.12: TRL Standards (a) True (b) Line (c) Reflect

As it is shown, these standards are hollow inside and contain two different error boxes. The error boxes have been designed by considering the input and output ports of PSIW power divider. For avoiding any radiation effects the reflect standard is a short circuit. The through standard is made by connecting the two error boxes directly together.

At the TRL calibration procedure in [57], the S-parameter of DUT is calculated by assumption of two identical error boxes. But in PSIW standards, error boxes are different from each other. Also, by selecting the TRL mode in the VNA, the process can be completed. The mathematical calculation of DUT parameters has been done as follows.

Signal flow graph for line standard with two different error boxes are shown in Figure.6-13.

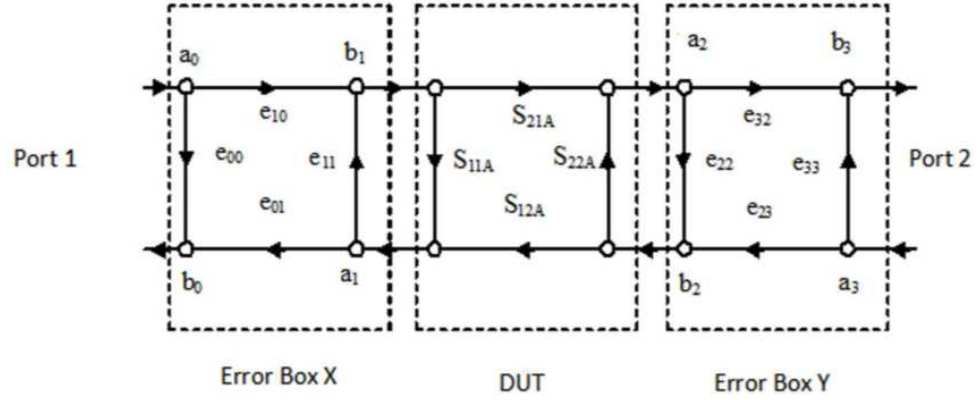


Figure 6.13: Signal flow graph for Line connection

By using the T-parameters or cascading parameters, it can be written:

$$[T_m] = [T_x][T_A][T_y] \quad (6.21)$$

$$[T_m] \stackrel{def}{=} \begin{pmatrix} T_{11m} & T_{12m} \\ T_{21m} & T_{22m} \end{pmatrix} = \frac{1}{S_{21m}} \begin{pmatrix} S_{21m}S_{12m} - S_{11m}S_{22m} & S_{11m} \\ -S_{22m} & 1 \end{pmatrix} \quad (6.22)$$

$$[T_A] \stackrel{def}{=} \begin{pmatrix} T_{11A} & T_{12A} \\ T_{21A} & T_{22A} \end{pmatrix} = \frac{1}{S_{21A}} \begin{pmatrix} S_{21A}S_{12A} - S_{11A}S_{22A} & S_{11A} \\ -S_{22A} & 1 \end{pmatrix} \quad (6.23)$$

$$[T_X] \stackrel{def}{=} \begin{pmatrix} X_{11} & X_{12} \\ X_{21} & X_{22} \end{pmatrix} = \frac{1}{e_{10}} \begin{pmatrix} e_{10}e_{01} - e_{00}e_{11} & e_{00} \\ -e_{11} & 1 \end{pmatrix} \quad (6.24)$$

$$[T_Y] \stackrel{def}{=} \begin{pmatrix} Y_{11} & Y_{12} \\ Y_{21} & Y_{22} \end{pmatrix} = \frac{1}{e_{32}} \begin{pmatrix} e_{32}e_{23} - e_{22}e_{33} & e_{22} \\ -e_{33} & 1 \end{pmatrix} \quad (6.25)$$

The thru has been applied so:

$$[T_{mt}] = [T_x][T_{At}][T_y] = [T_x][T_y] \quad (6.26)$$

Since for thru connection:

$$[T_{At}] \stackrel{def}{=} \begin{pmatrix} 1 & 0 \\ 0 & 1 \end{pmatrix} \quad (6.27)$$

The line has been applied so:

$$[T_{md}] = [T_x][T_{Ad}][T_y] \quad (6.28)$$

where

$$[T_{Ad}] \stackrel{def}{=} \begin{pmatrix} e^{-\gamma l} & 0 \\ 0 & e^{-\gamma l} \end{pmatrix} \quad (6.29)$$

For this matched line $S_{11A} = S_{22A}$ means that $T_{21A} = T_{12A}$

$$[T_y] = [T_x]^{-1}[T_{mt}] \quad (6.30)$$

Substituting into (6-28) :

$$[M][T_x] = [T_x][A_d] \quad (6.31)$$

where

$$[M] \stackrel{def}{=} [T_{md}][T_{mt}]^{-1} = \begin{pmatrix} m_{11} & m_{12} \\ m_{21} & m_{22} \end{pmatrix} \quad (6.32)$$

Rewriting (6-31) gives:

$$\begin{pmatrix} m_{11} & m_{12} \\ m_{21} & m_{22} \end{pmatrix} \begin{pmatrix} X_{11} & X_{12} \\ X_{21} & X_{22} \end{pmatrix} = \begin{pmatrix} X_{11} & X_{12} \\ X_{21} & X_{22} \end{pmatrix} \begin{pmatrix} e^{-\gamma l} & 0 \\ 0 & e^{-\gamma l} \end{pmatrix} \quad (6.33)$$

$$m_{11}X_{11} + m_{12}X_{12} = X_{11}e^{-\gamma l} \quad (6.34)$$

$$m_{21}X_{11} + m_{22}X_{21} = X_{21}e^{-\gamma l} \quad (6.35)$$

$$m_{11}X_{12} + m_{12}X_{22} = X_{21}e^{-\gamma l} \quad (6.36)$$

$$m_{21}X_{12} + m_{22}X_{22} = X_{22}e^{-\gamma l} \quad (6.37)$$

Eliminating $e^{-\gamma l}$ from (6-34) and (6-35) yields

$$m_{21}\left(\frac{X_{11}}{X_{21}}\right)^2 + (m_{22} - m_{11})\left(\frac{X_{11}}{X_{21}}\right) - m_{12} = 0 \quad (6.38)$$

Eliminating $e^{-\gamma l}$ from (6-36) and (6-37) yields

$$m_{21}\left(\frac{X_{12}}{X_{22}}\right)^2 + (m_{22} - m_{11})\left(\frac{X_{12}}{X_{22}}\right) - m_{12} = 0 \quad (6.39)$$

The solution for (6-38) and (6-39) are the same, but root choices must be done.

$$\left(\frac{X_{11}}{X_{21}}\right) \stackrel{def}{=} a = e_{00} - \frac{e_{01}e_{10}}{e_{11}} \quad (6.40)$$

$$\left(\frac{X_{12}}{X_{22}}\right) \stackrel{def}{=} b = e_{00} \quad (6.41)$$

$$e_{00} = b \quad (6.42)$$

$$\frac{(e_{01}e_{10})}{e_{11}} = b - a \quad (6.43)$$

Similar procedure can be used for $[T_Y]$.

$$[T_Y][N] = [T_{Ad}][T_Y] \quad (6.44)$$

where

$$[N] = [T_{mr}]^{-1}[T_{md}] = \begin{pmatrix} n_{11} & n_{12} \\ n_{21} & n_{22} \end{pmatrix} \quad (6.45)$$

Finally two equation are found as follows:

$$n_{12}\left(\frac{Y_{11}}{Y_{12}}\right)^2 + (n_{22} - n_{11})\left(\frac{Y_{11}}{Y_{12}}\right) - n_{12} = 0 \quad (6.46)$$

And

$$n_{12}\left(\frac{Y_{21}}{Y_{22}}\right)^2 + (n_{22} - n_{11})\left(\frac{Y_{21}}{Y_{22}}\right) - n_{21} = 0 \quad (6.47)$$

There are some definitions.

$$\left(\frac{Y_{11}}{Y_{12}}\right) \stackrel{def}{=} c = -e_{33} + \frac{e_{23}e_{32}}{e_{22}} \quad (6.48)$$

$$\left(\frac{Y_{21}}{Y_{22}}\right) \stackrel{def}{=} d = -e_{33} \quad (6.49)$$

$$e_{33} = -d \quad (6.50)$$

$$\frac{e_{23}e_{32}}{e_{22}} = c - d \quad (6.51)$$

Reflect standard has been used to find e_{11} and e_{22} . With reflection Γ_A coefficient at port 1 of error box X:

$$\Gamma_{mx} = e_{00} + \frac{(e_{10}e_{01}\Gamma_A)}{1 - e_{11}\Gamma_A} \quad (6.52)$$

$$\Gamma_A = \frac{1}{e_{11}} + \frac{b - \Gamma_{ma}}{a - \Gamma_{mx}} \quad (6.53)$$

With the same termination Γ_A on port 2 of the error box Y:

$$\Gamma_{my} = e_{33} + \frac{(e_{23}e_{32}\Gamma_A)}{1 - e_{22}\Gamma_A} \quad (6.54)$$

$$\Gamma_A = \frac{1}{e_{22}} + \frac{d + \Gamma_{my}}{c + \Gamma_{my}} \quad (6.55)$$

Eliminating Γ_A from (7-53) and(7-55):

$$\frac{1}{e_{22}} = \frac{1}{e_{11}} \left(\frac{c + \Gamma_{my}}{d + \Gamma_{my}} \right) \left(\frac{b - \Gamma_{mx}}{a - \Gamma_{mx}} \right) \quad (6.56)$$

During the thru connection, e_{22} with the port 1 reflection Γ_{m1} can be calculated.

$$\Gamma_{m1} = e_{00} + \frac{(e_{10}e_{01})e_{22}}{1 - e_{11}e_{22}} \quad (6.57)$$

$$e_{11} = \frac{1}{e_{22}} \left(\frac{b - \Gamma_{m1}}{a - \Gamma_{m1}} \right) \quad (6.58)$$

the value of $\frac{1}{e_{22}}$ from (7-56) and (7-58):

$$e_{11} = \left[\left(\frac{b - \Gamma_{mx}}{a - \Gamma_{mx}} \right) \left(\frac{c + \Gamma_{my}}{d + \Gamma_{my}} \right) \left(\frac{b - \Gamma_{m1}}{a - \Gamma_{m1}} \right) \right]^{\frac{1}{2}} \quad (6.59)$$

And from(7-58):

$$e_{22} = \frac{1}{e_{11}} \left(\frac{b - \Gamma_{m1}}{a - \Gamma_{m1}} \right) \quad (6.60)$$

$$(e_{10}e_{01}) = (b - a)e_{11} \quad (6.61)$$

$$(e_{23}e_{32}) = (c - d)e_{22} \quad (6.62)$$

from thru connection:

$$S_{21m} = e_{10}e_{32} \frac{1}{1 - e_{11}e_{22}} \rightarrow e_{10}e_{32} = S_{21m}(1 - e_{11}e_{22}) \quad (6.63)$$

$$S_{12m} = e_{01}e_{23} \frac{1}{1 - e_{11}e_{22}} \rightarrow e_{01}e_{23} = S_{12m}(1 - e_{11}e_{22}) \quad (6.64)$$

Γ_A and γl can be found as:

$$\Gamma_A = \frac{1}{e_{11}} \left(\frac{b - \Gamma_{mx}}{a - \Gamma_{mx}} \right) \quad (6.65)$$

$$e^{2\gamma l} = \frac{bm_{21+m22}}{\frac{1}{a}m_{12} + m_{11}}$$

In this way error boxes have been characterized and the S-parameters of DUT can be calculated.

6.7 Experimental Results of Three-Port PSIW Power Divider

Picture of fabricated PSIW power divider is shown in Figure 6-14. Port 1 is the input port and ports 2 and 3 are the output ports. Two RO4003 substrate with $\epsilon_r=3.55$, $\tan\delta=0.0027$ and 0.51 mm thickness are used to create the first and third layers. The second layer is a piece of copper with 0.3 mm thickness. These layers have been attached together and covered with two RO4003 substrates as top and bottom layers. Figure 6-15 shows the comparison of simulated and measurement results of PSIW, return loss and transmissions.

These parameters have been measured with TRL calibration method, so they present the

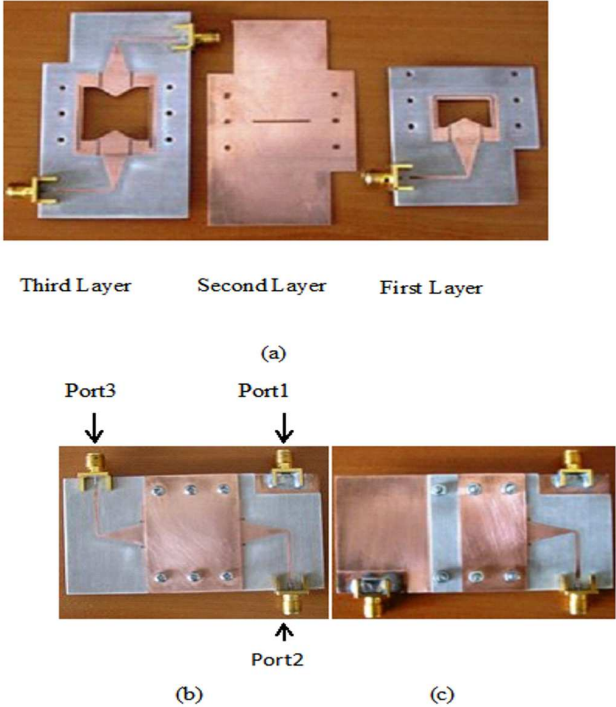
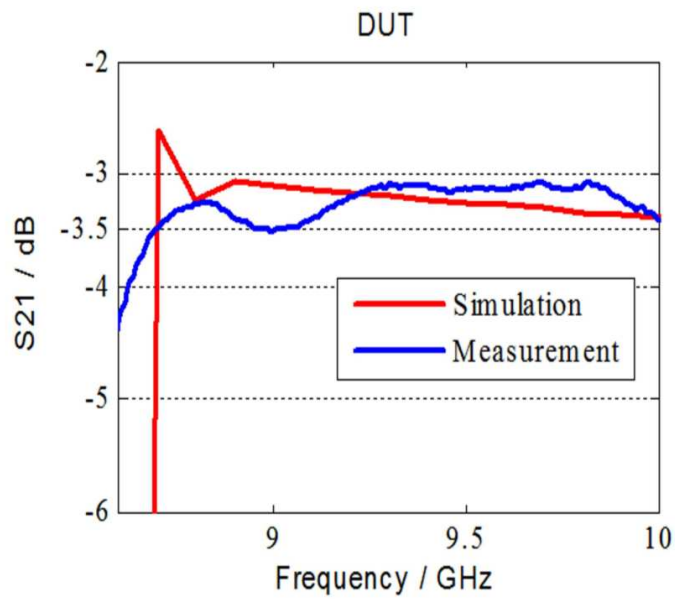
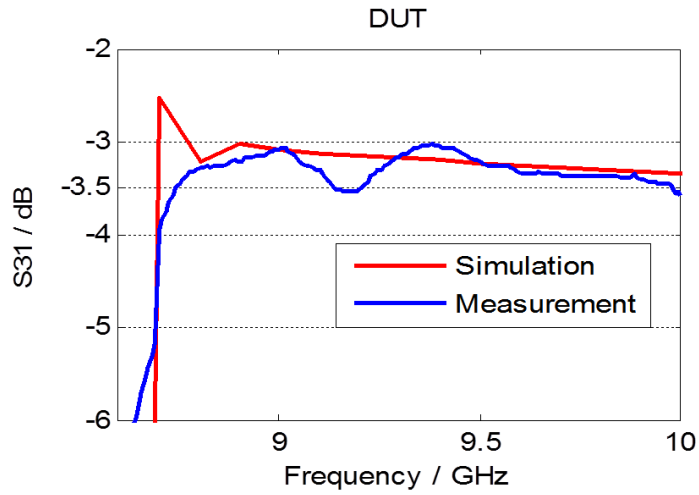
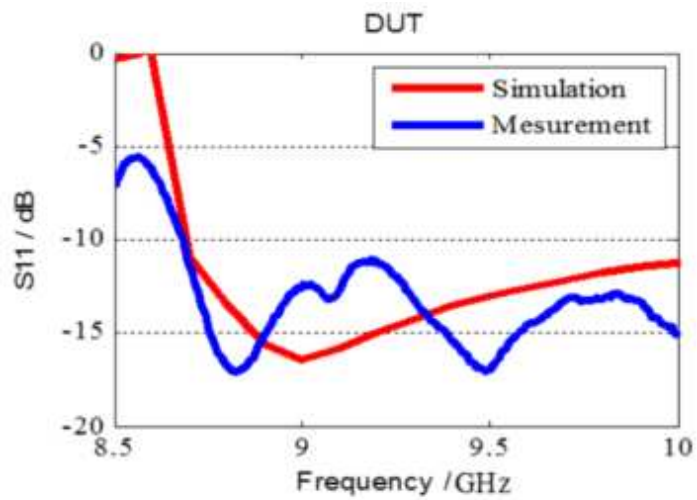


Figure 6.14: (a)Three layers of fabricated PSIW (b) Top view (c) Bottom view

S-parameters of device under test (DUT) without any effect of transition parts. The measured transmission coefficients are between -3 dB and -3.5 dB from 8.75 GHz to 10 GHz. Return loss is less than 10 dB at the same frequency band. Simulation and measurement results are in a good agreement with each other. As shown in Figure 6-16, the measured amplitude balance is between ± 0.2 dB from 8.75 GHz to 10 GHz. The measured phase difference between $\angle S_{21}$ and $\angle S_{31}$ is about $\pm 4^\circ$. It shows that the amplitude balance and phase balance is not too sensitive to frequency of operation.

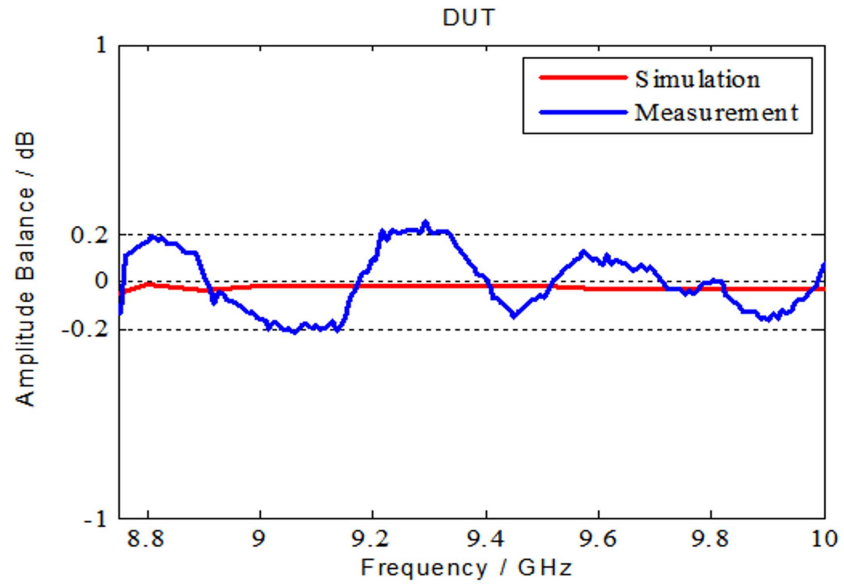


(b)

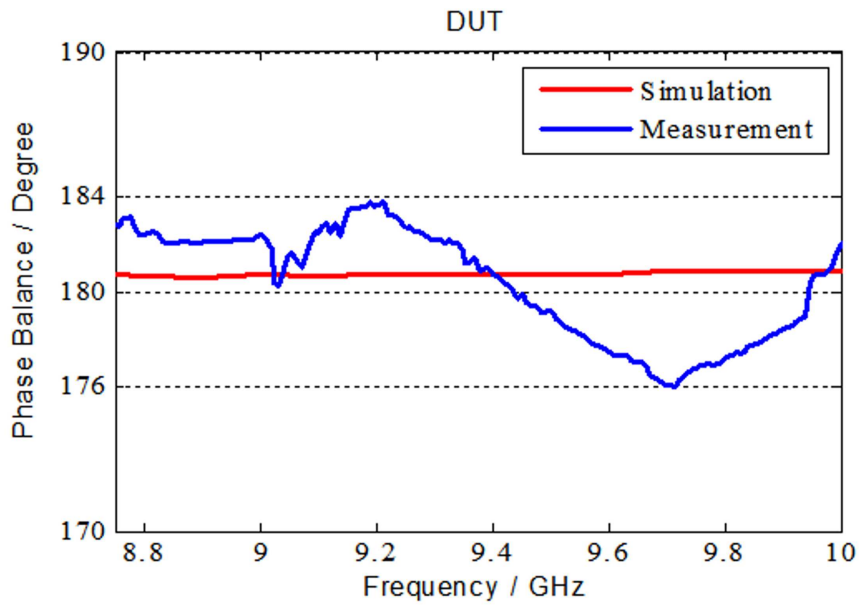


(c)

Figure 6.15: Simulation and measurement results of PSIWpower divider (a-b) Transmissions (c) Return Loss



(a)



(b)

Figure 6.16: (a) Amplitude balance (b) Phase balance of PSIW power divider

6.8 Five-Port PSIW Power Divider Design

A five-port PSIW power divider has been designed and simulated. RO4003 substrate with $\epsilon_r=3.55$, $\tan\delta=0.0027$ and 0.51 mm thickness has been used for simulation. The port positions are shown in Figure 6-17. Different layers have been shown in Figure 6-18 individually.

The tapered parts and transition parts design procedure are similar to three-ports PSIW power

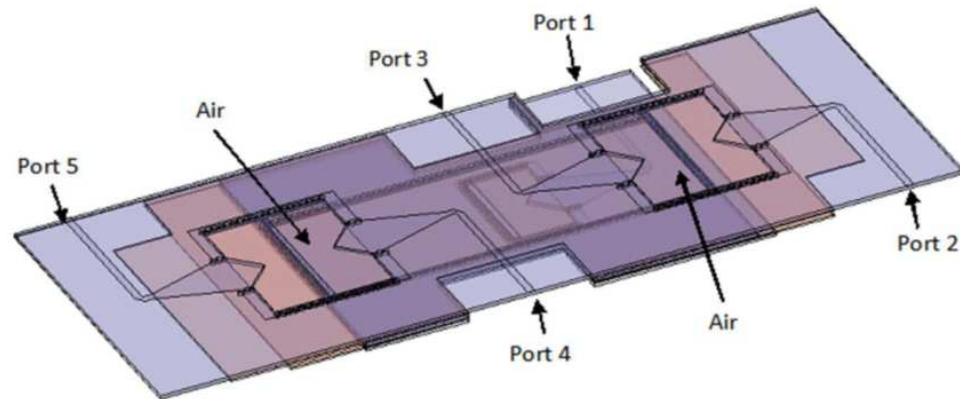


Figure 6.17: Five-port PSIW power divider

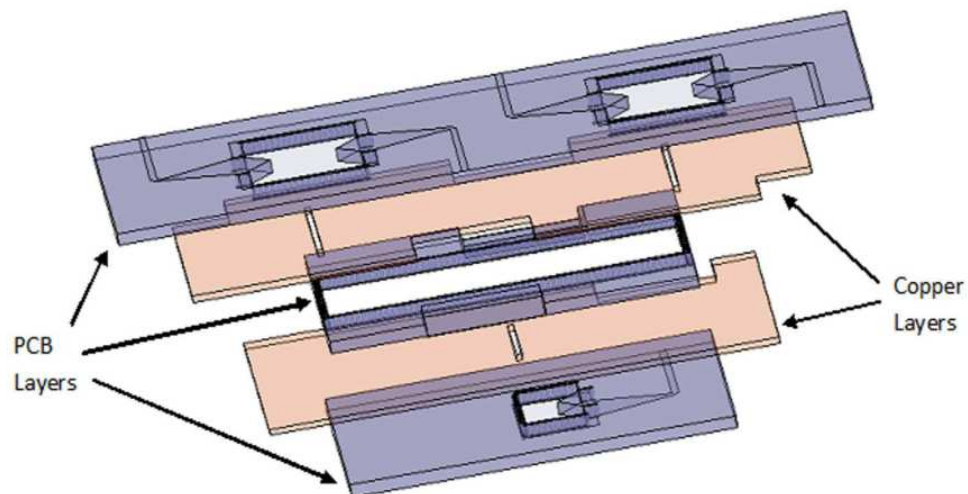


Figure 6.18: Configuration of five-port PSIW power divider

divider. The input port transition parts are different from output ports transition parts, so the TRL standards have different error boxes in their two ports. It consists of three PCB layers

and two copper layers with 0.3 mm thickness as shown in Figure 6-18. The dielectric layers have been cut inside and dielectric part has been removed. These parts have been covered by copper layers. There is one slot in the first copper and two slots in the second copper. The slot position is symmetric due to upper layer. The electromagnetic wave has been propagated from these slots to upper layers. The slot width is 1 mm. The via diameter and the space between vias is 0.8 mm and 1 mm respectively. Transition part width and length are 8 mm and 12.48 mm respectively. The tapered part has 8 mm width and 4 mm length. S-parameter of whole PSIW structure without transition part is a matter of concern. The DUT of the five-port PSIW is shown in Figure 6-19. The dimension of DUT is given in Table 6-2.

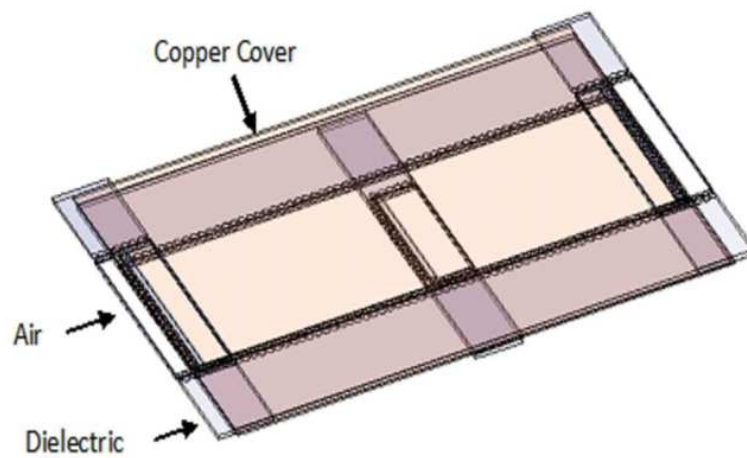


Figure 6.19: DUT of five-port PSIW power divider

Table 6.2: Dimensions of five-ports PSIW power divider (mm).

	Length	Width
First Layer	6	15.6
Second Layer	60	20.6
Third Layer	11	22.6
Transition Part	12.5	8

The simulation results of five-port PSIW power divider are shown below. According to the Figure 6-20 the return loss is below than 10 dB from 9 GHz to 11 GHz. The transmissions in Figure 6-21 are between 6 dB and 6.5 dB at the same frequency band.

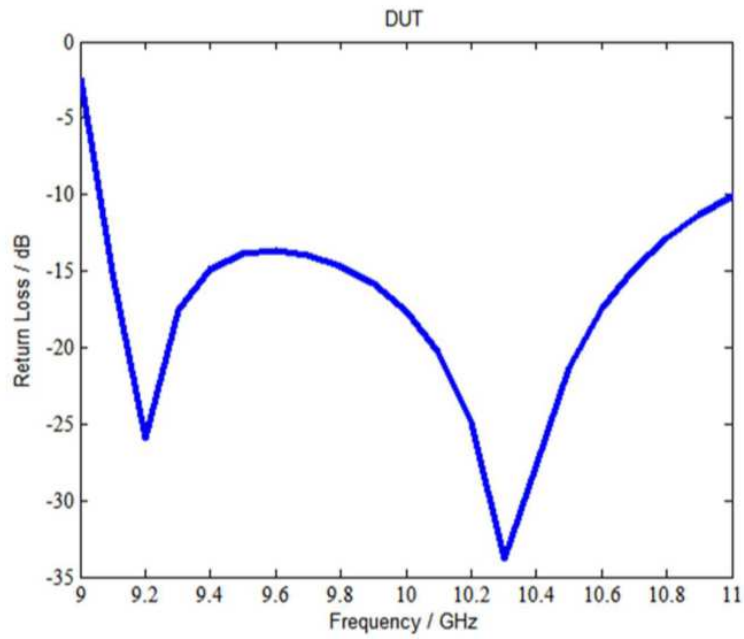


Figure 6.20: Simulation results of five-port PSIW power divider, Return loss

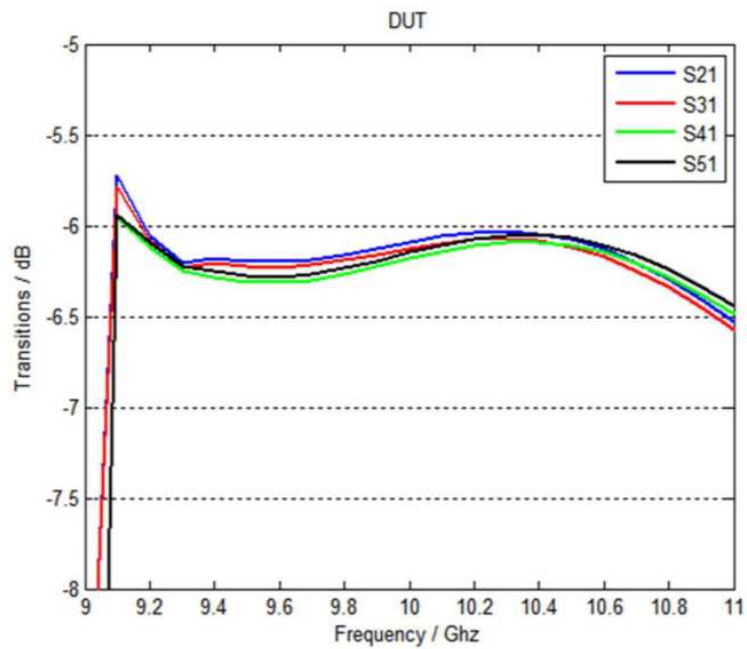


Figure 6.21: Simulation results of five-port PSIW power divider, Transmissions

Isolation between port 2 and port 3 is shown in Figure 6-22. There is not a good isolation be-

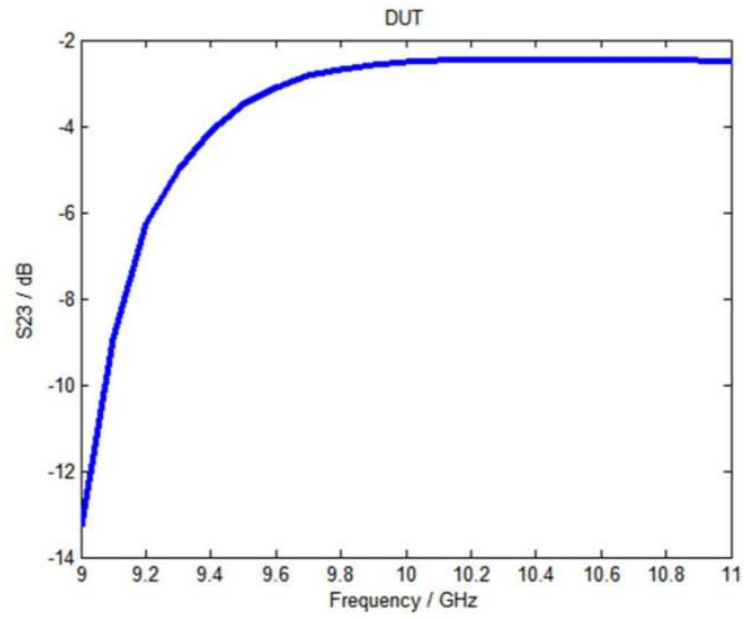


Figure 6.22: Simulation results of five-port PSIW power divider, Isolation

tween output ports as expected, because there is not any resistance between outputs. Isolation between other ports is similar to that shown in Figure 6-22.

CHAPTER 7

CONCLUSIONS

7.1 Thesis Summary and Conclusions

SIW based component has some advantages like low cost, low weight, and capability to integration with other components. The three-port and five-port SIW power dividers have been designed and fabricated. Compact in size and the capability of being developed into n-port are two important factors in design process. Generally, the design procedure has two main parts. First part is SIW design, which is done based on the similarity between SIW and rectangular waveguide. Second part is SIW power divider design which has been completed based on similarity between SIW power divider and E-plane power divider. The measurement results are in a good agreement with simulations. As it has been explained in chapter 4, a novel measurement set up has been established for TRL calibration of multi-port device. This set up has been used for reconstruction of the S-parameters of both structures. The fabrication process and the measurement results can be summarized as follows:

- For three-port SIW power divider the return loss below -10 dB has been achieved from 9 GHz to 11 GHz. Transmissions are between -3.5 dB to -4 dB at the same frequency band. There is a poor isolation between output ports as expected, because there is not any resistance between output ports. Measured amplitude balance is less than ± 0.5 dB from 9.5 GHz to 11 GHz and the measured phase difference between $\angle S_{21}$ and $\angle S_{31}$ is about $\pm 4^\circ$. It can be concluded that the amplitude balance and phase balance is not too sensitive to frequency of operation.
- For five-port SIW power divider, transmissions are approximately between -6.5 dB to -7 dB from 9.5 GHz to 10.5 GHz. There is a poor isolation between output ports as expected,

because there is not any resistance between output ports. Measured amplitude balance is less than ± 0.5 dB from 9.5 GHz to 10.8 GHz, and the phase balance is approximately $\pm 0.5^\circ$. The phase balance and amplitude balance are not sensitive to operation frequency in the desired band. There are similar results between other output ports.

- Loss mechanism in SIW structure has been investigated. Dielectric loss is considerably larger than the other losses. PSIW structure has been proposed, in which dielectric loss has been significantly decreased. At the PSIW structure transmission medium is air instead of dielectric. Three- port PSIW power divider has been designed and fabricated. Its measurement has been accomplished with TRL standards. These TRL standards have been constructed with two different error boxes. The design and measurement procedure is similar to the full SIW power dividers.
- For a three-port PSIW power divider, transmission coefficients are between -3 dB and -3.5 dB from 8.75 GHz to 10 GHz. Return loss is less than 10 dB at the same frequency band. Measured amplitude balance is less than ± 0.2 dB from 8.75 GHz to 10 GHz. The measured phase difference between $\angle S_{21}$ and $\angle S_{31}$ is about 4° . So it can be concluded that the amplitude balance and phase balance is not too sensitive to frequency of operation .
- For a five-port PSIW power divider, simulation the results show that return loss is below than 10 dB from 9 GHz to 11 GHz. The transmissions are between 6 dB and 6.5 dB at the same frequency band. As expected isolation between output ports is poor, because there is not any resistance between outputs.

7.2 Suggestions for Future Studies

SIW power dividers which have been reported in this thesis can be extended to focus on other related areas. These areas might specifically deal with the following topics:

- There is low isolation between output ports in proposed SIW power dividers, so it seems that by adding resistance between output ports high isolation can be achieved. The resistance value and its positions may be critical issues.
- A five-port PSIW power divider can be used as a feed network for array antenna with four elements. Therefore it is valuable to proceed with manufacturing the five-port PSIW

power divider. Measurement results of five-port PSIW power divider can be compared with a fully dielectric five-port SIW power divider. Good measurement results encourage the future researchers to use it as a beam forming network for array antenna.

- The simulation and measurement results for SIW power dividers which have been realized in this thesis show narrow frequency band. Thus increasing the frequency band of the structure will be a valuable subject.
- Unequal power divider is another important issue. The unequal power divider has been used with strict restrictions, in both designing and fabricating. The most common unequal power dividers reported [108]-[115] have been based on microstrip technology. These structures require a microstrip line with very high impedance, i.e. extremely low aspect ratio (W/H) or very thin conductor width. It is almost impractical to realize a high impedance line using the conventional microstrip structure. Although recently Defected Ground Structure (DGS) microstrip line has been reported to overcome the characteristic impedance problem [109], they have been used for low frequencies. Dual band microstrip power divider in [111] has been focused on operation centre frequency, but the performance at the frequencies between these desired two bands has not been considered.

A multiway dual band planar power divider with arbitrary power division in [115] has been reported. It is a very complicated structure and its operation frequency is low. The above mentioned structures have the inherent limitation of the microstrip line like radiation loss. Especially in array systems employing microstrip feeding network, the beam forming network (BFN) becomes more complicated as a number of array elements increases resulting in a significant radiation loss caused by the conductor in microstrip line.

SIW as a high integrated microwave component can be employed for the design of low loss unequal power divider. SIW is an interference free component, so it is suitable for BFN applications. Some SIW unequal power dividers in [89] and [91] have been reported. There is not a clear design equation for calculation of the amount of power desired to deliver to the specific port. Moreover they are not compact in size, so by increasing the number of ports the size problem becomes critical. Therefore an unequal SIW power divider which is similar to SIW power divider in this thesis, can overcome some of the above mentioned disadvantages. The proposed SIW unequal power divider is illustrated in Figure 7-1. It includes two layers which are attached to each other. There is a slot between layers for electromagnetic coupling. The characteristic impedances of two output ports are different from each other due

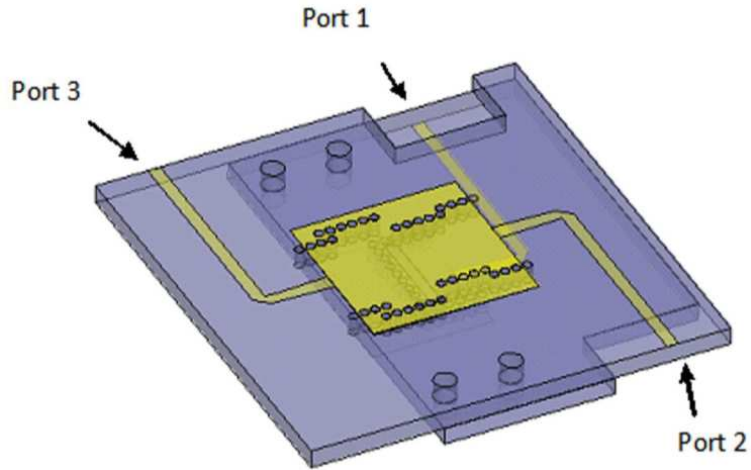


Figure 7.1: Unequal SIW power divider

to different dimensions of the ports. So the amount of power which has been propagated to the ports can be controlled with ports' dimensions. This idea can be developed for designing PSIW unequal power dividers. The simulation results of unequal SIW power divide is shown in Figure 7-2 and Figure 7-3. Table 7-1 shows the dimensions of the structure.

Table 7.1: Dimensions of unequal SIW power divider (mm).

	Length	Width
First Layer	8.2	9
Second Port	4	11.5
Third Port	4	17.5
Transition Part	4.6	1.5

Simulation results shows that return loss is below than 10 dB from 9 GHz to 11 GHz. Transmissions show that there is approximately 2 dB difference between output ports from 9.2 GHz to 10.4 GHz. These results are very satisfactory when compared with the available unequal power dividers which have been designed for a single frequency or dual mode structure have been focused on center frequency of dual band.

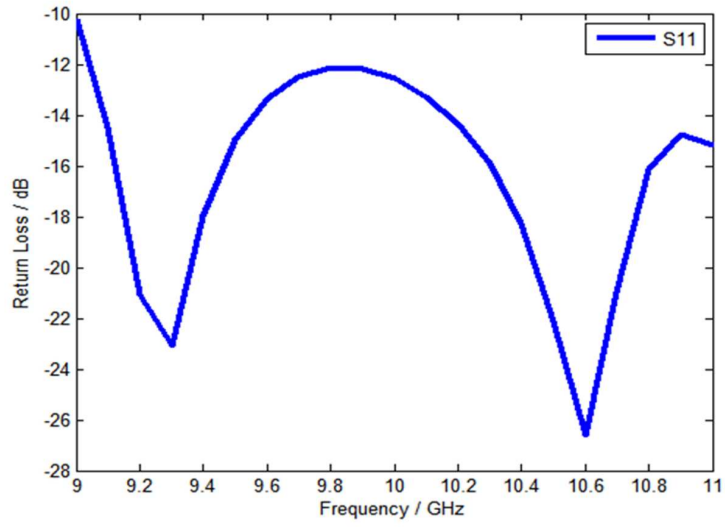


Figure 7.2: Return Loss of Unequal SIW power divider

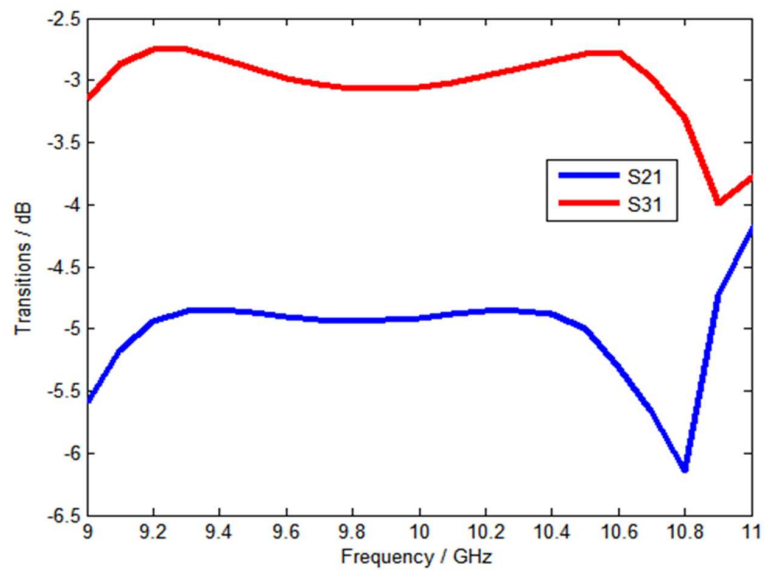


Figure 7.3: Transmissions of unequal SIW power divider

REFERENCES

- [1] J. Hirokawa and M. Ando, "Single-layer feed waveguide consisting of posts for plane TEM wave excitation in parallel plates," *Antennas and Propagation, IEEE Transactions on*, vol. 46, pp. 625-630, 1998.
- [2] Y. Cassivi, L. Perregrini, P. Arcioni, M. Bressan, K. Wu, and G. Conciauro, "Dispersion characteristics of substrate integrated rectangular waveguide," *Microwave and Wireless Components Letters, IEEE*, vol. 12, pp. 333-335, 2002.
- [3] D. Deslandes and K. Wu, "Integrated microstrip and rectangular waveguide in planar form," *Microwave and Wireless Components Letters, IEEE*, vol. 11, pp. 68-70, 2001.
- [4] S. Germain, D. Deslandes, and K. Wu, "Development of substrate integrated waveguide power dividers," in *Electrical and Computer Engineering, 2003. IEEE CCECE 2003. Canadian Conference on*, 2003, pp. 1921-1924 vol.3.
- [5] W. Ke, D. Deslandes, and Y. Cassivi, "The substrate integrated circuits - a new concept for high-frequency electronics and optoelectronics," in *Telecommunications in Modern Satellite, Cable and Broadcasting Service, 2003. TELSIKS 2003. 6th International Conference on*, 2003, pp. P-III-P-X vol.1.
- [6] A. Zeid and H. Baudrand, "Electromagnetic scattering by metallic holes and its applications in microwave circuit design," *Microwave Theory and Techniques, IEEE Transactions on*, vol. 50, pp. 1198-1206, 2002.
- [7] D. Deslandes and K. Wu, "Design Consideration and Performance Analysis of Substrate Integrated Waveguide Components," in *Microwave Conference, 2002. 32nd European*, 2002, pp. 1-4.
- [8] L. Yan, W. Hong, K. Wu, and T. J. Cui, "Investigations on the propagation characteristics of the substrate integrated waveguide based on the method of lines," *Microwaves, Antennas and Propagation, IEE Proceedings -*, vol. 152, pp. 35-42, 2005.
- [9] C. Xiao-Ping and W. Ke, "Accurate and efficient design approach of substrate integrated waveguide filter using numerical TRL calibration technique," in *Microwave Symposium Digest, 2008 IEEE MTT-S International*, 2008, pp. 1231-1234.
- [10] D. Deslandes, "Design equations for tapered microstrip-to-Substrate Integrated Waveguide transitions," in *Microwave Symposium Digest (MTT), 2010 IEEE MTT-S International*, 2010, pp. 704-707.
- [11] E. Miralles, H. Esteban, C. Bachiller, A. Belenguer, and V. E. Boria, "Improvement for the design equations for tapered Microstrip-to-Substrate Integrated Waveguide transitions," in *Electromagnetics in Advanced Applications (ICEAA), 2011 International Conference on*, 2011, pp. 652-655.

- [12] B. N. Das, K. V. S. V. R. Prasad, and K. V. S. Rao, "Excitation of Waveguide by Stripline- and Microstrip-Line-Fed Slots," *Microwave Theory and Techniques, IEEE Transactions on*, vol. 34, pp. 321-327, 1986.
- [13] W. Grabherr, W. G. B. Huder, and W. Menzel, "Microstrip to waveguide transition compatible with MM-wave integrated circuits," *Microwave Theory and Techniques, IEEE Transactions on*, vol. 42, pp. 1842-1843, 1994.
- [14] D. Deslandes and W. Ke, "Integrated transition of coplanar to rectangular waveguides," in *Microwave Symposium Digest, 2001 IEEE MTT-S International, 2001*, pp. 619-622 vol.2.
- [15] L. Sunho, J. Sangwoon, and L. Hai-Young, "Ultra-Wideband CPW-to-Substrate Integrated Waveguide Transition Using an Elevated-CPW Section," *Microwave and Wireless Components Letters, IEEE*, vol. 18, pp. 746-748, 2008.
- [16] A. Patrovsky, M. Daigle, and W. Ke, "Millimeter-wave wideband transition from CPW to substrate integrated waveguide on electrically thick high-permittivity substrates," in *Microwave Conference, 2007. European, 2007*, pp. 138-141.
- [17] N. Hee, Y. Tae-Soon, K. Ki-Byoung, Y. Ki-Cheol, and L. Jong-Chul, "Ku-band transition between microstrip and substrate integrated waveguide (SIW)," in *Microwave Conference Proceedings, 2005. APMC 2005. Asia-Pacific Conference Proceedings, 2005*, p. 4 pp.
- [18] W. Che, K. Deng, D. Wang, and Y. L. Chow, "Analytical equivalence between substrate-integrated waveguide and rectangular waveguide," *Microwaves, Antennas, Propagation, IET*, vol. 2, pp. 35-41, 2008.
- [19] D. Deslandes and W. Ke, "Single-substrate integration technique of planar circuits and waveguide filters," *Microwave Theory and Techniques, IEEE Transactions on*, vol. 51, pp. 593-596, 2003.
- [20] C. Wenquan, D. Kuan, and Y. L. Chow, "Equivalence between waveguides with side walls of cylinders (SIRW) and of regular solid sheets," in *Microwave Conference Proceedings, 2005. APMC 2005. Asia-Pacific Conference Proceedings, 2005*, p. 3 pp.
- [21] A. A. A. Apriyana and P. Zhang Yue, "A dual-band BPF for concurrent dual-band wireless transceiver," in *Electronics Packaging Technology, 2003 5th Conference (EPTC 2003), 2003*, pp. 145-149.
- [22] K. Jen-Tsai, Y. Tsung-Hsun, and Y. Chun-Cheng, "Design of microstrip bandpass filters with a dual-passband response," *Microwave Theory and Techniques, IEEE Transactions on*, vol. 53, pp. 1331-1337, 2005.
- [23] J. T. Kuo and C. Hung-Sen, "Design of quasi-elliptic function filters with a dual-passband response," *Microwave and Wireless Components Letters, IEEE*, vol. 14, pp. 472-474, 2004.
- [24] C. Quendo, E. Rius, A. Manchec, Y. Clavet, B. Potelon, J. F. Favennec, and C. Person, "Planar tri-band filter based on dual behavior resonator (DBR)," in *Microwave Conference, 2005 European, 2005*, p. 4 pp.

- [25] C. Quendo, E. Rius, and C. Person, "An original topology of dual-band filter with transmission zeros," in *Microwave Symposium Digest, 2003 IEEE MTT-S International*, 2003, pp. 1093-1096 vol.2.
- [26] C. Xiao-Ping, W. Ke, and L. Zhao-Long, "Dual-Band and Triple-Band Substrate Integrated Waveguide Filters With Chebyshev and Quasi-Elliptic Responses," *Microwave Theory and Techniques, IEEE Transactions on*, vol. 55, pp. 2569-2578, 2007.
- [27] M. Guglielmi, P. Jarry, E. Kerherve, O. Roquebrun, and D. Schmitt, "A new family of all-inductive dual-mode filters," *Microwave Theory and Techniques, IEEE Transactions on*, vol. 49, pp. 1764-1769, 2001.
- [28] D. Deslandes and K. Wu, "Millimeter-wave substrate integrated waveguide filters," in *Electrical and Computer Engineering, 2003. IEEE CCECE 2003. Canadian Conference on*, 2003, pp. 1917-1920 vol.3.
- [29] T. Shahvirdi and A. Banai, "Applying Contour Integral method for analysis of substrate integrated waveguide filters," in *Microwave Symposium (MMS), 2010 Mediterranean*, 2010, pp. 418-421.
- [30] H. Y. A. Yim and K. K. M. Cheng, "Novel dual-band planar resonator and admittance inverter for filter design and applications," in *Microwave Symposium Digest, 2005 IEEE MTT-S International*, 2005, p. 4 pp.
- [31] H. Wei, L. Bing, W. Yuanqing, L. Qinghua, T. Hongjun, Y. Xiao Xin, D. Yuan Dan, Z. Yan, and W. Ke, "Half Mode Substrate Integrated Waveguide: A New Guided Wave Structure for Microwave and Millimeter Wave Application," in *Infrared Millimeter Waves and 14th International Conference on Terahertz Electronics, 2006. IRMMW-THz 2006. Joint 31st International Conference on*, 2006, pp. 219-219.
- [32] W. Yuanqing, H. Wei, D. Yuandan, L. Bing, T. Hong Jun, C. Jixin, Y. Xiaoxin, and W. Ke, "Half Mode Substrate Integrated Waveguide (HMSIW) Bandpass Filter," *Microwave and Wireless Components Letters, IEEE*, vol. 17, pp. 265-267, 2007.
- [33] Y. F. Z. G. Zhang, Y. J. Cheng, and Y.-H. Zhang, "A compact multilayer dual-mode substrate integrated circular cavity (sicc) filter for x-band application," *Progress In Electromagnetics Research*, Vol. 122, 453-465, 2012. .
- [34] L.-S. W. R. Wang, and X.-L. Zhou, "Compact folded substrate integrated waveguide cavities and bandpass filter," *Progress In Electromagnetics Research*, Vol. 84, 135-147, 2008. .
- [35] R. E. COLLIN, *FOUNDATION FOR MICROWAVE ENGINEERING* MacGRAW-HILL, Inc. , 1992.
- [36] P.A. RIZZII, *MICROWAVE ENGINEERING PASSIVE CIRCUITS* Prentice - hall, Inc., 1998.
- [37] C. Peng, H. Guang, C. De Ting, W. Yuan Chun, and H. Wei, "A double layer crossed over Substrate Integrated Waveguide wide band directional coupler," in *Microwave Conference, 2008. APMC 2008. Asia-Pacific*, 2008, pp. 1-4.
- [38] F. Carrera, D. Navarro, M. Baquero-Escudero, P. Rodrigo, x00F, and V. M. arrocha, "Compact substrate integrated waveguide directional couplers in Ku and K bands," in *Microwave Conference (EuMC), 2010 European*, 2010, pp. 1178-1181.

- [39] V. A. Labay and J. Bornemann, "Design of dual-band substrate-integrated waveguide E-plane directional couplers," in *Microwave Conference, 2009. APMC 2009. Asia Pacific, 2009*, pp. 2116-2119.
- [40] B. Liu, W. Hong, Y. Q. Wang, Q. H. Lai, and K. Wu, "Half Mode Substrate Integrated Waveguide (HMSIW) 3-dB Coupler," *Microwave and Wireless Components Letters, IEEE*, vol. 17, pp. 22-24, 2007.
- [41] V. A. Labay and J. Bornemann, "E-plane directional couplers in substrate-integrated waveguide technology," in *Microwave Conference, 2008. APMC 2008. Asia-Pacific, 2008*, pp. 1-3.
- [42] W. Chao, C. Wenquan, L. Chao, and P. Russer, "Multi-way microwave power dividing/combining network based on substrate-integrated waveguide (SIW) directional couplers," in *Microwave and Millimeter Wave Technology, 2008. ICMMT 2008. International Conference on, 2008*, pp. 18-21.
- [43] Z. C. Hao, W. Hong, J. X. Chen, H. X. Zhou, and K. Wu, "Single-layer substrate integrated waveguide directional couplers," *Microwaves, Antennas and Propagation, IEE Proceedings -*, vol. 153, pp. 426-431, 2006.
- [44] R. Elliott, "An improved design procedure for small arrays of shunt slots," *Antennas and Propagation, IEEE Transactions on*, vol. 31, pp. 48-53, 1983.
- [45] M. Bozzi, A. Georgiadis, and K. Wu, "Review of substrate-integrated waveguide circuits and antennas," *Microwaves, Antennas Propagation, IET*, vol. 5, pp. 909-920, 2011.
- [46] W. Zi-bin, G. Rong, and J. Yong-chang, "Design and Experiment on Substrate Integrated Waveguide Resonant Slot Array Antenna at Ku-Band," in *Antennas, Propagation and EM Theory, 2006. ISAPE '06. 7th International Symposium on, 2006*, pp. 1-3.
- [47] C. Yu Jian, H. Wei, and W. Ke, "Millimeter-Wave Substrate Integrated Waveguide Multi-beam Antenna Based on the Parabolic Reflector Principle," *Antennas and Propagation, IEEE Transactions on*, vol. 56, pp. 3055-3058, 2008.
- [48] K. Kuhlmann, K. Rezer, and A. F. Jacob, "Far field measurement on Ka-band substrate-integrated waveguide antenna array with polarization multiplexing," in *Microwave Symposium Digest, 2008 IEEE MTT-S International, 2008*, pp. 1337-1340.
- [49] C. Jin, A. Alphones, and L. C. Ong, "Broadband leaky-wave antenna based on composite right/left handed substrate integrated waveguide," *Electronics Letters*, vol. 46, pp. 1584-1585, 2010.
- [50] L. Qing Hua, H. Wei, K. Zhen Qi, Z. Ying Song, and W. Ke, "Half-Mode Substrate Integrated Waveguide Transverse Slot Array Antennas," *Antennas and Propagation, IEEE Transactions on*, vol. 57, pp. 1064-1072, 2009.
- [51] L. Qinghua, C. Fumeaux, and H. Wei, "On the transition from radiating to guiding behavior of the half-mode substrate integrated waveguide," in *Microwave Conference Proceedings (APMC), 2010 Asia-Pacific, 2010*, pp. 1601-1604.
- [52] G. H. Zhai, W. Hong, K. Wu, and Z. Q. Kuai, "Wideband substrate integrated printed log-periodic dipole array antenna," *Microwaves, Antennas and Propagation, IET*, vol. 4, pp. 899-905, 2010.

- [53] A. Suntives and S. V. Hum, "An electronically tunable half-mode substrate integrated waveguide leaky-wave antenna," in Antennas and Propagation (EUCAP), Proceedings of the 5th European Conference on, 2011, pp. 3670-3674.
- [54] A. Borji, D. Busuioc, and S. Safavi-Naeini, "Efficient, Low-Cost Integrated Waveguide-Fed Planar Antenna Array for Ku-Band Applications," Antennas and Wireless Propagation Letters, IEEE, vol. 8, pp. 336-339, 2009.
- [55] D. Busuioc, M. Shahabadi, A. Borji, G. Shaker, and S. Safavi-Naeini, "Substrate integrated waveguide antenna feed - design methodology and validation," in Antennas and Propagation Society International Symposium, 2007 IEEE, 2007, pp. 2666-2669.
- [56] N. Marcuvitz, Waveguide Handbook: McGraw-Hill Book Company, Inc., 1951.
- [57] D. M. Pozar, Microwave Engineering, 3rd ed.: John Wiley, Sons, 2005.
- [58] M. Davidovitz, "Reconstruction of the S-matrix for a 3-port using measurements at only two ports," Microwave and Guided Wave Letters, IEEE, vol. 5, pp. 349-350, 1995.
- [59] S. Sercu and L. Martens, "Characterizing N-port packages and interconnections with a 2-port network analyzer," in Electrical Performance of Electronic Packaging, 1997., IEEE 6th Topical Meeting on, 1997, pp. 163-166.
- [60] A. Ferrero, U. Pisani, and K. J. Kerwin, "A new implementation of a multiport automatic network analyzer," Microwave Theory and Techniques, IEEE Transactions on, vol. 40, pp. 2078-2085, 1992.
- [61] A. Ferrero, F. Sanpietro, and U. Pisani, "Accurate coaxial standard verification by multiport vector network analyzer," in Microwave Symposium Digest, 1994., IEEE MTT-S International, 1994, pp. 1365-1368 vol.3.
- [62] A. Ferrero and F. Sanpietro, "A simplified algorithm for leaky network analyzer calibration," Microwave and Guided Wave Letters, IEEE, vol. 5, pp. 119-121, 1995.
- [63] R. A. Speciale and N. R. Franzen, "Super - TSD, A Generalization of the TSD Network Analyzer Calibration Procedure, Covering n - Port Measurements with Leakage," in Microwave Symposium Digest, 1977 IEEE MTT-S International, 1977, pp. 114-117.
- [64] J. C. Tippet and R. A. Speciale, "A Rigorous Technique for Measuring the Scattering Matrix of a Multiport Device with a 2-Port Network Analyzer," Microwave Theory and Techniques, IEEE Transactions on, vol. 30, pp. 661-666, 1982.
- [65] H. Dropkin, "Comments on A Rigorous Technique for Measuring the Scattering Matrix of a Multiport Device with a Two-Port Network Analyzer," Microwave Theory and Techniques, IEEE Transactions on, vol. 31, pp. 79-81, 1983.
- [66] D. Woods, "Multiport-network analysis by matrix renormalisation employing voltage-wave S-parameters with complex normalisation," Electrical Engineers, Proceedings of the Institution of, vol. 124, pp. 198-204, 1977.
- [67] D. F. Williams and D. K. Walker, "In-Line Multiport Calibration," in ARFTG Conference Digest-Spring, 51st, 1998, pp. 88-90.

- [68] L. Weigan and R. Chengli, "Measurement and calibration of a universal six-port network analyzer," *Microwave Theory and Techniques, IEEE Transactions on*, vol. 37, pp. 734-742, 1989.
- [69] C. Chih-Jung and C. Tah-Hsiung, "Virtual Auxiliary Termination for Multiport Scattering Matrix Measurement Using Two-Port Network Analyzer," *Microwave Theory and Techniques, IEEE Transactions on*, vol. 55, pp. 1801-1810, 2007.
- [70] C. Chih-Jung and C. Tah-Hsiung, "Measurement of Noncoaxial Multiport Devices Up to the Intrinsic Ports," *Microwave Theory and Techniques, IEEE Transactions on*, vol. 57, pp. 1230-1236, 2009.
- [71] L. Hsin-Chia and C. Tah-Hsiung, "Multiport scattering matrix measurement using a reduced-port network analyzer," *Microwave Theory and Techniques, IEEE Transactions on*, vol. 51, pp. 1525-1533, 2003.
- [72] L. Yu, T. Yu, G. Bo, and T. Ling, "An improved method for TRL calibration," in *Microwave and Millimeter Wave Technology (ICMMT), 2010 International Conference on*, 2010, pp. 696-698.
- [73] J. E. Zuiga-Juarez, J. A. Reynoso-Hernandez, and M. C. Maya-Sanchez, "An improved multiline TRL method," in *ARFTG Conference, 2006 67th*, 2006, pp. 139-142.
- [74] R. R. Pantoja, M. J. Howes, J. R. Richardson, and R. D. Pollard, "Improved calibration and measurement of the scattering parameters of microwave integrated circuits," *Microwave Theory and Techniques, IEEE Transactions on*, vol. 37, pp. 1675-1680, 1989.
- [75] J. C. Rautio, "Techniques for Correcting Scattering Parameter Data of an Imperfectly Terminated Multiport When Measured with a Two-Port Network Analyzer," *Microwave Theory and Techniques, IEEE Transactions on*, vol. 31, pp. 407-412, 1983.
- [76] L. Hsin-Chia and C. Tah-Hsiung, "Port reduction methods for scattering matrix measurement of an n-port network," *Microwave Theory and Techniques, IEEE Transactions on*, vol. 48, pp. 959-968, 2000.
- [77] N. A. Smith and R. Abhari, "Compact substrate integrated waveguide Wilkinson power dividers," in *Antennas and Propagation Society International Symposium, 2009. AP-SURSI '09. IEEE*, 2009, pp. 1-4.
- [78] F. Wenjie, C. Wenquan, and D. Kuan, "Compact Planar Magic-T Using E-Plane Substrate Integrated Waveguide (SIW) Power Divider and Slotline Transition," *Microwave and Wireless Components Letters, IEEE*, vol. 20, pp. 331-333, 2010.
- [79] J. Yuan, L. Xian Qi, Z. Zhong Bo, S. Peng, and F. Yong, "An improved compact power divider/combiner designed using HMSIW structure," in *Antennas Propagation and EM Theory (ISAPE), 2010 9th International Symposium on*, 2010, pp. 1109-1112.
- [80] P. Mohammadi and S. Demir, "Two layers substrate integrated waveguide power divider," in *General Assembly and Scientific Symposium, 2011 XXXth URSI*, 2011, pp. 1-4.
- [81] X. Zhongshan, L. Bing, Z. Yongjiu, T. Bo, and J. Shengli, "A novel Ka band multi-layer SIW power divider," in *Cross Strait Quad-Regional Radio Science and Wireless Technology Conference (CSQRWC), 2011, 2011*, pp. 634-636.

- [82] Z. Zhen-Yu and W. Ke, "Broadband half-mode substrate integrated waveguide (HMSIW) Wilkinson power divider," in *Microwave Symposium Digest, 2008 IEEE MTT-S International*, 2008, pp. 879-882.
- [83] K. Sarhadi and M. Shahabadi, "Wideband substrate integrated waveguide power splitter with high isolation," *Microwaves, Antennas, Propagation, IET*, vol. 4, pp. 817-821, 2010.
- [84] F. He, K. Wu, X. Chen, L. Han, and W. Hong, "A planar magic-T structure using substrate integrated circuits concept," in *Microwave Symposium Digest (MTT), 2010 IEEE MTT-S International*, 2010, pp. 1-1.
- [85] J. Haiyan and W. Guangjun, "A Novel Four-Way Ka-Band Spatial Power Combiner Based on HMSIW," *Microwave and Wireless Components Letters, IEEE*, vol. 18, pp. 515-517, 2008.
- [86] Y. Jiawei, J. Yuan, L. Xianqi, Z. Zhongbo, and F. Yong, "A four-way half-mode SIW power divider with improved impedance match," in *Microwave, Antenna, Propagation, and EMC Technologies for Wireless Communications (MAPE), 2011 IEEE 4th International Symposium on*, 2011, pp. 306-308.
- [87] S. Kaijun, F. Yong, and Z. Yonghong, "Eight-Way Substrate Integrated Waveguide Power Divider With Low Insertion Loss," *Microwave Theory and Techniques, IEEE Transactions on*, vol. 56, pp. 1473-1477, 2008.
- [88] Y. Ning, C. Caloz, and W. Ke, "Substrate integrated waveguide power divider based on multimode interference imaging," in *Microwave Symposium Digest, 2008 IEEE MTT-S International*, 2008, pp. 883-886.
- [89] Y. Songnan and A. E. Fathy, "Synthesis of an Arbitrary Power Split Ratio Divider Using Substrate Integrated Waveguides," in *Microwave Symposium, 2007. IEEE/MTT-S International*, 2007, pp. 427-430.
- [90] Z. Meiyong, Y. Zhenfeng, S. Zhenhai, L. Lianfu, and Z. Xueyong, "Design of Ka-band substrate integrated waveguide power dividers/combiners," in *Computational Problem-Solving (ICCP), 2011 International Conference on*, 2011, pp. 361-363.
- [91] T. Y. Seo, J. W. Lee, C. Choon Sik, and T. K. Lee, "Radial guided 4-way unequal power divider using substrate integrated waveguide with center-fed structure," in *Microwave Conference, 2009. APMC 2009. Asia Pacific*, 2009, pp. 2758-2761.
- [92] K. Song and Y. Fan, "Broadband travelling-wave power divider based on substrate integrated rectangular waveguide," *Electronics Letters*, vol. 45, pp. 631-632, 2009.
- [93] K. Song, Y. Fan, and X. Zhou, "X-band broadband substrate integrated rectangular waveguide power divider," *Electronics Letters*, vol. 44, pp. 211-213, 2008.
- [94] L.-n. Wu, X.-c. Zhang, C.-m. Tong, and M. Zhou, "A new substrate integrated waveguide six-port circuit," in *Microwave and Millimeter Wave Technology (ICMMT), 2010 International Conference on*, 2010, pp. 59-61.
- [95] H. Yuping and L. Yilong, "Design of a substrate integrated waveguide based 1-to-6 non-uniform power divider," in *Microwave Conference, 2008. APMC 2008. Asia-Pacific*, 2008, pp. 1-4.

- [96] H. ZhargCheng, H. Wei, L. Hao, Z. Hua, and W. Ke, "Multiway broadband substrate integrated waveguide (SIW) power divider," in *Antennas and Propagation Society International Symposium, 2005 IEEE*, 2005, pp. 639-642 Vol. 1A.
- [97] X. Zou, C. M. Tong, and D. W. Yu, "Y-junction power divider based on substrate integrated waveguide," *Electronics Letters*, vol. 47, pp. 1375-1376, 2011.
- [98] N. Ranjkesh and M. Shahabadi. (2006, Reduction of dielectric losses in substrate integrated waveguide. *Electronics Letters* 42(21), 1230-1231.
- [99] M. Bozzi, L. Perregrini, and W. Ke, "Modeling of Conductor, Dielectric, and Radiation Losses in Substrate Integrated Waveguide by the Boundary Integral-Resonant Mode Expansion Method," *Microwave Theory and Techniques, IEEE Transactions on*, vol. 56, pp. 3153-3161, 2008.
- [100] X. Feng, Z. Yulin, H. Wei, W. Ke, and C. Tie Jun, "Finite-difference frequency-domain algorithm for modeling guided-wave properties of substrate integrated waveguide," *Microwave Theory and Techniques, IEEE Transactions on*, vol. 51, pp. 2221-2227, 2003.
- [101] X. Feng and W. Ke, "Guided-wave and leakage characteristics of substrate integrated waveguide," *Microwave Theory and Techniques, IEEE Transactions on*, vol. 53, pp. 66-73, 2005.
- [102] D. Deslandes and W. Ke, "Accurate modeling, wave mechanisms, and design considerations of a substrate integrated waveguide," *Microwave Theory and Techniques, IEEE Transactions on*, vol. 54, pp. 2516-2526, 2006.
- [103] P. Mohammadi and a. S. Demir, "MULTI-LAYER SUBSTRATE INTEGRATED WAVEGUIDE E-PLANE POWER DIVIDER," *Progress In Electromagnetics Research C*, Vol. 30, 159-172, 2012.
- [104] K. D. W. Che, D. Wang and Y.L. Chow, "Analytical equivalence between substrate-integrated waveguide and rectangular waveguide," *IET Microw. Antennas Propag.*, Vol. 2, No. 1, February 2008.
- [105] W. H. L. Yan, K. Wu and T.J. Cui, "Investigations on the propagation characteristics of the substrate integrated waveguide based on the method of lines," *IEE Proc.-Microw. Antennas Propag.*, Vol. 152, No. 1, February 2005.
- [106] L. P. Y. Cassivi, P. Arcioni, M. Bressan, K. Wu, and G. Conciauro, "Dispersion Characteristics of Substrate Integrated Rectangular Waveguide," *IEEE MICROWAVE AND WIRELESS COMPONENTS LETTERS*, VOL. 12, NO. 9, SEPTEMBER 2002
- [107] R. F. Harrington, *Time Harmonic Electromagnetic Fields*: Wiley-IEEE Press, 2001.
- [108] G. Ge and H. K. Wen, "Research on microstrip multiway unequal power divider/combiner," *Microwaves, Antennas and Propagation, IEE Proceedings -*, vol. 143, pp. 437-440, 1996.
- [109] L. Jeng-Sik, L. Sung-Won, K. Chul-Soo, P. Jun-Seek, A. Dal, and N. Sangwook, "A 4.1 unequal Wilkinson power divider," *Microwave and Wireless Components Letters, IEEE*, vol. 11, pp. 124-126, 2001.

- [110] O. Seongmin, K. Jae-Jin, H. Mun-Su, P. Chunseon, J. Yong-Chae, L. Jong-Sik, C. Kwan-Sun, and A. Dal, "An Unequal Wilkinson Power Divider with Variable Dividing Ratio," in *Microwave Symposium, 2007. IEEE/MTT-S International, 2007*, pp. 411-414.
- [111] Y. Wu, Y. Liu, and S. Li, "Unequal dual-frequency Wilkinson power divider including series resistor-inductor-capacitor isolation structure," *Microwaves, Antennas , Propagation, IET*, vol. 3, pp. 1079-1085, 2009.
- [112] L. Bo, W. Xidong, and W. Wen, "A 10:1 Unequal Wilkinson Power Divider Using Coupled Lines With Two Shorts," *Microwave and Wireless Components Letters, IEEE*, vol. 19, pp. 789-791, 2009.
- [113] C. Li-Na, X. Huan-Huan, J. Yong-Chang, and Z. Fu-Shun, "A novel 4:1 unequal dual-frequency Wilkinson power divider," in *Microwave and Millimeter Wave Technology (ICMMT), 2010 International Conference on, 2010*, pp. 1290-1293.
- [114] W. Yongle, L. Yuanan, X. Quan, L. Shulan, and Y. Cuiping, "Analytical Design Method of Multiway Dual-Band Planar Power Dividers With Arbitrary Power Division," *Microwave Theory and Techniques, IEEE Transactions on*, vol. 58, pp. 3832-3841, 2010.
- [115] Z. Hong Lin, H. Bin Jie, and Z. Xiu Yin, "Compact Equal and Unequal Dual-Frequency Power Dividers Based on Composite Right-/Left-Handed Transmission Lines," *Industrial Electronics, IEEE Transactions on*, vol. 59, pp. 3464-3472, 2012.

VITA

Pejman Mohammadi was born in Tehran, Iran in 1973. He received Ph.D. degree from Electrical and Electronic Engineering of Middle East Technical University in 2012 December. His main research is microwave systems and antennas. He has experiences in design and manufacturing of Substrate Integrated Waveguide based components. His publication are:

1. P.Mohammadi, S.Demir, "Two layers substrate integrated waveguide power divider," General Assembly and Scientific Symposium, 2011 XXXth URSI , pp.1-4, 13-20 Aug. 2011.
2. P. Mohammadi and S. Demir, "Multi-layer substrate integrated waveguide e-plane power divider," Progress In Electromagnetics Research C, Vol. 30, 159-172, 2012.
3. P. Mohammadi and a. S. Demir, "Substrate Integrated Waveguide Unequal Power Divider with Adjustable Dividing Ratio, " The first Iranian Conference on Electromagnetic Engineering (ICEME) Iran University Of Science And Technology in 26-27 Dec. 2012